DEVELOPMENT OF 3D PRINTED FLEXIBLE SUPERCAPACITORS: DESIGN, MANUFACTURE, AND TESTING

A thesis submitted in fulfilment of the requirements

for the Degree of Doctor of Philosophy (Ph.D.)

by

Milad Areir

College of Engineering, Design and Physical Sciences

Brunel University London

Uxbridge, UB8 3PH

United Kingdom

January 2018

I. Abstract

The development of energy storage devices has represented a significant technological challenge for the past few years. Electrochemical double-layer capacitors (EDLCs), also named as supercapacitors, are a likely competitor for alternative energy storage because of their low-cost, high power density, and high fast charge/discharge rate. The recent development of EDLCs requires them to be lightweight and flexible. There are many fabrication techniques used to manufacture flexible EDLCs, and these methods can include pre-treatment to ensure more efficient penetration of activated carbon (AC) patterns onto the substrate, or those that utilise masks for the definitions of patterns on substrates. However, these methods are inconvenient for building cost-effective devices. Therefore, it was necessary to find a suitable process to reduce the steps of manufacture and to be able to print multiple materials uniformly. This research work describes the first use of a 3D printing technology to produce flexible EDLCs for energy storage.

In this research work, the four essential elements for the EDLCs substrate, current collector, activated electrode, and gel electrolyte were investigated. The AC powder was milled by ball milling to optimise the paste deposition and the electrochemical performance. A flexible composite EDLC was designed and manufactured by 3D printing. The electrochemical performance of the flexible composite EDLCs was then examined. Being highly flexible is one of the critical demands for the recent development of EDLCs. Therefore, highly flexible EDLCs were designed and manufactured by only one single extrusion process. The 3D highly flexible EDLC maintains significant electrochemical performance under a mechanical bending test. To meet the power and energy requirements, the EDLCs were connected and tested in series and parallel circuits. A supercapacitor based on printed AC material displays an area specific capacitance of 1.48 F/cm^2 at the scan rate of 20 mV/s. The coulombic efficiency for the flexible EDLC was found to be 59.91%, and the cycling stability was achieved to be 56% after 500 cycles. These findings indicate that 3D printing technology may be increasingly used to develop more sophisticated flexible wearable electronic devices.

II. Acknowledgments

First, my most humble gratitude to God. Only with His blessings and perseverance that was bestowed upon me in making this PhD journey possible.

My heartfelt thanks to my principal supervisor, Dr Yanmeng Xu who been a great inspiration and advisor during my PhD study. His supervision and encouragement in my research had refined my knowledge in the field of electronics. I am very proud and honoured for being a student under your guidance. I would like to express my deepest gratitude to Prof. David Harrison, Prof. John Fyson, and my second supervisors Dr Eujin Pei, for their advice and support throughout my PhD study, without whom this project would have been impossible.

I would like to thank Dr Ruirong Zhang, Mr Anan Tanwilaisiri, Dr Marco Cavallaro, Dr Timothy Minton, Prof. P. Kathirgamanathan, Dr Peter Evan and Dr Abdul Chaudhary, Mr Matthew Smith, whose enthusiasm, support, provision of facilities and equipment were essential for the research. Dr Esteban Schunemann for collaborating with me during the research and bringing in valuable interest, feedback and his professional suggestions to improve the experiment. I would also like to express my appreciation to Prof. Michael Turner, Dr Stuart Higgins, Dr Michael Renn, Dr Harrison Lee, Dr Catherine Ramsdale, Prof. Zhong Lin Wang, Dr Fernando Castro and other anonymous referees for their useful suggestions during the conference of Large-Area Electronics 2016 and 2017. Prof. Tony Anson from experimental techniques centre whose extensive expertise for carbon coatings and other advanced manufacturing applications for his support of the work as a judge in Research Institutes 2nd conference. Also, I must extend my heartfelt thanks to Dr Charles Mire from Structur3D printing for his valuable support in paste extrusion tool. Sincere thanks are extended to the Ministry of Higher Education of Libya for their funding. Finally, I thank my parents for their constant and unconditional support and my wife, brothers, sisters, and parents in law. I would like to thank all of my friends who have supported me socially and emotionally throughout my PhD journey.

III. Author's Declaration

I as a result of this declaration that the work in this thesis was carried out following the requirements of the University's Regulations for PhD and that it has not been submitted for any other academic award. Except where indicated by specific reference in the text, this work is my work. Work done in collaboration with, or with the assistance of others, is indicated as such. I have identified all material in this thesis that is not my work through appropriate referencing and acknowledgement. Where I have quoted or otherwise incorporated material, which is the work of others, I have included the source in the references. Any views expressed in the thesis, other than referenced material, are those of the author.

SIGNED…… DATE: ……

(Signature of student)

IV. Publication and Conference Emergent From This Work

The work detailed in this thesis has resulted in number of refereed publications, as follows:

Journal papers

1. **M. Areir**, Y. Xu, D. Harrison, J. Fyson, R. Zhang (2017) 'Development of 3D printing technology for the manufacture of flexible electric double-layer capacitors', Materials and Manufacturing Processes, 1-7, Taylor & Francis. DOI: 10.1080/10426914.2017.1401712.

2. **M. Areir**, Y. Xu, D. Harrison, J. Fyson (2017) '3D printing of highly flexible supercapacitor designed for wearable energy storage', Materials Science & Engineering B, 226, 29-38, Elsevier. DOI: 10.1016/j.mseb.2017.09.004.

3. **M. Areir**, Y. Xu, D. Harrison, J. Fyson (2017) 'A study of 3D printed flexible supercapacitors onto silicone rubber substrates', Journal of Materials Science: Materials in Electronics, 28, 1-9, Springer. DOI: 10.1007/s10854-017-7774-9.

4. **M. Areir**, Y. Xu, R. Zhang, D. Harrison, J. Fyson, E. Pei (2017) 'A study of 3D printed active carbon electrode for the manufacture of electric double-layer capacitors', Journal of Manufacturing Processes, 25, 351–356, Elsevier. DOI: 10.1016/j.jmapro.2016.12.020.

5. A. Tanwilaisiri, Y. Xu, R. Zhang, D. Harrison, J. Fyson, **M. Areir** (2018) 'Design and fabrication of modular supercapacitors using 3D printing', Journal of Energy Storage, 16, 1-7, Elsevier. DOI: 10.1016/j.est.2017.12.020.

Conferences

1. **M. Areir**, Y. Xu, D. Harrison, J. Fyson (2017) 'A study of 3D printed flexible supercapacitors onto silicone rubber substrates', EPSRC Centre for Innovative Manufacturing in Large-Area Electronics (InnoLAE) Conference, Cambridge, UK, 31st Jan.

2. **M. Areir**, Y. Xu, D. Harrison, J. Fyson (2016) 'Development of a method for the manufacture of hybrid energy storage using 3D printing technology', EPSRC Centre for Innovative Manufacturing in Large-Area Electronics (innoLAE) Conference, Cambridge, UK, 1st- 2nd Feb.

3. **M. Areir**, Y. Xu, D. Harrison, J. Fyson (2016) '3D printed flexible supercapacitors', Research Institutes 2nd Annual Conference, Brunel University London, UK, 30th Nov.

V. Table of contents

VI. List of Figures

VII. List of Tables

VIII. List of Equations

IX. Acronyms and Abbreviations

A list below is a brief overview of the terms, acronyms, and symbol used throughout this research.

Acronyms	Definition
ABS	Acrylonitrile butadiene styrene
AC	Activated carbon
Ag	Silver powder
AM	Additive manufacturing
CAD	Computer aided design
CMC	Carboxymethyl cellulose
CNC	Computer numerical control
CNT	Carbon nanotube

Code	Program instructions
CV	Cyclic voltammetry
CVD	Chemical vapour deposition
ED	Ethylene carbonate
EDLCs	Electric double-layer capacitors
EIS	Electrochemical impedance spectroscopy
EPD	Electrophoretic deposition technique
ESR	Equivalent series resistance
FDM	Fused deposition modelling
Firmware	Built in software to the machine
GC	Glassy carbon
GCD	Galvanostatic charge and discharge
G-code	Program containing build parameters and machine instructions
GO	Graphene oxide
GPE	Gel polymer electrolytes
H_2SO_4	Sulfuric acid
H_3PO_4	Phosphoric acid
LAYWOO-D3	Wood/polymer composite filament

M codes	Machine code (programming language)
MSCs	Micro supercapacitors
MWCNT	Multi-walled carbon nanotubes
NinjaFlex	Flexible filament material made from thermoplastic polyurethane
NMP	1-methyl-2-pyrrolidinone
PAN	Polyacrylonitrile
PANI	Polyaniline
PC	Propylene carbonate
PDM	Paste deposition modelling
PEDOT:PSS	Poly(3,4-ethylenedioxythiophene)polystyrene sulfonate
PET	Polyethylene terephthalate
PLA	Polylactic acid
PLC	Programmable logic and controller
Polyjet 3D	Photo-curing resin 3D printer
PPy	Polypyrrole
PTFE	Polytetrafluoroethylene
PUR	Polyurethane
PVA	Polyvinyl alcohol powder

PVDF-HFP	Polyvinylidene fluoride-co-hexafluoropropylene
R2R	Roll to roll
RepRap	Self-replicating manufacturing machine
rGO	Reduce graphene oxide
RP	Rapid prototyping
SemiFlex	Semi flexible filament combination of flexibility and firmness
Simplify3D	3D Slicer software for 3D printers
SLA	Stereolithography
Slic3r	Slicing software for FDM printer
SLM	Selective laser melting
SLS	Selective laser sintering
SolidWorks	Drawing cad software
SPE	Solid polymer electrolyte
SSA	Specific surface area
STL	Standard tessellation language
SWNTs	Single-walled carbon nanotubes
Symbol	**Definition (Units)**
$\triangle V$	Change in voltage (V)

$\Delta V/\Delta t$	Scan rate (V/s)
C	Capacitance (F)
C_a	Area specific capacitance (F/cm^2)
C_s	Specific capacitance (F/g)
i	Current (A)
iR drop	Voltage drop (V)
iR_{comp}	Cell resistance (Ω)
m	Mass of electrode (g)
Q_{total}	Stored charge (C)
V_f and V_i	Final voltage (V_f) and initial voltage (V_i) are the potential limits of the CV curve (V)

Chapter 1 Introduction

1.1 Background

There is an ever-increasing need for flexible electronic devices such as flexible displays, electronic solar cells and flexible energy storage devices, especially flexible supercapacitors (Zhang et al., 2015; Yoon et al., 2013; Zhou et al., 2015; Qiu et al., 2014; Jeong et al., 2015). Based on the energy storage charging mechanism and active materials used, these devices can be divided into three types: pseudo-capacitors, hybrid capacitors, and EDLCs. In these devices, the charge is stored by the surface charge separation of charged ions at the electrode-electrolyte interface, so they have a higher capacity than conventional capacitors (Sun et al., 2015). Supercapacitors benefit from the electro-ionic charge storage that can be generated in the electrochemical layer of a high-surface area of carbon particles (Dubal et al., 2015). EDLCs show a higher power density, are lightweight, and low cost with more cyclic stability than pseudocapacitors; however, they have a low energy density (He et al., 2013). EDLCs are usually used in energy sources for hybrid vehicles, power backup electronics, wearable electronics, flexible displays, and energy harvesting powered systems. The typical structure of supercapacitors consists of two conducting layers as current collectors, two conducting electrodes separated by a layer of dielectric material and the substrate frame. There are many fabrication techniques used to produce active layers for supercapacitors, for instance, a light scribe DVD burner, coating, screen printing, roll-to-roll, inkjet printing, and 3D printing selective laser melting. However, it is almost certain these methods require a long manufacturing time and pre-treatment techniques to increase the adhesions between the printed layers and the frame. The challenge therefore is to develop a simple, inexpensive fabrication method that does not require coating blades or masks.

In the recent years, rapid prototyping (RP) has been used as an alternative for additive manufacturing (AM) (Gibson & Stucker, 2014, p.11). AMintroduces a process in which digital 3D design data is used to build up a sample in layers by depositing material. AM identified as 3D printing technology has recently become more accurate in building up parts in a layer-wise manner, printing materials that are available in several forms, e.g. solid filament, powder, and resin. This additive fabrication process utilises very accurate deposition to incrementally melt and deposit thin layers of filaments to complete a 3D structure. It provides a facile and cost-effective approach to producing a

3D structure (Godoi et al., 2016). Many types of 3D printing techniques, for instance, fused deposition modelling (FDM), ink and Polyjet deposition techniques allow the users to print conductive materials to create intelligent applications. In contrast, they possibly need to undergo other processes to optimise the material properties for the particular purpose. Nevertheless, the development of technology to enable 3D printing of a flexible composite object for end-use applications in several fields due to material developments can be seen as an essential part of 3D printing innovation. Evidence from this thesis supports the fact that 3D printing technology is another suitable technique for flexible energy storage manufacturing industries. The direction of this work is to optimise the AM process, with the main goal of creating and using novel materials.

1.2 Motivation

Recently, there have been continuous interest and developing markets for flexible and rollable devices, organic electronics, and harvest and/or energy storage (Wang et al., 2014; Zuo et al., 2017). There would seem to be a great need for innovation to meet a corporate future for these types of products. In addition, many applications of electronics require portable sources of energy that are thin, flexible, and cost-effective. However, flexible EDLCs have applications for powering an active short duration peak power boost, short-term peak power back up, and as memory protection in several electronic devices. The main motivation behind this study is three fold and is explained as follows:

Different techniques of the flexible EDLCs require various processes to design and fabricate flexible EDLCs. The transfer of electrode patterns onto flexible substrates may influence the electrochemical performance. One solution to these challenges is the development of the manufacturing process of flexible EDLC. 3D printing technology has become the most widely adopted in electronics (Macdonald et al., 2014). However, a commercial 3D printing machine is limited by the types of extrusion head that can print the EDLC materials (Fu et al., 2017). This research work utilises 3D dual head extrusion, which allows the creation of multiple material forms. The main principle of 3D dual head printing is extruding a thin filament of molten thermoplastic by a heated tip nozzle onto a heated plate, while another nozzle sequentially deposits

paste materials, whose flow is controlled by a paste extruder tool (Gao et al., 2015). The challenge for the 3D dual head printing process is to manage this technique and control where the filaments are deposited. Because of the high cost of EDLCs materials components, minimizing the quantity of conductive and active material in the final printed sample is a significant goal. A possible explanation is that material compatibility is an important consideration for successful printing of EDLCs. The paste material should be printable, which means it needs the appropriate rheological properties.

Demand for a flexible EDLC is rapidly increasing with the emerging of wearable and portable devices and electric vehicles. It is believed that the current manufacturing processes of flexible EDLC are basic in their design, with limited materials, and limited process parameters available to expand the manufacturing process to allow more complex designed EDLCs to be created. Although potentially this could also be achieved by inkjet printing, the viscosity of the AC materials makes them unsuitable for this approach. The use of 3D printing allows more rapid prototyping of EDLCs than other printing methods such as roll-to-roll printing (R2R) or screen-printing. A commercial 3D printer based on fused deposition extrusion can use several materials for a homogenous substrate of EDLC. Nonetheless, the materials are limited in properties and restricted to the thermoplastic and its flexibility (Oropallo & Piegl, 2016). This is a significant challenge, and without addressing it, the technology may not be suitable for flexible electronics. A new approach to increasing the flexibility of printed substrate of the EDLC is to fabricate by single extrusion (paste), with rapid changes possible between the dispensing of the different materials, and no requirement to use fused extrusion, or to remove the substrate material from the printer between printing passes.

Finally, the electrochemical performance of the 3D printed supercapacitor under bending conditions is one of the most significant challenging issues (Fu et al., 2017; Wei et al., 2017). 3D deposition with user-created parameters and multi-range of EDLC flexible properties materials can be difficult. The flexible material becomes most challenging in complex AM technologies (Singh et al., 2017). Therefore, printing flexible EDLC by the 3D printer with optimised and selected materials would ensure optimum electrochemical performance under a bending test. The motivation is to

design and create a flexible energy storage device that can obtain high energy and power density, and the ability to store energy at high flexibility.

1.3 Main Aims

This research aims to develop a novel 3D printing method to manufacture flexible supercapacitors. The primary goal is to utilise a range of tools to explore 3D additive processes and suitable materials involved in producing flexible supercapacitors in order to optimise the mechanical and electrical performance of the supercapacitors developed.

1.4 Research Objectives

The purpose of this research is to develop a 3D printing process to manufacture a flexible supercapacitor. Detailed objectives are as following:

- To develop and modify the 3D printing processes using dual or single extrusion to manufacture flexible supercapacitors.
- To optimise conductive paste, AC materials and gel electrolyte for current collectors, electrodes and separator for 3D printing process, and for enhancing the electrochemical performance of flexible EDLCs.
- To demonstrate the effect of parameters in the manufacturing process on the performance of flexible EDLCs and to optimise the 3D printing process parameters.
- To manufacture complex shaped supercapacitors with various designed structures.
- To test an electrochemical performance for supercapacitors developed and manufactured in this study.
- To evaluate the performance of the flexible supercapacitors under the mechanical testing condition.

1.5 Structure of Thesis

Chapter 1

This chapter is an initial overview of the field of energy storage devices and additive manufacturing. Furthermore, it sets the aims and objectives, and it introduces specific content and arguments of the thesis detailing its structure and layout.

Chapter 2

This chapter covers a broad review of the current state of the art and previous investigations that involved the principle, materials, and manufacturing of the flexible supercapacitors. It also contains an extensive review of conventional 3D printing technology and 3D printer based on paste extrusion. These are discussed referring to authoritative published sources.

Chapter 3

The majority of this chapter is concerned with the experimental methods. Materials and manufacturing processes are evaluated to the needs of the research. It also discusses the measurement techniques of the energy storage devices.

Chapter 4

This chapter contains the result from the manufacture of flexible supercapacitors by dual printing extrusion, with the materials in the form of paste and flexible solid filament. The 3D process evaluation and electrochemical performance are included.

Chapter 5

Here further investigation of the 3D printed EDLCs is carried out. This concerns the effects of the thickness of AC and gel electrolyte layer on electrochemical performance. Moreover, a comprehensive optimisation of the 3D manufacturing process for the activated carbon paste is undertaken to provide an optimum deposition.

Chapter 6

The 3D paste deposition method is used to manufacture a highly flexible energy storage device in one single process. An electrochemical study is then performed to investigate the influence of the infill structure. The electrochemical performance of flexible EDLC was examined under a bending test. This chapter also presents the effect of some parameters on EDLC based on three electrodes design.

Chapter 7

The main contributions of the study to knowledge and suggestions for future work are presented.

Chapter 2 Literature Review

2.1 Introduction

There has been a recent upsurge of interest in flexible energy storage devices to meet the various requirements of modern applications, such as wearable electronics. Thus, there is a considerable need to use energy efficiently and to develop renewable and clean energy sources to facilitate sustainable development. An energy storage device is manufactured to save energy in some form that can be transferred to where it is required. Such storage devices include, for instance, batteries, capacitors, fuel cells, and supercapacitors. Every type of device has advantages and disadvantages, for example, performance, reliability, cost, and lifespan (Bae et al., 2011; Zhang et al., 2009; Tyagi et al., 2015). Based on electrostatic action, supercapacitors are essential on circuit boards and other electronic products as opposed to batteries. They can replace or act as complementary batteries in electrical energy storage when high power delivery or absorption is needed. Furthermore, supercapacitors can deliver higher power than batteries and store more energy than conventional capacitors (Bae et al., 2011). In addition, conventional capacitors are heavy and bulky, and it remains a significant challenge to achieve high-efficiency energy storage devices that are flexible. In early 1975, one of the technology leaders, Nippon Electric Company (NEC) of Japan, having made significant progress in research, rapidly developed a manufacturing capability, and began selling the product to the market as a supercapacitor. Nonetheless, electrochemical capacitor technology still requires significant development concerning technical requirements and practical applicability. This research work is focused mostly on the manufacture of flexible supercapacitors and on how to increase the energy density of supercapacitors based on the development of materials. This chapter will compare different energy storage devices and manufacturing techniques, and it will discuss the definitions, structures, fundamental working principles, and manufacturing of flexible energy storage devices.

2.2 The Beginning of Supercapacitors

Electric double-layer capacitors (EDLCs) are usually called supercapacitors, which is abbreviated to supercaps. Hermann von Helmholtz first mentioned the concept of double-layer capacitance in the middle of the eighteenth century (González et al., 2016), but the first attempt to store electrical energy as a low voltage electrolytic device was made by Howard I. Becker, who was a general electric engineer (Becker, 1957). As shown in Figure 2.1, the cell device was made with two porous carbon electrodes, which were immersed and separated in sulfuric acid and water as the electrolyte. Carbon materials have long been incorporated into the electrodes of energy storage devices in various forms. To obtain a carbon form without it eventually breaking and cracking, Standard Oil of Ohio Company (SOHIO) and Donald L. Boos successfully developed a flexible electrolytic carbon paste by mixing finely ground carbon particles with an electrolyte to produce EDLCs by compressing the paste to 20,000 psi to form the electrodes (Boos, 1970).

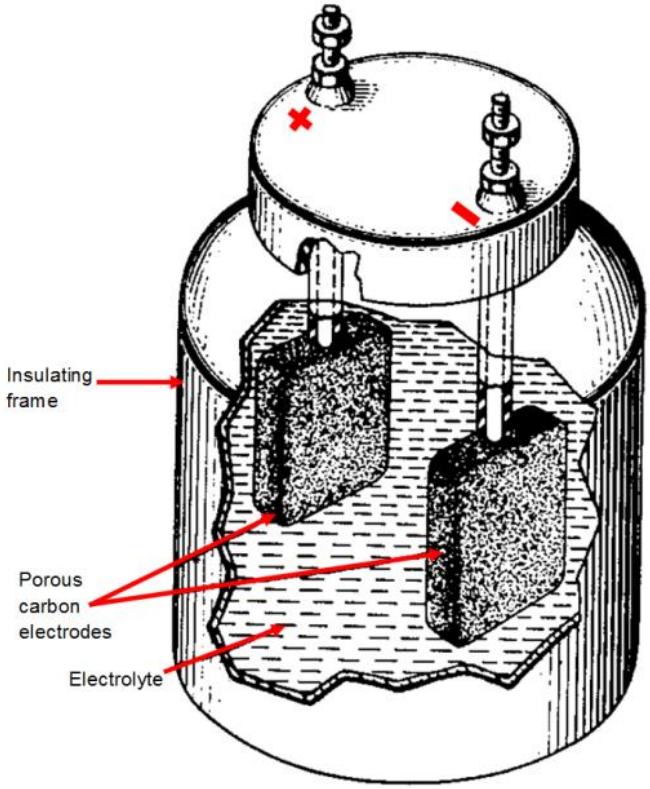

Figure 2.1: Schematic illustration of the principles of capacitor (Becker, 1957)

The need for flexible supercapacitors is growing rapidly nowadays, as they play a crucial role in many fields (Chuizhou, 2013). One of the important components in supercapacitors is the electrode, and this has been investigated based on the use of innovative materials. The most recent attempts made have been to optimise the charge storage mechanisms in flexible EDLCs, particularly in terms of electrode materials, such as graphene (Sheng et al., 2012; Liu et al., 2012; El-kady & Kaner, 2013; Sun et al., 2015), single-walled carbon nanotubes (SWNT), multi-walled carbon nanotubes (MWNT) (Ujjain et al., 2016), carbon nanomaterials (Xu et al., 2015; Chen & Dai, 2014), reduced graphene oxide (rGO)- polypyrrole (PPy) (Zhao et al., 2015), a graphene-activated carbon composite (Chen et al., 2012), and rGO (10%)-SWNTs (90%)-Polyurethane (PUR) (Jeong et al., 2015). It is acknowledged in the current literature that the most recent electrode material utilised in producing flexible supercapacitors, and especially in micro-supercapacitors, is graphene (MSCs).

The exploration of innovative materials with high performance for flexible supercapacitors to meet the requirements for various applications presents significant challenges. As shown in Figure 2.2, Winter and Ralph (2004) have demonstrated and compared supercapacitors to an internal combustion engine, fuel cells, and conventional capacitors, showing that supercapacitors can provide higher specific power (power density) than fuel cells and batteries, but lower specific power than traditional capacitors and a combustion engine. Nevertheless, flexible EDLCs are attracting significant attention based on their promising advantages, for example, having a relatively small size, and being lightweight and flexible. The EDLCs in low or high voltage apparatus have been used in many different applications. In fact, an ELDC has a lower energy density than a battery, but has a higher power density except for batteries made with thin film electrodes, which show a similar power density to supercapacitors (Hwang et al., 2017).

Recently, many companies have introduced several types of technology to produce non-flexible EDLCs that have very high performance. Maxwell® Co., Ltd. presented a new technology named DuraBlue to enhance shock and vibration performance. This technique is a combination of a dry electrode with an innovative cell structure (Hsieh, 2017). Next, Murata Co., Ltd. introduced the temperature compensation type chip monolithic ceramic capacitor measuring less than a millimetre in size. However, the

challenge currently is that most EDLCs need to be much more affordable than a conventional capacitor or lithium battery that stores the same amount or higher energy before they can be used to replace the batteries in some electronic equipment, such as smartphones or electrical city buses.

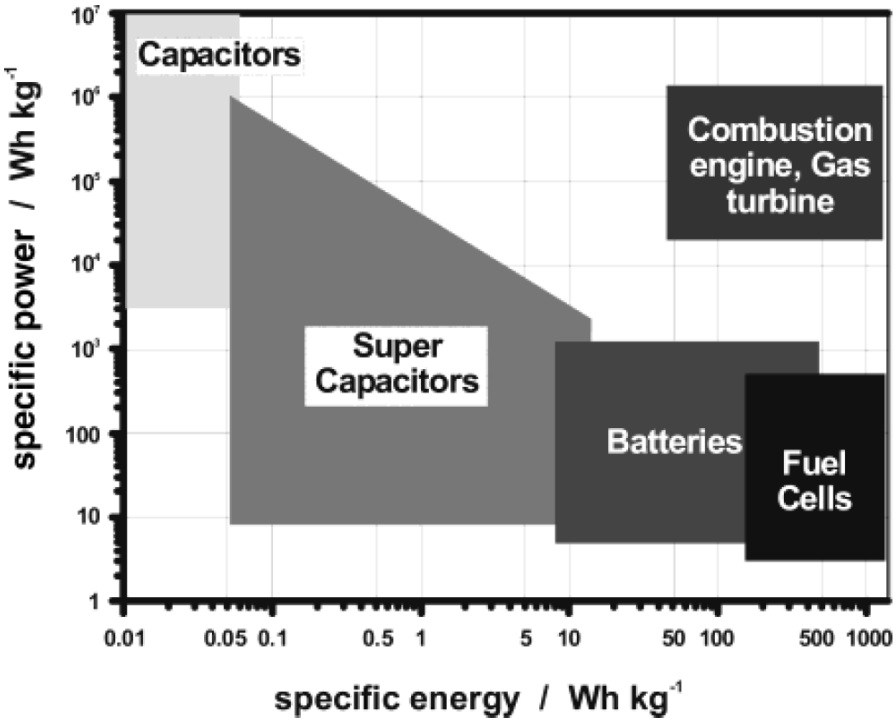

Figure 2.2: Ragone plot for various energy storage domains, conversion devices and combustion engines (Winter and Ralph, 2004)

2.3 Electrical Double-Layer Capacitors (EDLCs)

Based on the charge-storage mechanism, supercapacitors store energy with mainly three types of capacitive mechanisms: the EDLC, redox pseudocapacitance, and hybrid capacitors. An EDLC takes advantage of the electro-ionic charge storage induced in the electrochemical double layer of high-surface-area carbons, i.e., it stores energy through a physical process of ion adsorption. EDLCs present a higher power density and excellent cyclic stability than pseudocapacitors (He et al., 2013). On the other hand, they have a comparably low energy density. EDLCs can be divided into different types based on electrode materials, such as carbon aerogels, activated carbon, carbon nanotubes, conducting polymers, and graphene-based supercapacitors. All of these EDLCs have the same mechanism for storing energy. Applying the voltage to two electrodes means the ions are drawn to the surface of the EDL, and charged ions in the electrolyte migrate towards the electrodes of opposite polarity due to the electric field between the two charged electrodes. This means that when a current is applied to the EDLC, a voltage is generated and maintained between the surface and the ions of an electrolyte. An EDL is a structure that originates when a charged electrode is employed between gels; then, the balancing charge for this charged electrode surface will form in the gel near the surface, and the distance (d) from the surface to the ions is called the Helmholtz theory. Usually, there are two more additional theories for this space, namely, the Gouy–Chapman (diffuse layer) and the Stern theories (Stern-diffuse layer). To avoid confusion regarding the behaviour of the ions, González et al. (2016) claimed that the Gouy–Chapman theory is closer to reality than the Helmholtz theory. Due to the wide range of carbon structures, especially nanostructures, it is important to clarify the EDLC construction, as three types of structural components are required to complete a working EDLC.

2.4 EDLC construction

The construction of the EDLC is shown schematically in Figure 2.3. An EDLC consists of two current collectors and two electrodes; these are separated or immersed in a dielectric material, which is called the electrolyte, to prevent them short circuiting.

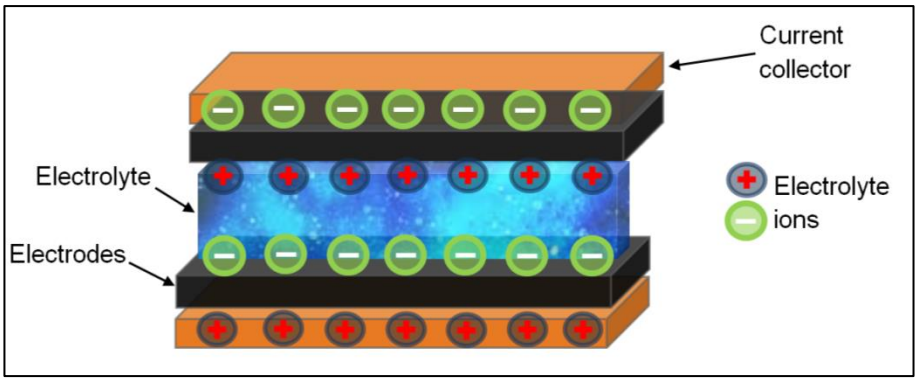

Figure 2.3: Schematic diagram of an EDLC

Each of the EDLC component materials can affect the performance of the supercapacitor. Their selection will be based on the application in which the EDLC is needed. For example, a flexible EDLC means all of these components must be flexible and be able work properly under different mechanical actions, such as bending or twisting. However, it is difficult to match flexible EDLCs in an application that requires a high voltage due to the limited selection of the ionisation of an electrolyte; in addition, it is hard to obtain flexible current collectors in different forms, such as a paste form.

2.4.1 Flexible current collector

The high performance of flexible EDLCs is related to the high conductivity, electrochemical stability, and excellent flexibility of the current collectors. The properties of the current collectors in EDLCs depend on the selection of the substrate (frame), the shape of the EDLCs, and the conductivity of the electrode materials. The most widely used flexible current collectors are of stainless steel, which has superior properties compared to other fabrics. Stainless steel is considered to be a good candidate for current collectors; for example, Zhang et al. (2017) reported the manufacture of a strip EDLC that used stainless steel as a current collector which was sealed by a laminator to act simultaneously as a frame. However, stainless steel is expensive, has a rough surface, and exhibits chemical instability in the EDLC, usually when in contact with the GPE. The high conductivity of active electrodes leads to avoiding using them as current collectors. The electrodes can act as both functional active materials and current collectors. Zhang et al. (2015) used aligned CNT coated onto an elastic polymer fibre to work as both a current collector and an active material. However, the aim is to avoid using highly expensive materials, for instance, CNT, which is also highly toxic to humans, or stainless steel, which has a rough surface. The critical challenges in manufacturing flexible EDLCs are the selection of environmentally friendly bendable current collectors with excellent mechanical properties, high adhesion, and superior conductivity. The conductor inks or pastes currently available are highly expensive, require a heat cure, and have limited flexibility and a weak bonding to the frame substrate, such as thermoplastic polymers. For example, silver (Ag) conductive adhesive paint would cost £73.81 for a 20 g bottle from RS Components Ltd. Zhao et al. (2017) reported on the use of silver ink was reported on the surface of PET as a current collector by using the screen printing method, although PET is susceptible to oxidation. A flexible, highly adhesive, and high conductive current collector in paste form is usually based on the selection of the binder (for further details of preparation, see 0).

2.4.2 Flexible electrodes

Researchers have paid more attention to active electrode materials to improve the capacitance performance and cycling stability. These materials are conducting polymers, such as PPy and Polyaniline (PANI). Because of their high electric conductivity (104 S/cm) and a high specific capacitance, these materials have been used to make electrodes in flexible supercapacitors in composite structures. Given the poor cycling stability of PPy and the slow kinetics of ion transport, Zhao et al. (2015) developed a stretchable/flexible composite electrode based on PPy/reduced graphene oxide (rGO). PANI is also a good candidate for flexible supercapacitors when it is composed of mesoporous carbon. PANI and PPy have the advantage of providing environmental stability and excellent electrical conductivity. However, they are very expensive, brittle polymers, and they show a non-uniform and non-smooth surface when coated onto fabric substrates. The use of PPy on the surface of cotton fabric as an electrode is complicated by the requirement for complex polymerisation, and insufficient proton activity in the electrolyte has been reported (Cetiner, 2014; Xu et al., 2015). PANI and PPy are pseudocapacitive materials, as they use a redox reaction to store charge in the material, and they show high specific capacitance compared to carbon-based EDLCs.

Current manufacture techniques of supercapacitors use materials that have been specially made for the operation of the proposed method. Five forms of carbon have been used in flexible supercapacitors: carbon aerogels, carbon fibres, carbon blacks (Cakici et al., 2017; Ju et al., 2014; Wang et al., 2014), glassy carbon, and carbon nanostructures (Ujjain et al., 2016; Bärtsch et al., 1998). Numerous studies have been conducted to improve specific capacitance behaviours and the energy density of flexible supercapacitors. Therefore, it is necessary to identify the synthesised structure of these materials; the majority of these materials are AC on which is usually blended a conductive carbon black. An extensive guide to the description of carbon material properties and their role in supercapacitors is available (Pandolfo & Hollenkamp, 2006). One of the highest attractions of using AC, especially porous AC, for electrodes is that it has high SSA, high electronic conductivity, and low cost, and it is easy to prepare into electrodes that can be controlled and converted into a liquid or paste form.

Generally speaking, it is difficult for AC electrodes to reach high capacitance in EDLCs in comparison with other materials, such as graphene. Much time and effort has been devoted to improving the AC electrodes, but the low conductivity and the limited surface area of AC cause low energy density. Therefore, the focus has been switched to other materials, such as conductive polymers and graphene. Recently, there have been cases of EDLCs based on these materials working as both current collectors and electrodes. Table 2.1 shows the comparative data of electrochemical EDLC materials based on different processes. It can be seen that a nanocomposite of layered vanadium phosphates ($VOPO_4$) and graphene nano-sheets reaches a high specific capacitance of 527.9 F/g at current density 0.5 A/g (Lee et al., 2015). This is mainly due to the increase in the SSA of graphene nano-sheets by an ice-templated self-assembly method, which shortens the ion diffusion length for the electrolyte. Also, it can be seen from the table that the improved capacitance reached 235 F/g by utilising ink-jet printed functionalized MWCNT onto a polyethylene terephthalate (PET). A printed MWCNT worked both as a current collector and as an active electrode, resulting in reduced contact resistance (Ujjain et al., 2016).

Table 2.1: Comparative data of electrochemical capacitors materials

Fabrication process	Electrode/ Substrate	Electrolyte	Current Collectors	C_s	Energy density	Ref.:
3D printed SLM	PPy coated titanium/ Fine powder	PVA/H_3PO_4	Ag/AgCl	2.4 F/cm^3	213.5 W/m^3	Zhao et al., (2014)
3D printing direct-ink writing	graphene composite aerogel	--	--	63.6 F/g	0.14 mWh/cm^3	Zhu et al., (2016)
Coated	rGO/PPy/ Nylon	1.0 M Li_2SO_4	rGO sheet	114 F/g	2.53 Wh/kg	Zhao et al., (2015)
Coated	Electrochemically rGO	KOH	graphene sheet	283 micF/cm^2	--	Sheng et al., (2012)
Coated	GO/cotton composite	6 M KOH	nickel wire	326.8 F/g	7.13 Wh/kg	Liu et al., (2012)
Coated	AC slurry	1 M $C_{16}H_{36}BF_4N$	stainless steel	0.2725 F	8 Wh/kg	Zhang et al. (2015)
Dipping & drying, annealing process	rGO/carbonized cotton fabric/ PET	filter paper	Copper foil	5.53 F/cm^3	767.36 micWh/cm^3	Zhou et al., (2015)
Electrochemically polymerized	PPy films/ Silicone	0.3 M $LiCiO_4/H_2O$/ PVA	nickel	0.06 F/cm^2	2.2 mW/cm^2	Sun et al., (2009)
Hydraulic press at 1 ton	Nanocomposite	3 M KCl	titanium foil	0.81 F/cm^2	--	Zhang et al.,

	MnOx/CNT					(2010)
Ice-templating	VOPO4/graphene	6 M KOH	nickel foam	527.9 F/g	108 Wh/kg	Lee et al., (2015)
In situ polymerization	PPy nanorods/cotton/ fiber	2 M NaCl	PPy/cotton	325 F/g	24.7 Wh/kg	Xu et al., (2015)
Inkjet-printed	AC/CNTs/ Paper	Triacrylate polymer	Ag nanowire	---	---	Choi et al., (2016)
Inkjet-printed	Functionalized MWCNT/ PET	(EMIM)(BF_4) gel polymer	F-MWCNT	235 F/g	16.2 Wh/kg	Ujjain et al., (2016)
Lightscribe DVD	GO/ PET	ionogel	GO	2.35 F/cm^3	200 W/cm3	El-kady & Kaner (2013)
Micro extrusion	rGO/ PET	1 M PVA-H_2SO_4	free	56.5 F/cm^3	7.6 mWh/cm^2	Sun et al., (2015)
Pressing	Graphene-AC	1 M $EMIBF_4$, KOH	nickel meshes	122 F/g	6.1 Wh/kg	Chen et al., (2012)
Pressing	Glassy carbon	3 M H_2SO_4	GC	2.6 F	0.18 Wh/l	Bärtsch et al., (1998)
Pressing at 10 mPa	ACNWs/GENF	6 M KOH	nickel	176.5 F/g	4.8 Wh/kg	He et al., (2013)
Roll-to-Roll	AC/ PET film	3 M KCl	Ag ink	99.4	---	Yeo et

				F/g		al., (2014)
Screen printing	mesoporous / PET carbon/PANI	1 M H_2SO_4	Ag ink	50 F/m^2	---	Zhao et al., (2016)
Semi-automatically coating	carbon-based Chinese ink	PVA/H_3PO_4	Microwire	20.7 mF	0.22 mWh/cm^3	Qiu et al., (2014)
Spray coating	AC ink/ polyester-cotton	ammonium salt/PVA	stainless steel	10.6 F/g	---	Yong et al., (2015)
Spray coating	rGO/SWNTs/ polyurethane	1 M H_2SO_4	gold	265 F/g	---	Jeong et al., (2015)
Vacuum filtration deposition	Graphene/Nickel foam	6 M KOH	nickel foam	152 F/g	38 kW/kg	Zhang et al., (2012)
Wrapping & coating	PANI/CNT/ elastic polymer	PVA/H_3PO_4	CNT sheet	105.8 F/g	---	Zhang et al., (2015)
Electrophoretic deposition technique	MXene	PVA-KOH	nickel foam	140 F/g	---	Xu et al., (2017)

2.4.3 Flexible electrolyte

The electrolyte is a crucial component that plays a critical role in flexible EDLC performance. The studies on the electrical properties of aqueous, organic, and polymer electrolytes have attracted much attention over the years because of their application in flexible EDLCs. Polymer gel electrolytes were used as alternative electrolytes rather than organic electrolytes in flexible EDLCs. GPEs have been shown to combine the electrolyte and the separator into one part. It is frequently used in flexible EDLCs due to its quick preparation and low cost. It is made by incorporating ionic acid into a polymer matrix. PVA is one of the polymers most frequently used for gel electrolytes in flexible EDLCs because of its excellent mechanical properties, such as stretching to reach up to 400% (Zhang et al., 2015). GPE-based PVA is electrochemically and thermally stable, and has high conductivity and good bonding when fully encapsulated in the EDLCs, resulting in minimal leakage (Xia et al., 2017). The PVA gel electrolyte is able to penetrate into some carbon electrode materials, such as carbon nano sheets.

This means that ions in the electrolyte cannot diffuse quickly at the electrode/electrolyte during the charging and discharge process. The use of the polymer as the binder in gel electrolytes results in an increased distance between two placed electrodes. Therefore, increasing the concentration of the electrolyte and decreasing the polymer content improves the diffusion rate and accessibility of the counterions. In the literature, it is claimed that the addition of electrolyte concentration increases the capacitance of EDLCs and reduces the discharge capacity (Guan et al., 2015; Meissner, 1997). A low concentration means lower conductivity, which leads to higher resistance of GPEs (Rs) and a subsequent greater voltage drop. Moreover, the difference in the equivalent series resistance (ESR), also known as the internal resistance of the supercapacitor, is explained with regard to the conductivity of electrolytes. It can be calculated from the high-frequency intercept of the semi-circle on the real axis and can be obtained from the electrochemical impedance spectroscopy (EIS). Not only the concentration of the electrolyte, but also the thickness of the electrolyte layer can affect the Rs (Sun et al., 2009). In addition, some of the carbon electrode materials may have a low mesoporosity structure, which reduces electrolyte accessibility and increases the internal resistance of the supercapacitor.

The way the electrolyte in EDLCs is manufactured or applied can also affect the performance of the EDLCs. He et al. (2013) reported that a supercapacitor based on a 3D network of AC nanowhiskers with an aqueous solution of electrolyte 6 M potassium hydroxide (KOH) by using the electrospinning method gives a good performance and has higher power characteristics. This is because the electrolyte could permeate electrodes and become wet, and diffuse quickly. This method was used only with diameters ranging from a micrometre to the nanoscale. It is not only a very expensive and time-consuming method, but also it depends on a high number of complex parameters, such as the solution parameters, ambient conditions, and process parameters. The GPEs have a small potential range from 0.7 to 1.1 V in acidic aqueous electrolytes; therefore, the choice of GPE depends on the application of the flexible EDLCs. The GPEs seem to play a role in separating electrodes, and many parameters and other related mechanisms must be taken into consideration to describe and understand the physical properties of GPEs to obtain an excellent capacitance performance.

The properties of the electrode materials play an important role in the selection of the electrolyte, as they need to be compatible. Chen et al. (2012) reported that carbon-based EDLCs have the unique advantage of higher energy density and power density, and a longer lifespan when operated with inorganic electrolytes. As shown in Figure 2.4, Bae et al. (2011) compared the specific capacitance made by zinc oxide nanowires as electrodes in three different preparations of electrolytes: zinc oxide (ZnO) nano-wires in potassium nitrate (KNO_3), ZnO in a GPE of phosphoric acid (PVA/H_3PO_4), and manganese dioxide in sodium sulfate (Na_2SO_4). This shows that the specific capacitance of fibre EDLCs in the KNO_3 electrolyte is lower than that in the PVA/H_3PO_4 gel electrolyte. The GPE of PVA/H_3PO_4 showed a high specific capacitance of 2.4 mF/cm.

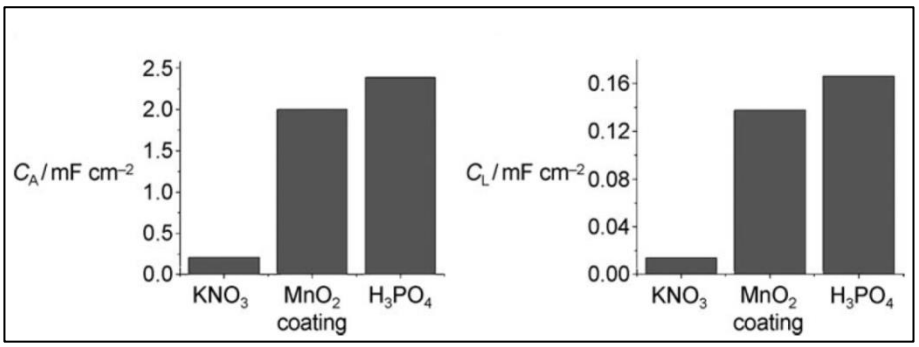

Figure 2.4: Specific capacitance values of fibre EDLCs with different electrolytes (Bae et al., 2011)

2.4.4 Flexible substrates (packaging materials)

The recent revolution in flexible EDLCs offers the potential to generate a high power density with different mechanical properties, and there has been a notable improvement in electrode, electrolyte, and packaging materials. However, there are some issues associated with packaging materials as regards their flexibility. For example, an aluminium casing of the supercapacitor is non-flexible, and only a limited number of electrolytes can be released (Xia et al., 2017).Furthermore, the flexible EDLCs are limited by their mechanical properties, such as bendability and stretchability. Therefore, flexible packaging materials offer a promising solution for energy storage devices. As shown in Figure 2.5, many packaging materials have been used for EDLCs, such as Kevlar fibre and nylon Lycra fabric (Zhao et al., 2015), elastic polymer fibre (Zhang et al., 2015), SiO_2/Si substrate (Sun et al., 2009), polyester-cotton fabric (Yong et al., 2015), as well as paper, flexible plastic, and polydimethylsiloxane film (PDMS) (Zang et al., 2014; Chuizhou, 2013; Kaempgen et al., 2009; Gilshteyn et al., 2016), with PET as the most preferable substrate (Zhao et al., 2017; Niu et al., 2013). As shown in Figure 2.5(d), Xu et al. (2013) used the unconventional substrate of a silicon wafer to maintain the capacity densities of 1.1 mAh/cm^2 under stretchability of up to 300%. However, a thin slice of silicone wafer is a weak absorption material; it has a much higher melting point and acts as a universal solvent when molten.

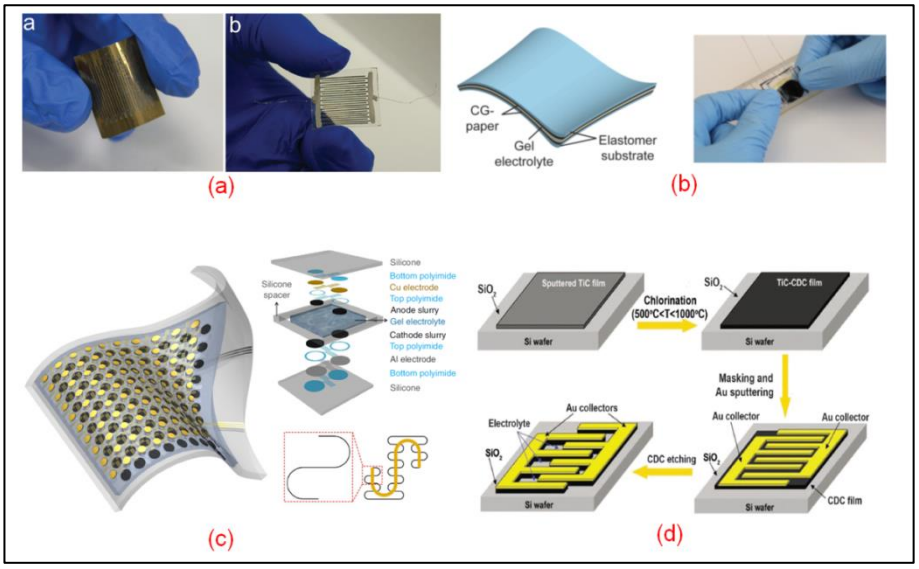

Figure 2.5: Images of various substrates: a) EDLCs on PET substrate (Niu et al., 2013),(b) EDLCs on paper (Zang et al., 2014),(c) aspects in battery layout and design onto silicone substrates (Wang et al., 2016) and (d) EDLC on Si wafer (Xu et al., 2013)

The rapid development of wearable and flexible electronics for integration into EDLCs is crucial for them to be fabricated and applied on flexible substrates, such as paper. The flexible EDLC applied to a paper substrate is brittle and needs treatment, such as being laminated, to be encapsulated and so sealed entirely. However, the laminator could affect the capacitance through the heating process. Therefore, flexible EDLCs with the capability of retaining their functionalities under different mechanical tests are urgently required. Cai et al. (2017) manufactured flexible MSCs by using a combination of laser direct writing and electrophoretic deposition techniques of interdigitated carbon/TiO_2 electrodes on flexible polyimide (PI) films at a thickness of 125 µm (Kapton 500H). The Kapton is a polyimide film developed by DuPont® in 1960. However, it has a relatively high moisture absorption and needs cleaning with water and ethanol before use. The next section introduces the current manufacturing methods that have been developed for the fabrication of flexible EDLCs and their components.

2.4.5 Types and design of flexible EDLCs

Based on the mechanism for storing charge, supercapacitors can be divided into three main types of capacitive mechanisms: double layer capacitors, pseudocapacitors, and hybrid capacitors. The charge storage of EDLCs involves an electrostatic and non-faradaic process in comparison with pseudocapacitors, which electrochemically charge storage (faradaic) including redox reaction. As shown in Figure 2.6, hybrid capacitors (supercapattery) apply a mechanism that uses a combination of two electrodes, with one electrode based on the electrochemical double layer and the other for the pseudocapacitor. A hybrid capacitor usually stores energy by using pseudocapacitance materials, such as redox metal oxide or redox polymer in the anode, while the cathode uses EDLC materials, such as carbon (Zhi et al., 2013). The types of EDLCs are usually classified based on the electrode materials; most are AC, carbon nanotubes, graphene, carbon aerogels, and composite (graphene and carbon nanotubes)-based EDLCs.

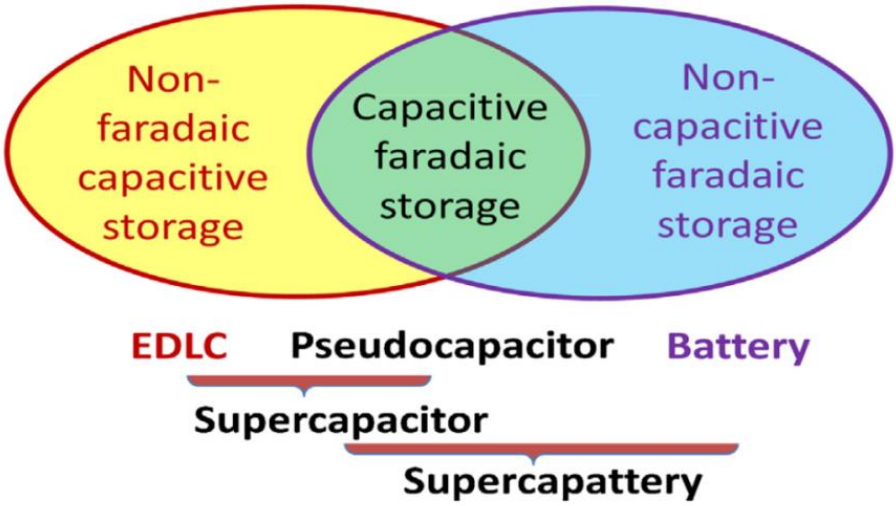

Figure 2.6: Comparison of capacitive and faradaic charge storage processes for EDLC, pseudocapacitors, hybrid (supercapattery), and battery (Guan et al., 2016)

There is an increasingly broad use of flexible EDLCs, as they are replacing batteries in some systems. Thus, much effort has been made by researcher and interested practitioners to enhance the performance and manufacturing process of supercapacitors; therefore, many complex designs and different manufacturing techniques have been examined, as shown in Figure 2.7.

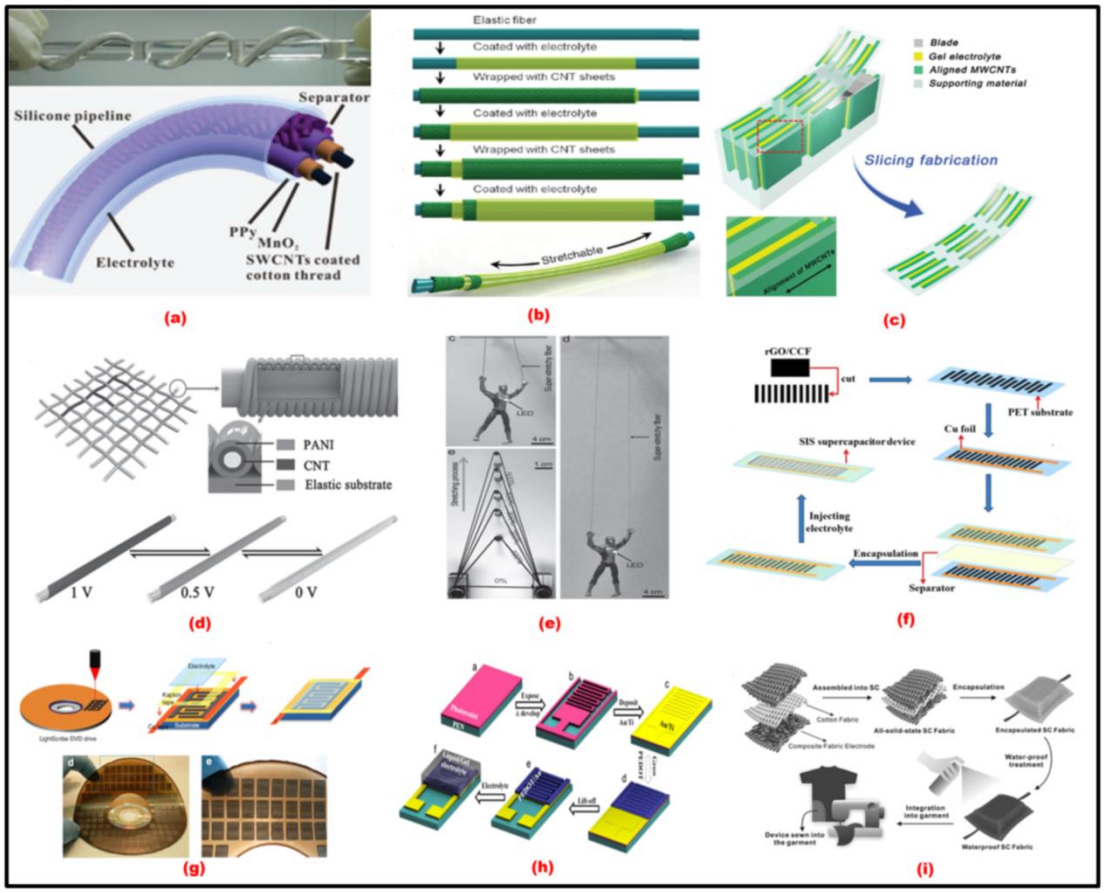

Figure 2.7: (a) Schematic diagram of cable type flexible supercapacitors (Liu et al., 2013), (b) fiber shaped supercapacitor (Yang et al., 2013), (c) thin supercapacitors (Sun et al., 2016), (d) wearable fiber shaped supercapacitor (Chen et al., 2014), (e) elastic fiber shaped supercapacitor (Zhang et al., 2015), (f) sandwich interdigital structure (Zhou et al., 2015), (g) flexible MSCs (El-kady & Kaner, 2013), (h) conducting polymer MSCs (Kurra et al., 2015), and (i) wearable supercapacitor fabrics (Yang et al., 2017)

The shape of energy storage devices depends on the principle components and the form of the supercapacitors, and on the technique of their manufacture. The shape of flexible supercapacitors has evolved over time. Figure 2.7 (a-i) shows the different shapes of flexible supercapacitors, such as fibre shaped supercapacitors (Zhang et al., 2015; Yang et al., 2013; Chen et al., 2014), cable type (Liu et al., 2013), sheet-like (Zhou et al., 2015), thin film shaped (Sun et al., 2016; Nyström et al., 2015), and MSCs (El-kady & Kaner, 2013). A rapid prototyping technique has the potential to fabricate energy storage devices of virtually any desired shape. As shown in Figure 2.8, Zhao et al. (2014) manufactured interdigitated supercapacitors based on 3D selective laser melting (SLM) printing technology to produce 3D titanium interdigitated electrodes.

They used a very expensive 3D printing machine to print metal powder as electrodes to fabricate non-flexible supercapacitors. In addition, they used a PPy coating technique to obtain a specific capacitance of 10.1 F/cm^3.

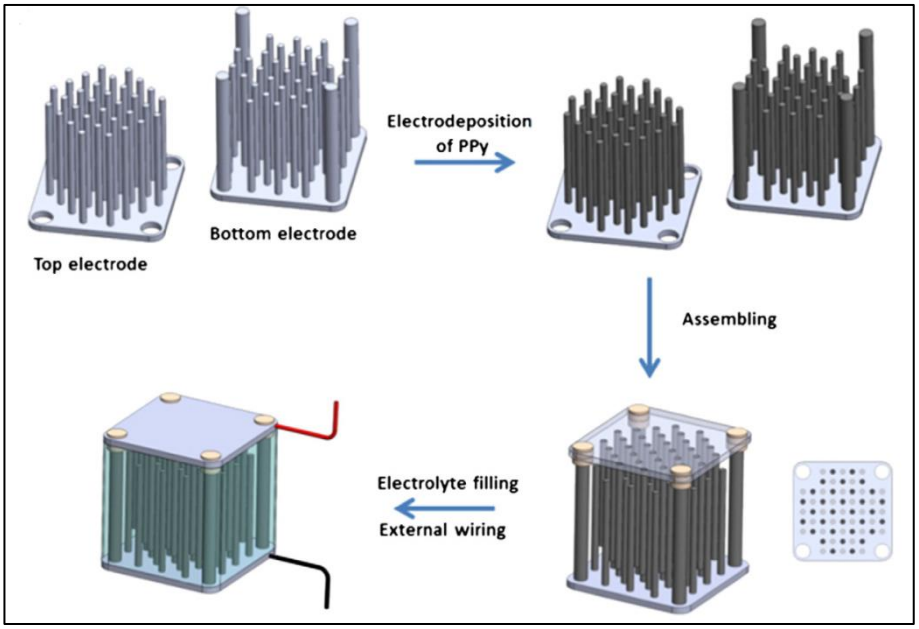

Figure 2.8: Schematic steps used to manufacture solid state supercapacitors (Zhao et al., 2014)

When engineers design flexible supercapacitors, and decide on their shapes and components, they have to be familiar with the process that will be used to fabricate the flexible EDLCs. For instance, when designing a flexible EDLC, several parameters must be kept in mind, such as the flexible properties of the EDLC's components. The next section introduces the latest flexible components that have been used in flexible EDLCs.

2.5 Manufacturing Methods of Supercapacitors

Increasingly, many of the flexible electronics developers and industries are using organic electrolyte-based EDLCs. Currently, a few of the industries offer energy storage devices based on non-toxic and non-flammable electrolytes, despite the fact that active electrode materials are mainly made of toxic materials, such as graphene. The novel manufacturing processes, materials, and design could open a new arena for manufacturing environmentally friendly flexible EDLCs with good capacitance performance. However, the manufacturing techniques for flexible EDLCs can be complicated. In this section, eleven manufacturing processes are discussed. These are critical processes and are key to reducing cost and time, and increasing ease when fabricating high-performance flexible EDLCs.

2.5.1 Coating

The method of manufacturing active electrodes and electrolytes is the same as the method for manufacturing EDLCs. The components of the EDLCs, such as current collectors and frames, usually require another method for them to be integrated into electrodes. Due to the low cost and speed of the mass production method, the coating technique is one of the most popular manufacturing processes for EDLCs (Zhao et al., 2015). It needs some tools based on the forms of the electrode material. Many techniques and tools have been used, such as spraying, brushing, doctor blade, spin-coated, dip, wire wound rod coating, knife, slot-die, mask, and semi-automatic motor using a dip coating. Pre-existing substrates with active electrode materials are usually coated with non-uniform thicknesses, and have holes and a non-uniform morphology due to the conditions of synthesis of active electrode materials. Besides, some of the active electrode materials are not symmetrical in their coating techniques and need both pre-treatment and time to dry. Zhao et al. (2015) reported that rGO showed a wrinkled surface morphology when coated on the surface of the fibres. The weight and thicknesses of the activated materials need to be controlled; interfaces with dimensions between EDLC components seem to present an advantageous characteristic. Therefore, the combination of the coating method with another method has become imperative to the manufacture of high fidelity energy storage devices.

The fabrication of flexible EDLCs can be complicated, and the influence of each parameter should be investigated to ensure good capacitance behaviour. Qiu et al. (2014) developed a semi-automatic system, using a dip coating method involving a multi-speed controlled motor and discs to produce uniform coatings for the manufacture of coaxial thread supercapacitors (Figure 2.9). However, a semi-automatic method using a multi-speed motor is controlled manually, and it may lead to non-effective thicknesses of coated electrode wires. In addition, this manufacturing process may be limited to a wire or wire-shaped substrate.

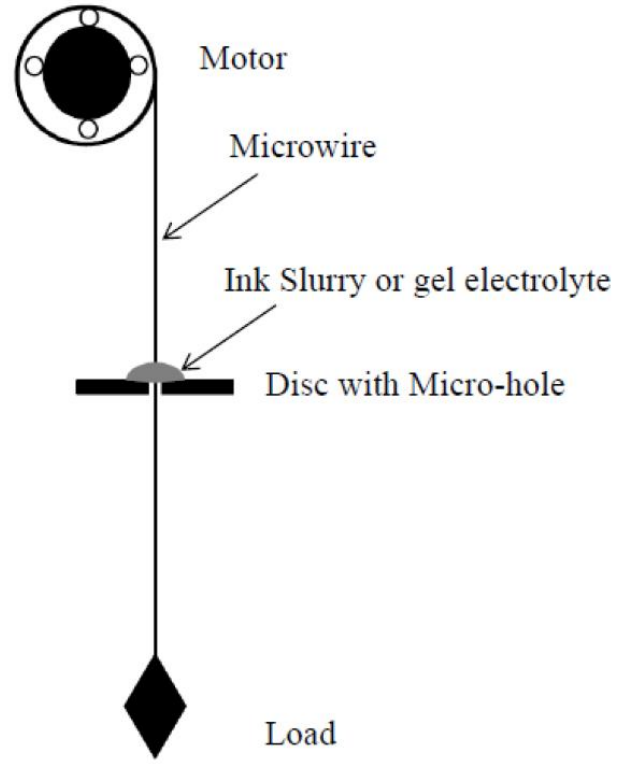

Figure 2.9: Schematic of semi-automatic using a dip coating method (Qiu et al., 2014)

In fact, there are many parameters affecting the performance of capacitance, for instance, type of electrolyte, conductivity of the materials, and SSA; indeed, the manufacturing process and the method of transferring EDLC components could influence the EDLCs' performance. However, despite steady advances in the manufacturing process, fabricating flexible EDLCs remains a challenging task. Each manufacturing process has advantages and disadvantages especially the manufacture of flexible EDLCs based on AC and GPE. Various techniques are considered for the uniform deposition or coating onto substrates.

2.5.2 Spraying and masking

The spray deposition technique is also a frequently used coating process, as it can be used on almost any type of substrate to fabricate active electrodes. The spray coating method has commonly been used to deposit conductive nanomaterials with an ink form. Many inks have been used for flexible supercapacitors, such as AC ink (Yong et al., 2015), MWCNT/rGO (Yang et al., 2017), MWNTs and SWCNT (Chuizhou, 2013; Kaempgen et al., 2009), and manganese oxide Mn_3O_4 and GO ink (Yadav et al., 2016; Fu et al., 2017). Such inks are easy to process and are frequently used to manufacture flexible EDLCs. They can be deposited randomly or used with a mask to obtain patterned layers, which is a critical requirement to achieve uniform layers.

Indeed, as shown in Table 2.1, the good performance of flexible EDLCs by using the spray coating technique of AC/ammonium salt GPE to reach a specific capacitance of 10.6 F/g has been reported (Yong et al., 2015). The patterned layers can be obtained via several other steps to achieve optimum deposition layers. However, the spray deposition technique is relatively complicated and significant attention is needed to avoid contaminants. The air compressor or Paasche airbrushes have been used to control the limited thickness of the deposited layers. However, in some cases, the spray process needs an optimum nozzle size to obtain a homogenous deposition. Also, some specific substrates need to be preheated to accelerate the evaporation of the droplets on the substrate.

2.5.3 Dipping and drying techniques

As mentioned in previous sections, the manufacturing techniques for EDLCs depend on electrode manufacture as an important function material in EDLCs. Many researchers aim to fabricate active electrodes for supercapacitors. As shown in Figure 2.7(f), Zhou et al. (2015) made lightweight graphene-cotton electrodes using the dipping and drying method. The electrode was prepared by a combination of an annealing process and a dipping process, with the electrode being dipped over five times to reduce the resistance and to increase the conductivity and thickness of the GO. The rGO/cotton electrode was made, cut into strips, and then integrated into a PET substrate to fabricate flexible supercapacitors.

Figure 2.10 shows how CNT and MnO_2 electrode materials were fabricated using the dipping and drying method to obtain a specific capacitance of 4.15 F/cm^2 in the electrolyte solution of H_2SO_4, as reported by Zhang et al. (2017). However, the drawback of the dipping method is the non-uniform coating thickness of the applied active materials, which leads to poor electrochemical performance. This method is commonly limited to high absorption fabrics, such as cotton, and has been used to improve flexibility, wear, and capacitance performance.

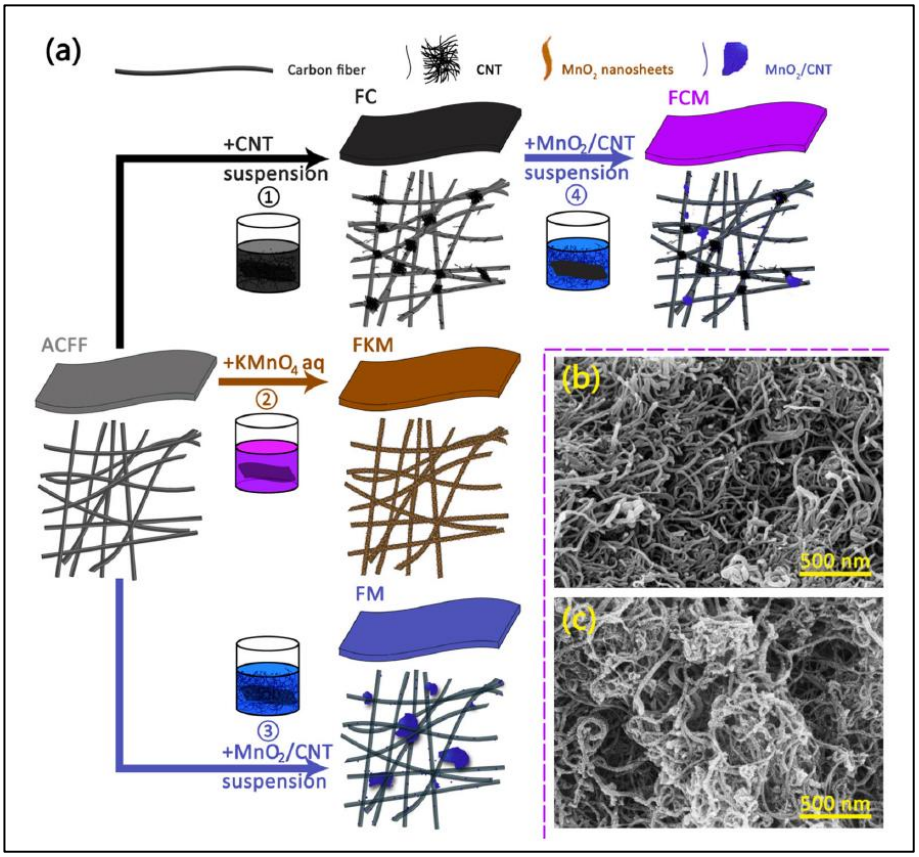

Figure 2.10: (a) Schematics of dipping and drying method with different textiles, (b) SEM images of CNT fillers, (c) MnO2/CNT fillers (Zhang et al., 2017)

2.5.4 Electrophoretic deposition technique (EPD)

As highlighted by the most recently published works that focus on flexible EDLCs, their manufacture via electrophoretic deposition (EPD) needs more consideration due to different aspects of the theory of EPD (Xu et al., 2017; Corni et al., 2008). In addition to the dipping and drying process, EPD has been used for depositing onto a broad range of different shapes and dimensions, due to its ability to achieve optimum deposition and thicknesses. The mechanism of EPD involves charging the particles of the materials in a suspension, usually ethanol, or acetone. The particles are introduced into the electrolyte and begin depositing onto two electrodes under an applied voltage of 30 to 50 V. The distance between the two electrodes is usually 1 cm. Xu et al. (2017) manufactured flexible MXene electrodes without any binder using the EPD method, and they employed supercapacitors to reach a specific capacitance of 140 F/g in the alkaline electrolyte (Figure 2.11).

Figure 2.11: Schematic illustration of the manufacturing process for flexible supercapacitor by EPD (Xu et al., 2017)

The EPD is quite complicated and problematic especially when it involves the deposition of two or more materials at the same time from the same suspension. The stability in the applied voltage is necessary for EPD, as the amount of deposition would increase with the increase in the applied voltage. Zhang et al. (2012) claimed that an EPD cannot store sufficient electricity for most practical applications. Also, an EPD is highly dependent on the conductivity of the electrode's substrate because of the movement of the particles. Therefore, it is limited to highly conductive electrode materials.

2.5.5 Roll-to-roll printing (R2R)

To reduce the production costs, many manufacturing companies have fabricated some flexible printed electronics with a combination of manufacturing processes. MicroFLEX® is one of the companies that have used a high-precision laser process with a roll-to-roll (R2R) printing process to manufacture flexible electronic devices. A wide range of deposition and patterning methods have been used, and each has its advantages and its drawbacks for flexible electronics. The drawbacks of these techniques are that they are highly expensive and are limited to specific substrate materials and active conductive materials. Based on recent research for flexible energy storage devices, many manufacturing processes have been used and investigated based on a range of requirements and parameters. The process selection would usually be based on the cost of the process, the time, and the capability of the flexible materials, the resolution of the electrodes, the packaging, and the type of dielectrics. The manufacturing industries of micro-sized flexible supercapacitors have used photolithography R2R and the ink-jet print process to achieve lower resolution flexible supercapacitors with a high capacitance performance.

R2R processes have been reported for flexible supercapacitors based on different electrodes and substrates. As shown in Figure 2.12(a), there are three main steps in the R2R process to produce flexible supercapacitors: deposition, patterning, finally, packaging. The limited thicknesses and deposition rate of the R2R process are the main drawbacks. As shown in Figure 2.12(b), CNT/PANI electrodes into PVA-H_2SO_4 electrolyte have been manufactured using the R2R method, as reported by Meng et al. (2010). Also, as shown in Figure 2.12(c), Huang et al. (2012) fabricated GPE film by

swelling the PAN-b-PEG-b-PAN copolymer with a $LiClO_4$/DMF LE for EDLCs. It is readily scalable and applicable to the R2R process. However, due to the surface morphology effect and mechanical defects, such as cracks by the R2R process, the R2R method can be classified as a high production process, and most of the applied materials were harmful nanoscale materials for use as a deposit and for improved processability.

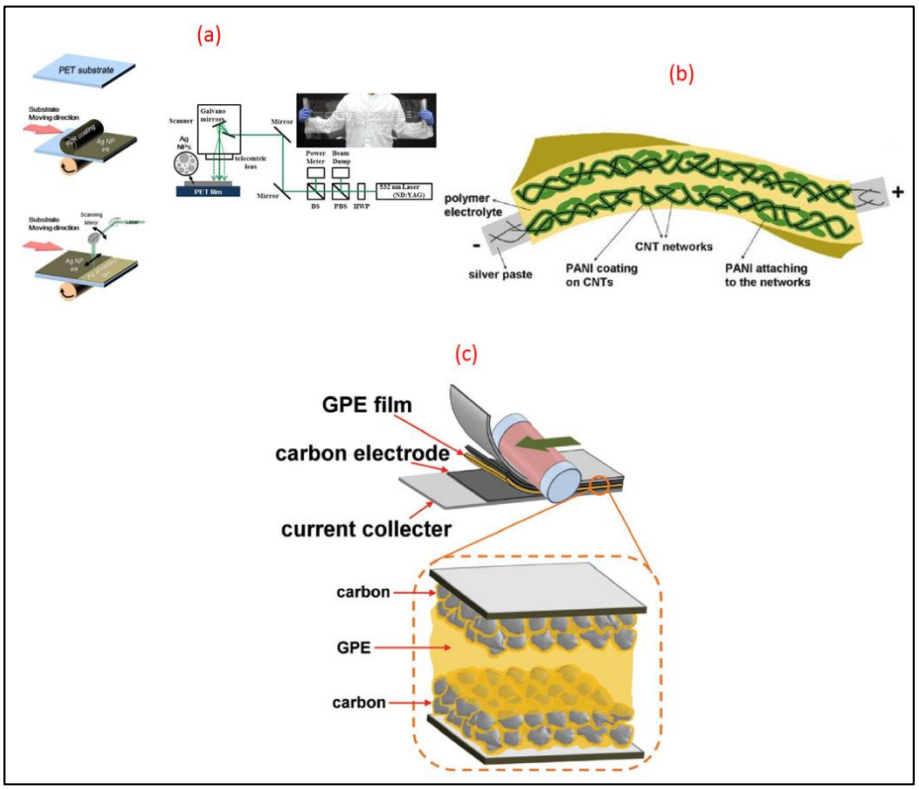

Figure 2.12: (a) Schematic illustration of the R2R fabrication process (Yeo et al., 2014), (b) Paper like polymer supercapacitors fabricated by R2R (Meng et al., 2010), and (c) R2R assembly of an EDLC using the developed GPE film (Huang et al., 2012)

2.5.6 Screen printing

An inexpensive and fast fabrication technique like screen printing is more reproducible in masses. Therefore, it has been reported as a very promising technique for manufacturing flexible EDLCs (Zhao et al., 2017). In brief, this method involves printing conductive ink onto flexible substrates through a prepared screen of fine materials. In some cases, a mask is used for patterning followed by a blade being moved across the screen. The disadvantage of this method is the time required for fabrication, as the main process involves the use of a manual flat-bed to build functional EDLCs. The viscosity of the deposited materials, such as inks and pastes, is usually based on a

conductive filler, which leads to the EDLC suffering from brittleness and even roughness. The repeated pressing of the materials increases the thickness and conductivity and can distort the patterns. Besides, the deposited material thickness is limited (5 mm to 10 mm) (Godino et al., 2012). Many different electrodes have been printed onto various substrates using screen-printing. The curing process step is essential to get high adhesion and conductivity. The material printed layers need to be flattened; otherwise, they would not be completely in contact with each other. The printed materials are mixed with the eco-friendly binder to give adhesion support to the particles. To improve electrode adhesion, different types of adhesive have been used with the electrode materials. Figure 2.13(a) shows rGO electrodes based on a polyvinylpyrrolidone (PVP) binder and deposited onto PET substrates by screen printing to get a specific capacitance of 201 F/g at the scan rate of 2 mV/s (Sudhakar et al., 2014). Therefore, significant research and development is needed to improve the characteristics of materials based on screen-printing. Screen-printing has been used for the production of large-sized flexible supercapacitors although the specific capacitances decrease with the increasing size of the electrodes. As shown in Figure 2.13(c), Sun et al. (2016) manufactured electrodes based on PANI/rGO on 100 cm^2 of a polyester textile sized using the screen printing technique to reach a capacitance of 69.3 F.

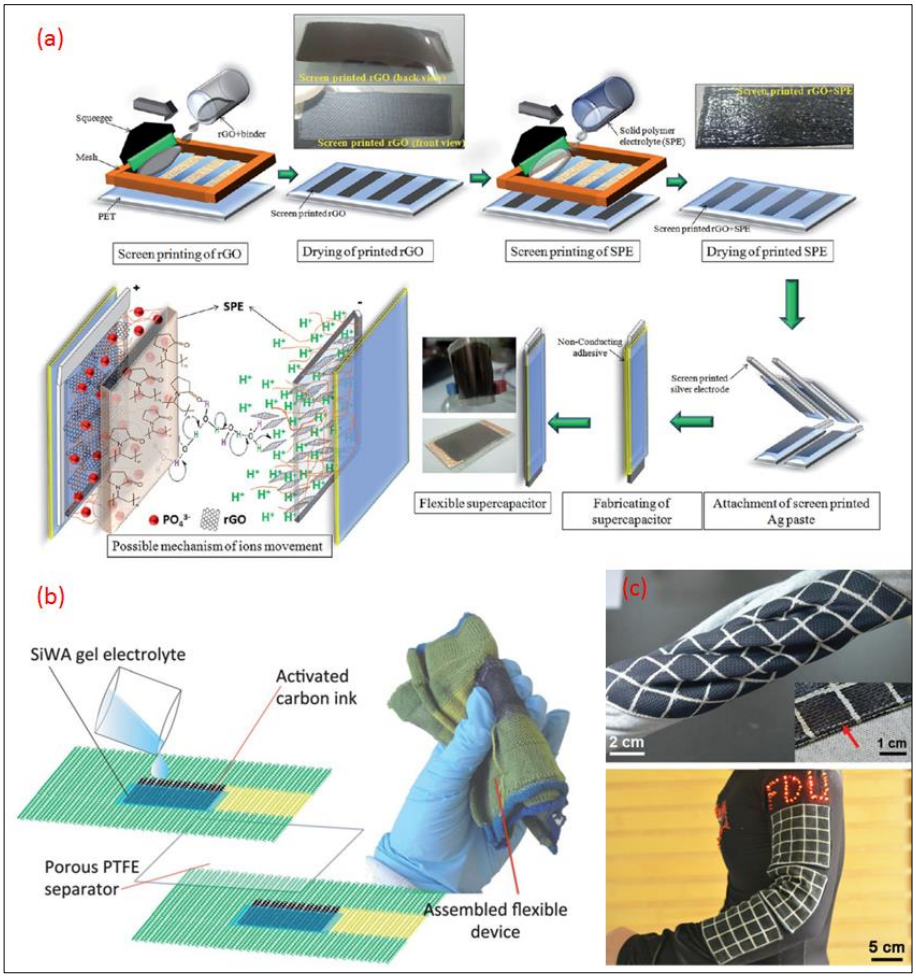

Figure 2.13: (a) rGO screen printed on PET and manufacture of EDLCs (Sudhakar et al., 2014), (b) EDLC based on carbon fiber current collector for knitted or woven (Jost et al., 2013), and (C) photographs of a 400 cm^2 EDLC textile woven into a T-shirt (Sun et al., 2016)

2.5.7 Inkjet-printing technology

An inkjet printing technology is a direct-write process. It is used for depositing designed patterns on thin substrates, such as paper, plastic, and silicon wafers. It is a frequently utilised method, as it allows designers to control the patterns and reduce the amount of waste materials. To date, the active materials have been inkjet-printed onto thin substrates for flexible supercapacitors/MSCs. These materials, which have been used in ink form, have been investigated recently, for example, carbon-based hybrid ink (Pei et al., 2017), pristine graphene (Li et al., 2016), exfoliated graphene (Liu et al., 2016), PEDOT:PSS/Ag (Cheng et al., 2016), graphene/molybdenum disulfide (Li et al., 2014), and SWNT (Chen et al., 2010), and MWCNT (Ujjain et al., 2016). Lee et al. (2014) invented flexible MSC; this was manufactured by graphene oxide flakes being reduced thermally to graphene and then directly deposited onto a substrate using an inkjet printer. The sizes of nozzles on the inkjet printer were in the range of 100–400 nm and were designed for a nominal drop volume. Based on the printer heads, two types of inkjet printers can be used for fabricated flexible supercapacitors, namely, piezoelectric and thermal inkjet printers. The standard ink jet heads for fabrics are piezoelectric. They provide printer producers with machines that are more robust and have greater flexibility. This process allows precise amounts of ink to be dropped on demand. However, it is difficult to manufacture a very thin conductive layer on the fabric substrate, as the substrate could not survive the long period of high temperatures during the curing process.

To enhance the conductivity of deposited ink layers, an increase in the amount of conductive filler is highly significant, but it might block the nozzles. Because of the technical challenges of ink materials, there have been only limited reports on the inkjet printers for flexible supercapacitors-based fabric. Therefore, graphene has attracted a significant amount of attention in most of the electronic fields due to the two-dimensional structure and high specific surface area. For instance, Liu et al. (2016) manufactured a flexible MSC, as shown in Figure 2.14, and commented that the exfoliated graphene sheet must measure less than 2 µm to be deposited onto an ultra-thin PET substrate when using the inkjet printer to avoid blocking the nozzles.

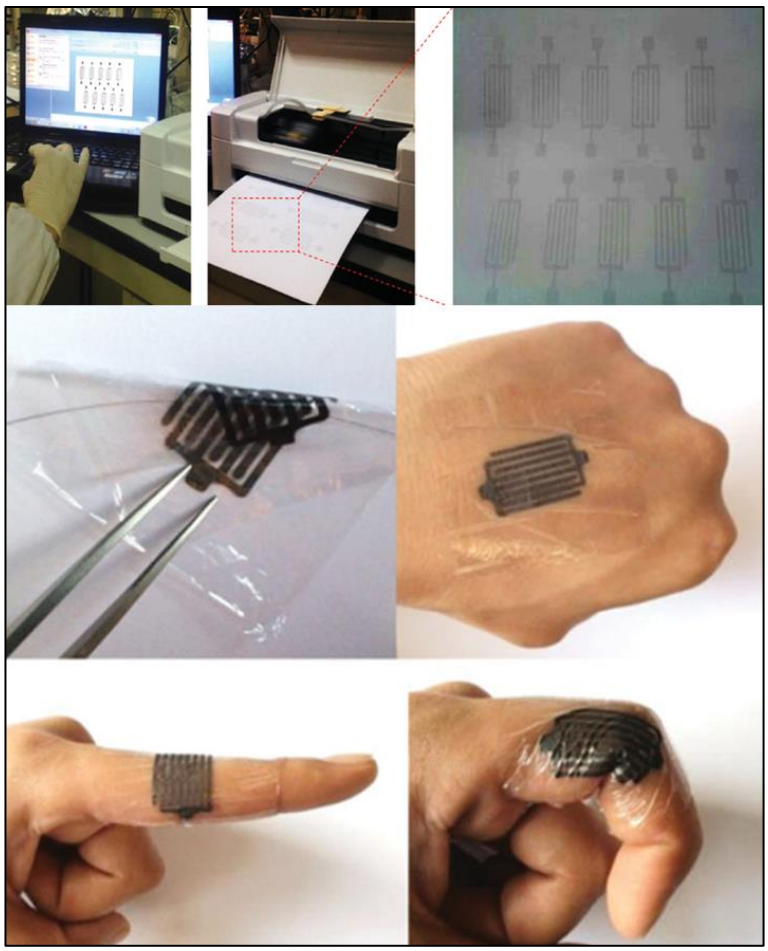

Figure 2.14: Schematic illustrations of the procedure for fabricating flexible MSCs based on pristine EG ink using the inkjet printing method indicating that the device is thinner than a human hair (Liu et al., 2016)

2.5.8 Micro-extrusion technique

It is important to address the issues of blocked nozzles and heat curing encountered in ink-jet printing technology, as 3D printing technologies have inspired a revolution in the electronic industry due to their ability to recreate 3D structures and patterns on different substrates. The micro-extrusion process is used to make flexible MSCs. The method involves extruding ink through a deposition nozzle via displacement pump drives; the speed is controlled by pre-programmed printing (Sun et al., 2015). There has been research in the field of 3D printing processes regarding the full fabrication of working energy storage devices because of the complexity of the material forms. To date, the 3D process has been used only to fabricate electrodes. For example, Sun et al. (2015) deposited just graphene ink onto glass and PET substrates using a micro-extrusion system. The coating method has also been used to coat gel electrolytes.

Therefore, not all the EDLC components have been deposited using the fabrication process of an expensive micro-extrusion system. There has been some slight research into the use of micro-extrusion for flexible MSCs. For example, Zhu et al. (2016) adapted 3D micro-extrusion (direct ink writing) for the manufacture of a 3D graphene composite aerogel for lightweight supercapacitors based on an aqueous electrolyte (KOH). They used a modified printer to deposit 1 mm thicknesses onto an isooctane bath to prevent structural shrinkage during printing. The supercapacitors achieved a power density of >4 kW/kg, and a good capacitive retention ca. 90% from 0.5 to 10 A/g. However, the micro-extrusion system is more typically used for making biodegradable polymers based on biomedical applications.

2.5.9 Light scribe DVD burning

Many applications are required to achieve thin layers, high resolution, and high conductivity. For this, the light scribe DVD method is a unique and valuable process. Laser-scribed graphene is fabricated to reach a high conductivity of 2.35 x 103 S/m with a large specific surface area of 1500 m^2/g. This makes it possible to employ the electrodes without the binder, so they can operate as both electrodes and current collectors for supercapacitors. Figure 2.7(g) shows the manufacturing process of laser scribing (HP DVD burner). A limited range of materials has been prepared with this technique, commonly graphene, and recently, manganese dioxide (MnO_2) and carbon nanotubes (El-kady & Kaner, 2013; Chen et al., 2016; Wen et al., 2014). To reduce graphene oxide (GO) to graphene by another method, the GO is coated onto a flexible substrate, usually PET. It is glued to the DVD disc and inserted into the optical drive for laser patterning and reduction. In the final step, the printed discs are coated with the electrolyte. The DVD burning method has been used to manufacture flexible MSC due to its low cost and its simpler, scalable, and high capacitance performance. However, several issues have been reported: the restacking issue results in a substantial drop in the amount of ion accessible surface of graphene and in the times of light scribe, and only limited electrode materials can be utilised. High capacitance performances have been reported by DVD burning to transfer layers of GO/CNT to be 3.10 F/cm^3 (Wen et al., 2014), and 202.98 F/cm^3 laser scribed graphene/MnO_2 (Chen et al., 2016), and 2.35 F/cm^3 of GO electrodes (El-kady & Kaner, 2013). This manufacturing process

demonstrates a superior electrochemical stability even under bending and twisting conditions.

2.5.10 Aerosol jet printing method

Among the manufacturing techniques of the flexible supercapacitor, the aerosol jet is one of the printed processes used for energy storage devices. The aerosol method is a sustainable process for large-scale production, as it allows supercapacitors to be accrued from precise micron-scale patterning with low waste and thin layer deposition. The aerosol method uses the AM process and refers to the suspension of liquid droplets, called atomisers, in a sheath gas. The printing system aerosol jet 300 series system® has been used to carry active ink (carbon nanoparticles) droplets to the substrates (Saengchairat et al., 2017). Sagu et al. (2016) used the aerosol-assisted chemical vapour deposition (CVD) technique for CNT in ethanol by using the electrolyte of 0.1 M tetrabutylammonium hexafluorophosphate (NBu_4PF_6) in propylene carbonate (PC); a maximum capacitance of 3.4 mF/cm^2 was obtained. The aerosol method is assisted by the spray-coated technique, and it is suitable for the fabrication of high-performance supercapacitors. For example, Jang et al. (2013) fabricated electrodes with a functionalized AC nanoparticles solution, which was propelled through a nozzle with a syringe pump to form an aerosol. Nitrogen (1 bar) has been used as a carrier gas to make injected aerosol solutions. This has made it possible to achieve a better specific capacitance of 154 F/g and energy density of 18 Wh/kg at a scan rate of 10 mV/s in a 1 M Na_2SO_4 electrolyte. In another study, by Gilshteyn et al. (2016), fabricated stretchable and transparent supercapacitors are based on aerosol synthesised SWCNTs to get a specific capacitance of 17.5 F/g in PVA/H_2SO_4 gel electrolyte. This can be stretched up to 120% with practically no variation in the electrochemical performance after 1000 stretches. It is a relatively new deposition method compared to other manufacturing processes. The advantages of this technique are that it is easy to control the cross-sectional profile of printed lines, such as the thickness. Similar to the ink-jet printing method, there is a more extensive range of compatible conductive and dielectric ink materials with different degrees of viscosity. In addition, it is possible to print a variety of nanowire-based inks for other materials, for instance, piezoelectric, carbon nanotubes, and thermoelectric.

2.5.11 3D printing technology

There have been a few attempts where designers have tried to print active and conductive material with low-cost 3D printers by developing a specific unique process, for example, the work presented by Leigh et al. (2012), Peterson et al. (2014), and Zhao et al. (2014). To date, there are 3D printer machines for electronics such as the 'Voxel8®', which is a dual printing technique using ink and solid filament deposition. This is printed by a pneumatic system, although air could lead to unstable drawing behaviour and these processes could not address all the needs of prototyping. As has been mentioned before, additive manufacture (AM) is a significant incorporative research area that covers electronics, materials, and chemical engineering. Indeed, incorporating the filament deposition method for several forms of conductive or active material will allow the present study to focus on the performance of conductive and active layers in comparison with other expensive methods less suited for prototyping. Typical materials used in 3D paste deposition printing include polymers, waxes, and paste filled with, for example, metal and ceramics. Using a CNC machine as the platform for 3D deposition of materials facilitates providing adequate control of deposit thickness and several pattern structures. However, many methods exist for controlling the flow of material from a syringe, such as a linear motor driving the syringe piston or a controlled flow of compressed air into the syringe (Valentine et al., 2017); the last method involves using constant pressure compressed air behind the material in the syringe with a controlled valve at the syringe tip.

The fabrication of fully working flexible EDLCs by an additive manufacturing process is innovative and requires more research. There are crucial steps to making energy storage devices with flexible properties by the manufacture of an additive. Zhao et al. (2014) used titanium materials for 3D SLM (SLM50, ReaLizer®) to manufacture 3D interdigitated electrodes for supercapacitors. As shown in Figure 2.8, the SLM method melts and fuses titanium powder with a laser beam. Subsequently, the 3D titanium electrode is coated by PPy to deliver a volumetric capacitance of 2.4 F/cm^3, and an energy density of 213.5 Wh/m^3 at a current density of 3.74 mA/cm^3 in PVA/H_3PO_4 electrolyte. The critical issue for printing a successful supercapacitor is the selection of an electrode and electrolyte material with excellent printability and a low cost of manufacture. Currently, SLM printers are the most expensive machines, and there is

no machine or printer that is capable of printing a working supercapacitor in a single process.

As shown in Figure 2.15, a 3D printed solid-state supercapacitor has been manufactured by a 3D graphene-based PLA filament using an FDM 3D printer as reported by Foster et al. (2017). The specific capacitance of 75.51 µF/g has been achieved at an applied current of 200 µA in 1.0 M PVA/H_2SO_4 electrolyte. This investigation, however, does not fully exploit the abilities of AM; it is a simple 3D FDM structure. In addition, the rest of the EDLC components were attached manually to manufacture the supercapacitors. Furthermore, there is a lack of material variety in AM, and these were developed specially for the FDM printer at a high cost. For instance, the price of the Blackmagic® filament is very high, at around £54 for 100 grams (BlackMagic3D, 2016).

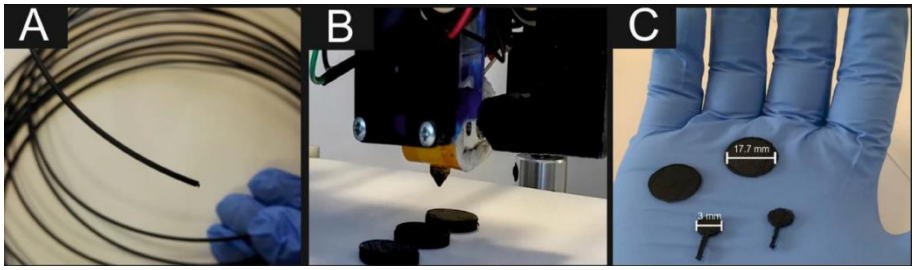

Figure 2.15: Photos of the 3D printable graphene/PLA (Foster et al., 2017)

2.6 Introduction to Additive Manufacturing (AM)

AM is used to describe a range of technologies that are able to translate virtual solid object data into physical objects in a fast and easy process. Each process has its advantages and disadvantages. In general, the main advantage to be gained by taking an AM approach is the ability to produce objects of virtually any geometrical complexity without the need for tooling, which means no extra cost. AM is a more common term than rapid prototyping (RP), as it defines any technology that generates parts or exclusive structures by adding-printing in a layer-by-layer process using high-speed CNC machining or rapid form copying processes after acquiring the initial objects. The RP technologies are described as offering quick self-service fabrication due to the notable time saving and due to the produced parts having an accuracy and surface finish that is inferior in comparison with other machines. They can be fabricated with physical parts of any shape and complex form. The various technologies used in AM have their particular design requirements, so the designer must have a definite idea of how to successfully design for a particular process. An AM machine must be set up before the build process, and issues will appear at the slicing stage. Layered manufacturing is a fundamental development in manufacturing. Therefore, several layer manufacture processes (LM) are currently available; some of the more familiar methods are stereolithography (SLA), selective laser melting SLM, selective laser sintering (SLS), laminated object manufacturing (LOM), and FDM 3D printing. RP emerged a decade ago and has been a primary concern of the scientific due to its ability to create 3D products directly from 3D computer-aided design systems (CAD). These are mostly STL files, which slice the part into several layers. The development of RP is closely related to the development of areas of computer numerical control (CNC) and CAD. This gives different results between RP as an additive machine and CNC as a subtractive machine prototype. For example, a CNC milling machine has standardised tools and so might require different cutting tools depending on the materials; hence, it can be used with a broad range of materials, e.g., metal alloys, woods, thermoplastics, acrylic, and wax.

2.7 Computer Numerical Control (CNC)

In the machine tool classification, CNC refers specifically to computer numerical control and is widely used for lathes, such as milling machines, drilling machines, and laser machines. Figure 2.16, CNC machine, which is defined as a computer, converts the design prepared by CAD into several numbers utilising a prepared program containing coded alphanumeric data.

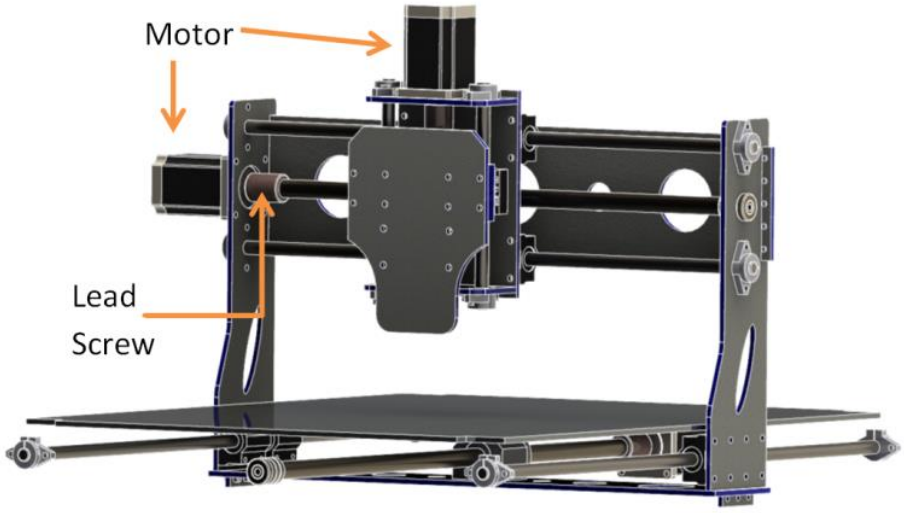

Figure 2.16: Rendering of assembled CNC Machine

The 3D X, Y, and Z axes control the motions of the head on a 3D CNC machine, and it is this that allows materials to be machined in 3D; however, the main head is instructed to move from one coordinate to another. The apparatus consists of two main components, namely, the data processing unit (software) and the control loops unit, which runs the drives attached to the machine leadscrews to move the build plate. As shown in Figure 2.17, the process is relatively direct; the open and closed loop defines the control process of an apparatus. The open loop denotes an apparatus where the communication between the controller system and the motor is one way and has no effect on the control of the input. It becomes a closed loop by including feedback. An important concept that is related to the open loop system is that motors must have virtually no backlash and must be stiff at a low temperature, such as a NEMA 17 stepper motor, which provides several advantages over reduction gears and no backlash that could affect accuracy and fewer moving parts that could break.

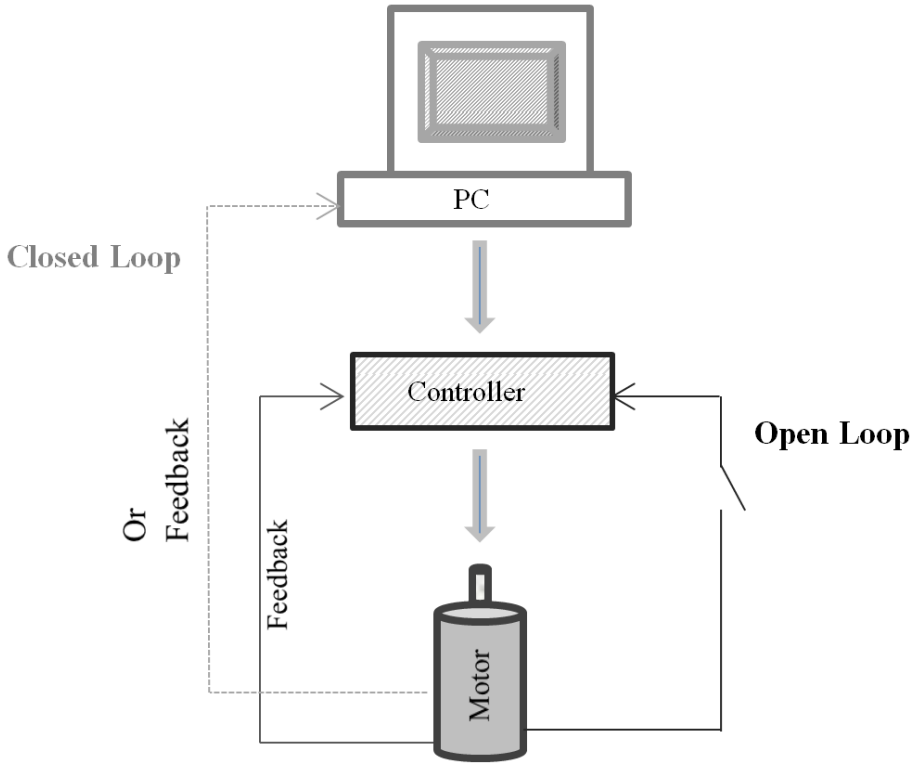

Figure 2.17: Primary types of CNC block

The differences between the CNC machine and the 3D printing machine are the tool head and the heated build platform; however, the CNC machines use spindles, in contrast to 3D printers, which use hot plastic extruders as FDMs. Many researchers have developed a 3D printing attachment that can be added to many CNC machines as a milling machine – this makes it possible for the machine to operate in three dimensions and allows designers print a thermoplastic prototype of a finished metal object on one machine. The CNC platform itself has a bearing on the results of the experiments. One example of a development made possible by Schunemann et al. (2015) is based on a CNC machine. An air-pressurised syringe was set up to deposit several viscous materials. They produced a body of work that developed the materials, process, and supporting technologies of CNC, AM, and RP machines and captured the advantages of many open-source projects, including RepRap; both projects cover the entire experimental set-up including the software and the hardware.

2.7.1 Motion control

Motion controllers play an essential role in the development of high-performance CNC machines. The design of many devices requires linear motion; this plays a vital role in a CNC machine and is generated by using a rotating screw and a nut that translates along the length of the screw. However, to allow them to match each other, there is usually a space, which leads to backlash. Therefore, to avoid this issue, an anti-backlash nut should be installed (Malone & Lipson, 2007, p.55). Typically, the leadscrew is prevented from rotating with the motor. Thus, the rotor motion is converted to linear motion, and this guides the machine in a precise motion with low friction.

In general, the head moves along the x and y-axes while depositing material, and the z-axis move down to present the object in the third dimension. Each axis uses a NEMA stepper motor with several sizes of bipolar with rotor mounted lead screws, the thread of which is responsible for controlling the resolution. The CNC controller and computer system work together to send out the instructions through the parallel ports to the motors and drive the system regarding in which direction to move, as this is usually ordered by the motion control software. Typical CNC machines use controllers with a high performance 60 MH Philips (LPC-2148 ARM7TDMI, Royal Philips Electronics N.V.) with large RAM space to buffer motion commands due to real-time motion that does not depend on variations in the communication bandwidth (Malone & Lipson, 2007, p.47).

However, the FDM printing machine has developed to become one of the most popular RP processes (Stratasys). It has increased the build speed by employing two axes in a high-speed motion control system that moves each of the two extrusion heads for part and support material independently. Most FDM 3D printers have the advantage that they can be connected to a PC as well as functioning as a stand-alone system that can print from G-code files from a removable storage port. The fabrication of 3D printed objects from CAD files is very easy: minor steps are fundamental to producing G-code files in a format, which is ready to be printed.

2.7.2 G-code, printer programming

Computer-aided manufacture (CAM) involves the use of a computer to assist in all operations of a manufacturing plant (Gibson, 2014, p.23). Currently, when converting geometric modelling into model production instructions, there is no fundamental difference regarding data preparation among the existing RP and manufacturing technologies. There are several different format files for data interfaces from CAD/CAM to RP, for instance, common layer interface (CLI) files, rapid prototyping interface (RPI) files, and the stereolithography (STL) file format (Chang et al., 2004). The STL file has become the de facto standard for the data input of the current 3D printing processes and machines. It can be generated by a 3D CAD system or other technology that can be used in conjunction with additive manufacture technology, and it is noteworthy that this file cannot eliminate errors, though there is software available for checking and correcting STL files such as Netfabb. These files need to be reduced to a series of processes which require input sensor and actuators. Therefore, 3D printing machines need microcontrollers to run these files. However, most standard microcontrollers are programmed only in the assembly language; for instance, Arduino microcontroller is an open-source prototyping platform based on flexible use hardware and software. The benefit of the STL format is that the skin of a CAD object can be reproduced with extreme accuracy using planar triangles via tessellation. The “slices” are printed in a particular format named G-code, which is a numerical control programming language that is presented as a set of instructions or commands for moving the instrument’s extruder head, laser, and cutter head along a path of the X, Y, and Z axes.

Therefore, there is CAD software as well as slicing software; Slic3r®, Skeinforge® and CURA® are some of the most common slicing software for open source system. However, concerning our research aim, we have chosen a slicer software called Simplify3D®, a dual extrusion wizard, due to its ability to generate a G-code by setting the geometric parameters (feed-rate, layer height, filling, and supporting material), in addition to allowing us to manipulate, slice, and repair. However, the G-code language implemented on the machine controller is based on Marlin firmware, which is compatible with Ultimaker^2 3D printers that have an Arduino microcontroller (ATmega 2560) installed. The basic G-code commands (Reprap, 2015) are listed in Table 2.2.

Table 2.2: List of G-code commands

Command	Description
M302	allow cold extrude
M92	set axis steps per unit (mm)
M104	set extruder temperature
M140	set bed temperature
M84	stop idle hold (disable motors)
G28	move to origin (home all axes)
G0	move
G92	set position
G1	move
F (n)	sets feed-rate
T (n)	select extruder
X, Y, Z	address to an individual axis

2.8 Introduction to 3D Printing Technology

The first 3D printing machine was made in early 1990 as a rapid prototyping machine. Based on materials' forms and structures, there are different 3D printing machines, such as FDM, wax deposition modelling, paste deposition modelling (PDM), polyjet, powder bed, and inkjet 3D printers. 3D printing machines have been restricted to using a small range of materials, such as thermoplastics (PLA or PLA-based, ABS, nylon), resins, and powders. Furthermore, 3D printers use several methods, as a 3D resin printer cannot conduct paste or solid freeform thermoplastic materials, and to date, there are no 3D printers that can work with several material characteristics. 3D printing machines serve to offer the freedom to design and fabricate extremely complex 3D geometric structures. However, significant difficulties are encountered in most of the processes required to achieve the accurate deposition of the layered base material; therefore, a large part of the challenge has been to turn AM into a production technique with a wide-ranging application that may support a revolution in manufacturing.

FDM and paste deposition involve additive manufacturing, while inkjet printing technology is similar to both techniques, as ink drops onto a substrate while other models jet layers of liquid photopolymer onto a build tray. Therefore, modern developments in printing technologies concerning extrusion nozzle technology offer a choice in the way ink or paste is deposited onto the substrates. FDM 3D printing machines are lower in cost than other AM machines and are easy to assemble from standard components, such as print heads, stepper motors, and build plates. Open-source 3D printing is an emergent industry and provides free access to a remarkable community of knowledgeable enthusiasts; the most impressive innovations might be related to the materials, although the system might need some change or modification to cope with the actual materials. 3D printers work on FDM build samples layer by layer, by heating thermoplastic filaments and depositing them in beds through an extrusion route. However, although this system is flexible to use and makes it possible to design complex geometries with high performance, there are some issues with this technology, given that it cannot print on all substrates, as the printing bed needs to be calibrated; additionally, the metal nozzle tips can become blocked with plastic debris. To help resolve these issues, due to the competitive situation among FDM machine

manufacturers, the machine user can usually obtain operational expertise from the machine's supplier, such as Ultimaker®, etc. Furthermore, FDM has the function of automatically driving the filament to provide stable working and to minimise sample defects: for example, the Bendlay® filament material is verified as being able to recreate a textile-based structure that is harder than polylactic acid (PLA) although not as brittle as ABS. Indeed, 3D printers are capable of creating even the smallest details when bringing electronic devices to life by integrating many processes, such as UV, IR, and photonics in one production line. For example, the 3D CeraPrinter® is a high-accuracy and high-speed 3D inkjet printer with automatic motorised rotation, allowing the embedding of many printing heads, which can change process with accuracy in each of the slots.

The 3D inkjet printer runs in two systems, for example, a piezo inkjet head and a pulsed inkjet head with a static electricity system and a polyjet system, meaning that rather than jetting drops of ink onto paper, polyjet printers jet layers of curable liquid photopolymer onto a build tray (Stratasys®). Consequently, due to the large number of piezo nozzles, the ink must have a lower viscosity and a higher surface tension. Therefore, major suppliers of thermal ink jet printers, such as Stratasys, HP Multi-Jet Fusion, T50 Epson, Cubify®, and Roland®, have established inkjet-based printing that can create naturally soft and flexible materials. According to Nakamura and Henmi (2008), inkjet printing technology has much more feasibility for providing a quick response than has conventional print technology. However, Tyler (2005) confirmed that the ink is ejected from the nozzles due to the bubble being formed and bursting while the ink heads are being heated; in addition, the ink could be affected, leading to the nozzles becoming blocked, thus reducing the print quality.

In contrast, PDM is used to build a design with several material structures instead of the filament as a solid or ink as a liquid. Thus, the principle of this method is simple, as it is specifically designed for ceramic paste printing. Usually, the extruder mechanism of 3D printing will exclude heating the nozzles and instead will drive paste extrusion, as the working device produces high pressure by using pistons or air pressure to control the flow speed of the extrusion. Indeed, the use of PDM 3D printing in our project will allow us to print conductive materials onto fabric substrates, since PDM will allow us to print conductive paste directly by using a stepper motor due to the ability to adjust

the flow rate at any time during the printing process. In this respect, the hardware developers from the Structur3D printing company have presented a Discov3ry tool that works as a paste extruder based on a syringe. It can be attached to any 3D desktop printing machine. In addition, this system has been updated to facilitate the open cartridge system that keeps the print materials separate (Structur3D®, 2014). Several types of 3D printing machines for PDM technology have been updated to print larger projects without the need to stop the machine during the print process, as well as reducing the labour involved. For example, research has been carried out by Deltabots, Mini Metal Maker, Zmorph, and Voxel8 team researchers to update an active 3D printer to work using dual printing heads for thermoplastic and conductive paste in order to design a novel electronic device. In several processes, including more recent 3D printing techniques, it would be useful to understand the concept of each technology, where the users can control the process to match the desired consequence, and this starts with the most common extrusion-based additive manufacture system, namely, FDM.

2.9 Fused Deposition Modelling (FDM)

In the FDM process (Figure 2.18), the machines have all been produced for a lower cost than previously. As the most modern development direction, reliable FDM machines are now available to home users. Scott Crump, who is the co-founder of the Stratasys®, registered the original FDM patent in 1992. FDM uses a heating extrusion to liquefy plastic, which is fed by a feeder motor into the system as a filament. The filament is extruded at a constant rate, meaning the first layer will be put in place while the extruder head moves through a predetermined path. When it is completed, the build plate is lowered to let the extrusion deposit the second layer. Hence, every layer is filled by ways according to a particular path, and these ways can be considered as the real building units of the process. Therefore, the extrusion path width depends on the diameter of the extrusion nozzle, as the maximum extrusion path width is two times the nozzle diameter. It is advisable to work with a smaller size of nozzle, as it can fabricate thinner walls and other complex geometries, but certain types of these nozzle diameters will lead to long fabrication times. FDM machines can run and build an object with several layer thicknesses due to the diameters of their nozzle tips, which are manually changeable. Some FDM machines have dual tip heads with different diameters. Therefore, FDM machines can print several different layer thicknesses, such as 0.01, 0.17, 0.25, and 0.33 mm, in solid thermoplastic.

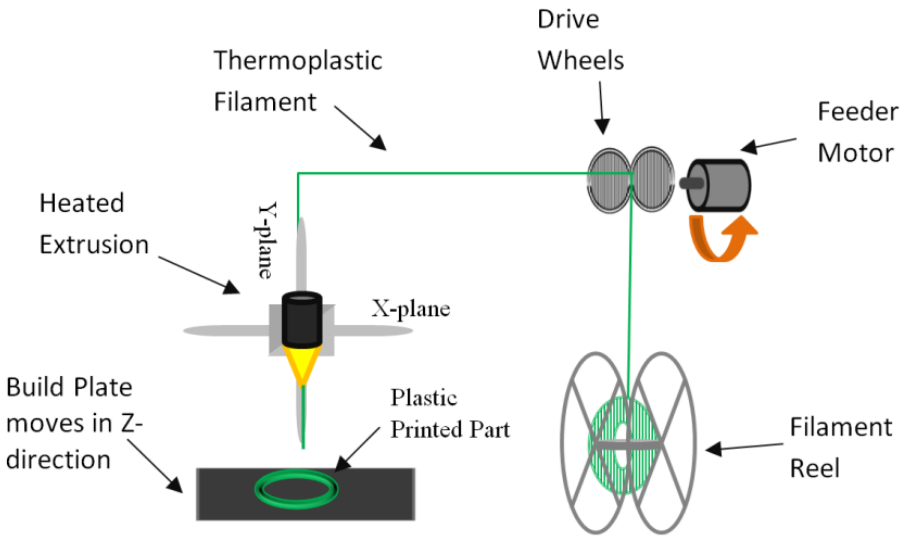

Figure 2.18: Schematic illustration of the FDM

The most common limitations of FDM machines are essentially in material density, accuracy, and layer thickness. Moreover, FDM cannot print sharp external corners due to the nozzle's circular shape, as there will be a radius equivalent to that of the nozzle at any corner (Gibson & Stucker, 2014, p.164). The layers must be in the shape of the object being designed, and it is necessary to balance the speed at which thick layers are deposited. The material could be deposited in the outer region, which is called an overlap, as can be seen in Figure 2.19. Undoubtedly, a software solution will present an excellent solution in each case, but care should be taken to ensure that excess material is not deposited to the extent that the geometry is partly adjusted (Gibson & Stucker, 2014, p.159).

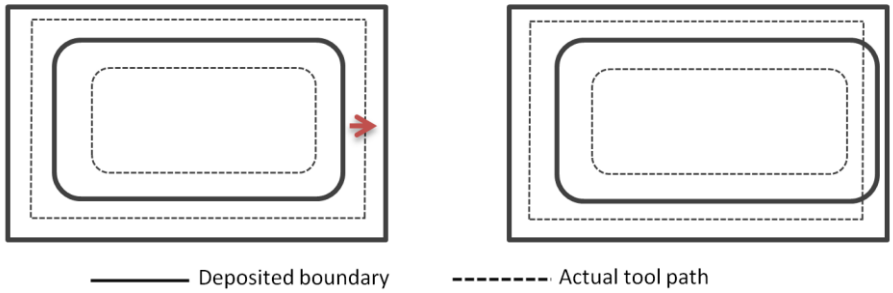

Figure 2.19: Primary extrusion materials (left) Overlap materials extrusion (right)

The FDM process is able to offer multi-material deposition, low repeatability, and a high operating temperature. With 200 µm resolution, FDM has been used for several applications. Interesting developments and modifications based on FDM printers are paste deposition modelling, resin deposition modelling, and contour crafting. These approaches have influenced many researchers to develop their concepts with open-source FDM machines. Some of them have focused on improving the properties of the part designs, such as multiple printing materials, while others have had a narrower focus and have investigated several parameters, such as wall and layer thickness, avoiding sharp corners, scanning patterns, build speed, perimeters, and nozzles. The next section deals with the FDM system-based single extrusion, as some key points need to be considered.

2.9.1 Extrusion

The precise control of extrusion is the most important issue for extrusion-based systems. Each model of extruder has its specific properties and application areas, but most extruder systems are combined in the processing steps. Single screw, twin screw, and multi-screw extruders are existing processes. There are several types of extrusion processes based on material forms: for instance, cold extrusion, micro-extrusion, and hot extrusion. Thermoplastic extrusion can become hot enough to melt plastic, as the hot end parts use thermoplastic filament materials that can withstand temperatures of up to 260°C. The temperature controlled extrusion head is fed with a thermoplastic modelling material that is heated to a semi-liquid state. These thermoplastic filaments are usually 1.8, 2.75, and 3 mm in diameter, and are driven by a gear connected to a stepper motor using simple screw geometry. The FDM materials are fed from a spool through an extrusion nozzle while the platform is moving. Then, the nozzle is heated to melt a filament of thermoplastic material that immediately hardens, solidifying it to the layer below, as seen in Figure 2.20.

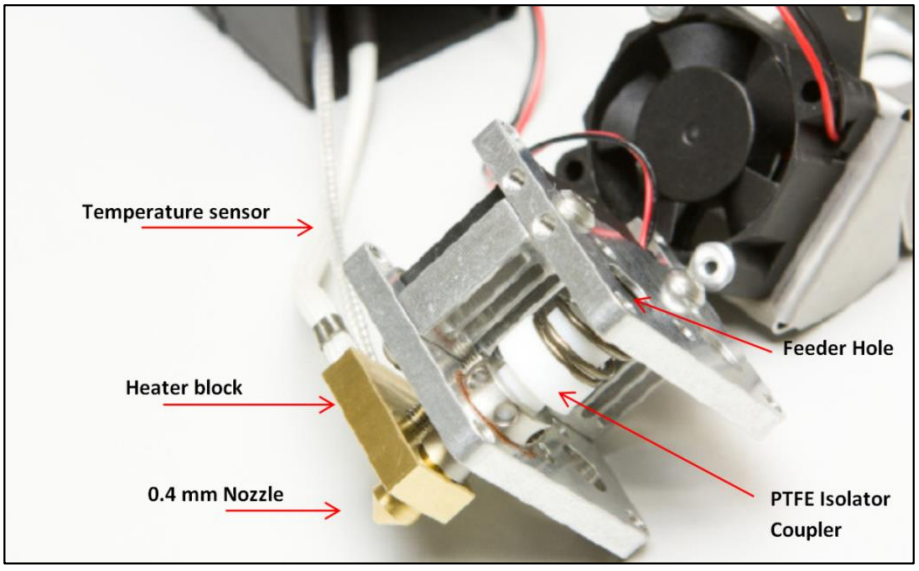

Figure 2.20: Filament extruder and components (Ultimaker[2])

However, some FDM machines present single extrusions with multiple nozzles, such as the 'Ultimaker®', which has an open filament system that allows the designers to combine different materials with different nozzle sizes in one build with an accurate finish. Other 3D printers use a dual extrusion head to deposit two material forms, an example of which can be seen on the 'Voxel8®' desktop 3D printer in Figure 2.21. The

advantage here is that it can print two materials, including conductive ink, thus allowing users to create 3D electronics as well as having wiping and purging stations for each head to ensure that the tips remain clean. The issue here is that at £6,000, it is still expensive; also, no functional materials or matrix can be used with its interchangeable print heads and ink cartridges.

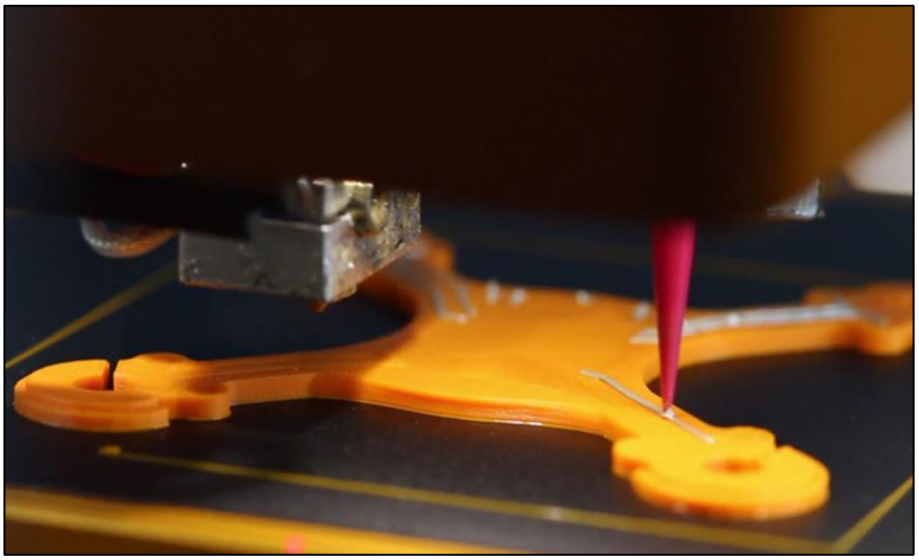

Figure 2.21: Dual extrusions head 3D printer side view (Voxel8®, 2014)

2.9.2 Materials

FDM has a broad range of materials for printing, including polylactic acid (PLA), acrylonitrile butadiene styrene (ABS), nylon, and flexible filaments. Many FDM printers come from a design history referred to as Rep-Rap. FDM printers that use a filament are the most practical for normal educational applications. Also, they are available at or below £1,000 in the United Kingdom. Several materials are available nowadays for FDM printing machines; Gibson and Stucker (2014, p. 164) mentioned that materials based on PC (PC-based) could provide higher tensile properties with a flexural strength of 104 M Pa.

We are going to focus on various materials types, but particularly, the most common flexible and semi-flexible filaments, such as Ninjaflex (NinjaFlex, 2014) and Laywoo-D3 FLEX by Kai Parthy (3ders., 2015). 3D FDM printers can print elastomer materials; these materials are usually made from rubber and other material mixes. NinjaFlex is designed for FDM extruders; it adheres well to the build platform and the bonding between layers with excellent strength and elasticity. Composite materials (alloy) mix

plastic with an additive, such as metal powder or recycled wood, such as the Laywoo-D3 filament. Soluble support materials, for example, thermoplastic polyvinyl alcohol filaments (PVA), dissolve in water, and they are particularly appropriate for different parts. LAY-CLOUD and LAY-AWAY are mainly dedicated for use with flexible prints for FDM printers. 3D printing with multiple extruders and materials is a relatively new phenomenon within the 3D printing world. However, it is crucial for many users to identify considerations regarding the materials selected for applications, such as mechanical properties, for example, friction and flexibility, tolerances and environment, as well as thermal and electrical properties. It is also important to identify what type of support materials need to hold the overhanging geometry in place as the model is created.

2.9.3 Wall thickness

FDM printers can deposit layers of different thickness due to the different nozzle diameters. An important design consideration when using this type of machine is to set up the wall thickness, as the minimum wall thickness for FDM samples changes based on the slice thickness that will be used to fabricate the part. A maximum value of wall thickness ensures that all gaps are closed completely, and this reduces the chance of leaks; however, it will increase the print time and consume a significant amount of material. The thickness of both the horizontal and vertical wall should be considered; for instance, the height of the surface should be a multiple of the slice thickness to achieve a better accuracy, as the horizontal surface is prepared by laying down slices of a fixed thickness. The wall line width presents the number of walls, and this can be calculated. For example, when using a wall line width of 0.6 mm, the wall thickness will be 1.8 mm (3 x 0.6); this means three walls will be printed, which will be sufficient to build a part. Many FDM printers have developed their specification with software that offers options to enhance the parts, especially thin parts. One of these options is to fill the gaps between walls or add an extra wall every other layer. For example, when using a 0.4 mm nozzle, the Ultimaker^2 can produce layer heights of 0.02 mm and offers swappable 0.25, 0.6, and 0.8 mm nozzles. Using CURA® software, it is possible to change the parameters, such as a shell thickness of 0.8 mm, which means that it will print two lines (two times the nozzle diameter of 0.4 mm).

2.9.4 Infill patterns

An FDM structure comes with unique strengths and drawbacks. Specifically, to be printed successfully, specific geometric features require support and infill structures. 3D software, such as Simplify3D®, Slicer®, and CURA®, propose settings to manipulate the infill pattern geometry. The infill density (%) percentage of the parts volume is filled with deposited material inside, while the infill pattern means where the nozzle pattern is drawing to fill the part. However, based on the types of parts and the users' design requirements, particular patterns would require filling. For example, the honeycomb fill pattern may suit mechanical parts more than other patterns due to each hexagon bonding with the same underlying pattern in each layer to form a strong vertical structure. Furthermore, it is useful to know that infill optimisation reduces weight while maintaining an excellent mechanical performance. The FDM process has a greater advantage, as it allows users to fabricate solid objects with a semi-hollow honeycomb interior. This means that these samples have a higher strength to weight ratio, resulting in a much lighter part than usual, but if the infill percentage is deficient, then there will be massive air gaps in the infill object. Infill patterns and density are a major factor, especially when users print with materials with a different rheology or highly expensive materials, such as conductive materials, due to the tremendous impact on weight. Specimens with the following infill patterns are shown in Figure 2.22.

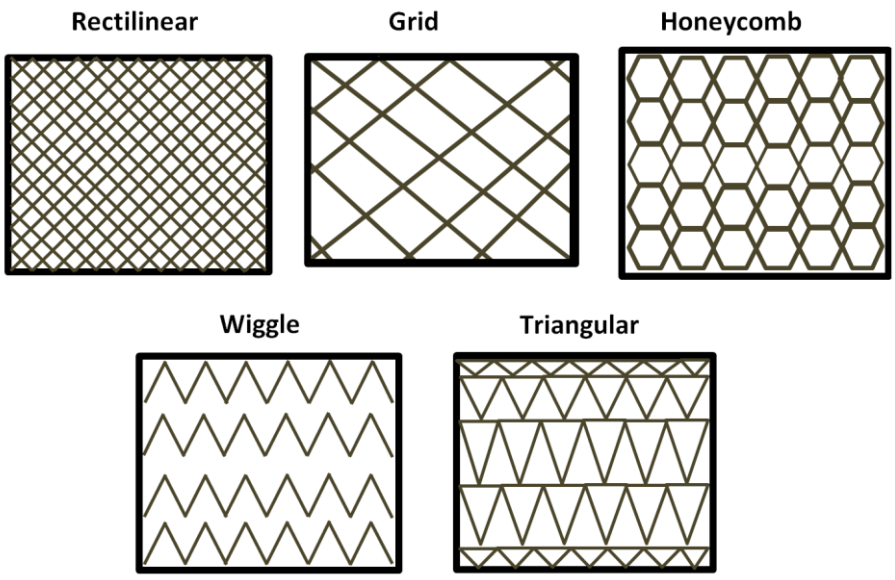

Figure 2.22: Infill patterns offered by Simplify3D® software

There are five types of different infills: rectilinear, grid, wiggle, hexagonal, and honeycomb. The fast honeycomb offers high strength compared to the amount of materials used. In addition, it is the most efficient infill and is faster to print than the other patterns. The minimum infill percentage used is 10%, but in some samples, it is impossible to print 10% infill density with very smooth and strong surfaces. However, some users have applied their algorithm by using FDM to print hollow parts without infill patterns to save a substantial amount of both time and material. Wei et al. (2016) printed a vase without infill patterns using Makerbot® Replicator 2X by creating three main parameters combining seed angle, down facing faced angle, and oriented angle.

2.9.5 Support and build orientation

Supports are used when the part has steep overhangs or unsupported areas, which makes it necessary to use supports to avoid deformation and drooping of the top layer. However, the support material has to be removed from the part after curing.

When creating objects with complex geometries in FDM type processes by using a removable support material, the automatic support generation options allow the software to provide users with a recommendation about where the support material is needed and placed. However, most of the angle parts greater than 45° degrees would start to require support material, as shown in Figure 2.23.

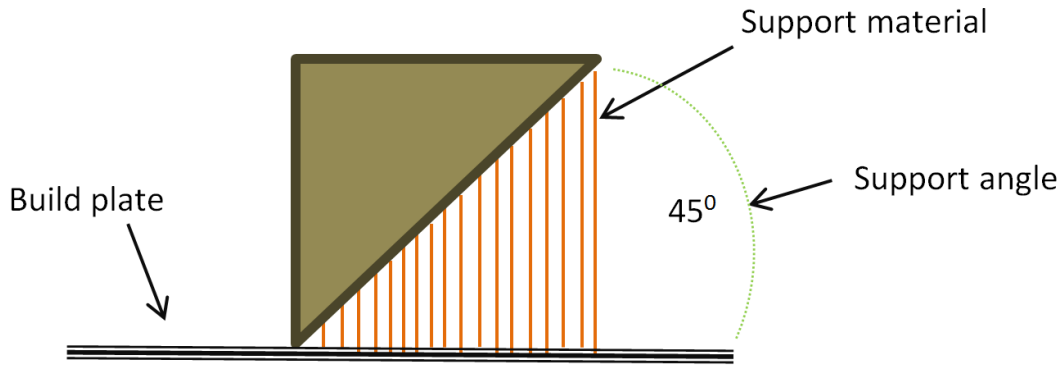

Figure 2.23: Support angle diagram

The orientation of the part during printing can affect the FDM build and might change the properties of the material. It might also affect the strength and functionality of parts; hence, it is possible to solve many large-scale and complicated engineering problems in reduced timescales or avoid printing supporting materials by utilising

design software. However, based on the shape's geometry, some orientations will produce highly accurate results. The build in the (x) direction results in high strength, while in the (y) direction, the last layers leading to the point will be very fragile; in the (z) direction, the build will be smooth, but weak. Therefore, users should keep in mind that an object's overall strength performance is geometry based.

2.9.6 Layer height

Also known as Z height, this is used to refer to the print resolution. Many 3D printer systems vary in their layer height capability. FDM is one of the desktop printers used; it has a maximum Z height of 0.02 mm (Ultimaker.com, 2015), the lower heights offer a higher resolution. However, the lower layer heights do not always indicate an excellent 3D printed result, as many factors influence the finished sample, such as the number of motor steps per turn, firmware settings, and Z-axis threaded rod steps. The nozzle diameters also play an important factor in the resolution, as the Z height cannot be greater than the nozzle diameter. Thus, we can identify an optimum minimum layer height by the size of the nozzle diameter, as the minimum height is equal to a 1/4 nozzle diameter. For instance, the Ultimaker^2, with a 0.4 mm nozzle, can deposit a layer height of 0.1 mm, thus manufacturing samples with a smooth finish while taking into account other parameters, such as high extrusion temperature, low feed-rate, and material properties. For example, when a layer of printed PLA or ABS materials is at too low a layer height, the retraction of the Z-axis can affect the layer height, and the extruder will struggle to push the filament in and back into the hot end. However, elastic materials, such as NinjaFlex, can deposit too low a layer height, as the retraction would be disabled due to the flexibility of the filament so that the extruder cannot push it in and back into the hot end.

It should be noted that layer height, which is limited by the filament thickness, refers to the vertical thickness of each layer of deposited materials to create samples, and therefore, it does not determine sample quality. Figure 2.24 shows that the smaller the layer thickness is, the more accurate and smoother the 3D sample is, but it leads to an increase in the manufacturing time, as it prints more slowly. Many users pay attention to only the first layer height and do not consider how appropriate the height of other consecutive layers might be. When starting printing, it is usually desirable to print a

smaller first layer to ensure a good solid adhesion to the 3D platform, and it is important to print at a low printing speed to avoid any imperfections. Some 3D software, for instance, CURA®, give an option to select only the first layer height and continuous layer, while Simplify3D® software provides a range of options related to the layer height values, which can be written in manually using G-code. However, inadequate adhesion in the first layer causes the sample to separate from the build plate; therefore, it is recommended to raise the first layer height to match the diameter of the FDM nozzle.

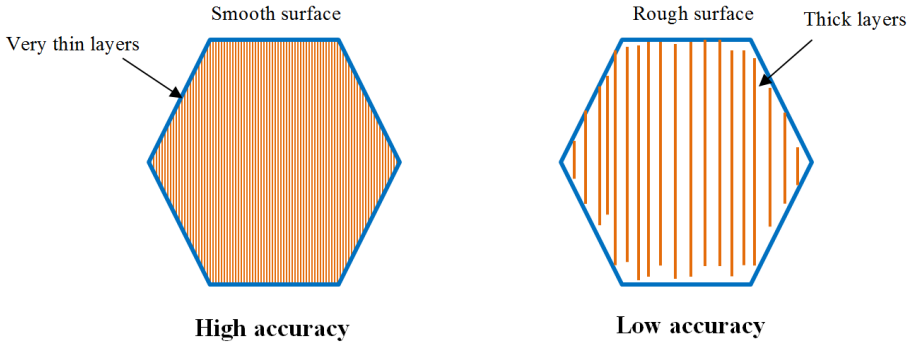

Figure 2.24: Effect of layer thickness on surface finish and an accuracy comparison

High accuracy and sample surface quality have become the focus of the rapid prototype community with the increased requirement of prototyped functional parts. Currently, many researchers have focused on the development of slicing thickness for slicing tessellated models to reduce manufacturing time. For example, Pandey et al. (2007) proposed a slicing procedure for FDM based on the real-time edge profile of deposited layers to enhance the surface quality and accuracy of parts. Other researchers have used their algorithms for variable or uniform slicing (Nadiyapara & Pande, 2017). High-resolution involves high accuracy and precision, and it is hard to achieve high accuracy with a 3D printer without high resolution and vice versa. Hence, the layer height is an essential selling point for commercial FDM printers.

2.10 Paste Deposition Method (PDM)

PDM based on 3D printing is a promising method to control the deposited layers, providing a highly adjustable and affordable method. In early 2007, a similar build process of FDM was introduced by Fab@home, as shown in Figure 2.25(a) (Malone & Lipson, 2007). Instead of s plastic solid filament extrusion, two stepper motor-driven syringes were installed. This system has allowed many users to modify both software and hardware to match their requirements by providing an open source software machine with a syringe tool that allows many fabricators to use a wider variety of materials. However, this expression does not fully achieve the potential of additive manufacturing systems; rather, it can be described as 3D-printed food sculptures. Based on indications by Fab@home, some other designers have integrated a commercial FDM 3D printer (such as Orion or SeeMeCNC®) and a paste extrusion tool (Discov3ry, Structur3d®); see Figure 2.25(b, c). For example, the Orion Delta™ 3D and Rostock MAX printer comes set up and calibrated from the beginning. Along with many other tools, they have two extrusion nozzles - one for thermoplastics and the other for paste material extrusion. Figure 2.25(d) shows the high potential of AM multi-material digital manufacturing (Voxel8®). It has the capability to print embedded electronics and various other devices in one process. However, this printer is very expensive, and has only one thermoplastic extrusion nozzle and another for ink extrusion, but it has no nozzle for paste.

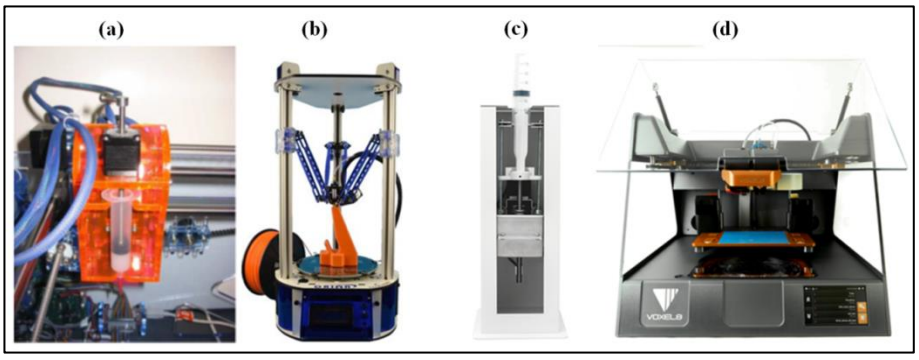

Figure 2.25: (a) Fab@Home syringe tool, driven by a linear stepper motor, (b) Orion delta 3D printer, (c) Discov3ry paste extrude, and (d) Voxel8 3D printer

To enable the composite slurry to be 3D printed, the cost-effective paste extrusion system is integrated with a commercial FDM 3D printer to produce a 3D part by

printing with active and conductive pastes. As indicated in the published work just reviewed, most designers and researchers decide to build the extrusion equipment according to the specifications of a particular application. However, there are three types of extruder, and the next subsection will give a brief overview of these.

2.10.1 Paste extrusions

Based on the materials' properties and rheology, a paste is prepared with an eco-friendly binder depending on the size of the material's particles. Material compatibility plays an important role in 3D build samples. Therefore, the first essential tool of a 3D paste printer is an extruder. There are three basic types of paste extruders, such as a direct drive paste extruder, which is a syringe pushed by a belt; a pump extruder, which is based on a progressive cavity pump; and a pneumatic paste extruder, which relies on air pressure. However, most of the cavity pump extruders need recalibration when there is a change of material; this creates pulsations in the extrusion and is mainly used in the manufacture of food. The deposition of high viscosity pastes would require constant maintenance because of the contact between the material and the mechanical elements inside the extrusion head. However, the disadvantage of the pneumatic paste extruder is that it is difficult to achieve an appropriate continuous feed system. Moreover, due to the complicated setup for controlling air pressure, most of the designers controlled the air manually, which is unreliable and has a negative effect on the printed layers. Therefore, Fab@home applied an appropriate application for the extrusion equipment, so that the equipment does not come into contact with the material, by using inexpensive syringes that exerted control with a linear actuator. This means that if clogging issues were to arise, then replacing the syringe would be simple. It can be altered based on the properties of the material being used, but it may not be possible to re-use the syringe. A paste extrusion tool works based on FDM 3D printers; it deposits several pastes through a user-filled syringe to a special extruder nozzle mounted on the 3D printer main head. Most of the extruders use a linear stepper motor, typically, NEMA17 stepper motors, to manipulate the syringe plunger position. However, using a linear stepper motor would run the risk of bending or stripping threads if the viscosity of the material is too high, and such a risk would potentially limit the range of materials that can be experimented with. However,

because the project aims at depositing active materials, the viscosity of the material will always be under controlled conditions.

Discov3ry paste extrusion is an economical paste extruder that can be attached to any 3D printer system that uses FDM. Discov3ry, as shown in Figure 2.26, has a direct drive NEMA 17 stepper motor that offers several advantages over reduction gears. It differs from gear systems, as there is no backlash that might affect accuracy, and there are fewer moving parts that could break. The Discov3ry paste extruder operates at about 100:1 of the speed (RPM) to obtain the equivalent output flow rate with a 48 rate torque. Due to this ratio, it creates a high-stress load on the stepper drivers when operated with higher viscosity pastes. However, 3D printed gears were added to this extruder to lower the cost further for FDM printer users. These are a double helix type to allow the apparatus to self-centre. This extruder head has the advantage that it can be mounted on any open source printers.

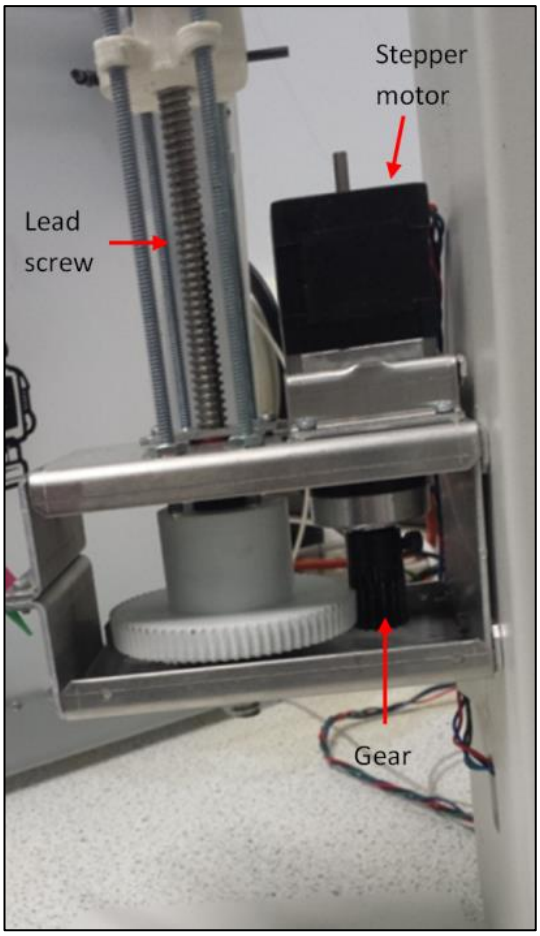

Figure 2.26: 3D Discov3ry extrusion

For full use to be made of an extrusion system there must be an understanding of the process being used. Park (2016) claimed that the Discov3ry extruder leads to unwanted material wastage of up to 3 mL. Therefore, it has been modified by the adoption of a hydraulic pumping mechanism to fabricate a 3D lithium battery (Figure 2.27). However, it increases the time of the fabrication process and requires many types of equipment, which leads to a higher cost. Hence, Wijnen et al. (2014) considered the cost of the paste extrusion system and developed a commercial syringe pump that has a similar performance, as shown in Figure 2.28. Nevertheless, the simplicity of their extrusion system means it has a limited materials viscosity and syringe size. Also, for example, the cost of the entire Discov3ry extruder is less than £330 including the six cartridge starter kit.

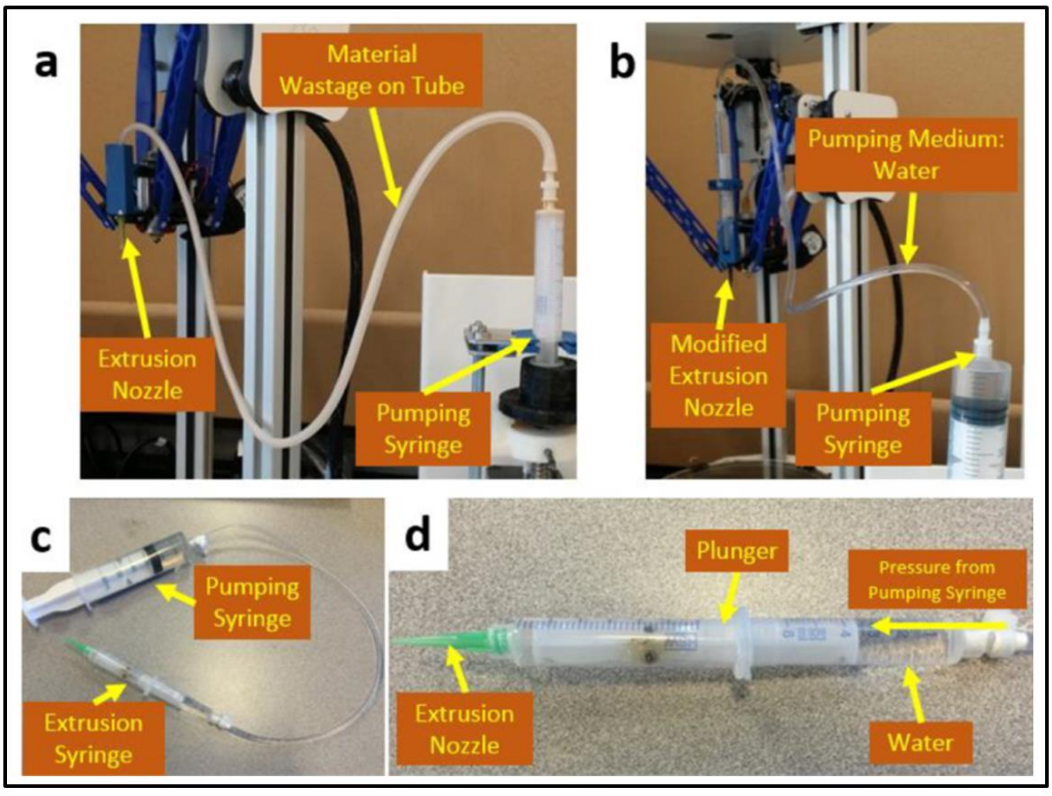

Figure 2.27: (a) Original Discov3ry extrusion system, (b) modified hydraulic pumping extrusion system, (c) hydraulic syringe pump and extrusion syringe, and (d) detailed view of the modified extrusion syringe (Park, 2016)

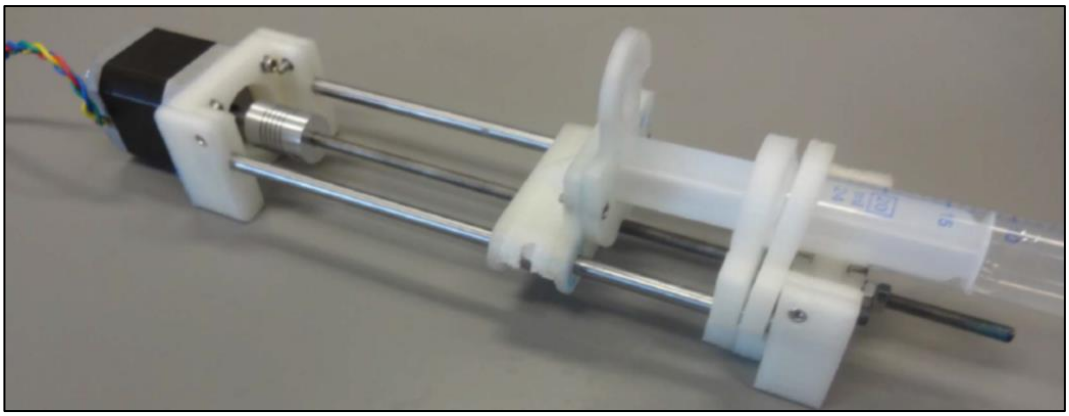

Figure 2.28: Open-source syringe pump with NEMA 17 stepper motor (Wijnen, et al., 2014)

2.10.2 Materials

Recently, a wide variety of different material forms has been made available for 3D printing technology and for use with AM applications. The drawback of the current RP is the limited choice of material properties with which the prototype can be manufactured. However, research into the further development of new materials is in progress. Particular materials have been developed recently for specific platforms operating applications, such as electronic products, with material properties that more precisely match the application (Park, 2016; Leigh et al., 2012; Peterson et al., 2014; Wardyn et al., 2015; Zhao et al. 2014; Gardner et al., 2016). In the FDM and most of the AM processes, there are no limitations to the geometry of the sample, and complex geometrical samples can be immediately built. The material extrusion FDM process is used to fabricate thermoplastic samples through the heated extrusion and deposition of materials in a layer-wise manner. The FDM process is most widely used, but there is a limitation regarding materials, especially conductive materials. Nowadays, there are some conductive filament materials that are used for FDM, for instance, a conductive graphene filament (BlackMagic3D, 2016), the F-Electric filament (Functionalize, 2014), and even flexible conductive filaments, but most of these filaments are based on PLA and ABS. The conductive filament produced should have high conductivity and an excellent surface adhesion. In RP technology, the demand for fabricating complex structures from the wide range of materials, such as polymers, ceramics, silicone, and conductive and semiconductor materials, has been observed. However, as was discussed in the previous subsection, to build electronic parts and

print conductive tracks with FDM, it is necessary to replace non-conductive thermoplastic extrusion with an extrudable conductive material.

Many different materials have been printed with 3D printing based on PDM, for example, silicone, wood filler, natural clay, royal frosting, and Nutella. The materials must be in a state of optimum viscosity to be able to be extruded from a nozzle size of at least 0.6 mm. To avoid any agglomerates from the paste mixture, other factors, such as strength, type of particles, binders, and time of curing, must be taken into consideration when selecting a 3D paste deposition process. Other 3D parameters are also important, such as feed-rate, layer height, the speed of printing, % of the infill pattern, and retraction issues.

2.10.3 Layer height

As discussed earlier, the first layer height and consecutive layer height are crucial, especially in PDM. The first layer height plays a significant role in the adhesion of the deposited paste on the build plate. Recently, layer height of 0.1 mm or less has become achievable using the cheapest FDM printer. As discussed in section 2.9.6, the FDM layer height is determined by the lead-screw pitch along with the steps/rotation of the stepper motor. Table 2.3 shows an overview of the different layer heights for various 3D printing processes.

The main differences between PDM and FDM are regarding the material selection, in that the strength of the binding force between the layers is lower than in FDM, and the mass of upper layers may squeeze the layers below. However, in open source printers, FDM and PDM, the height of the layers, whether the first layer or any consecutive layer, can manually be modified by G-code and M-code commands to include extrusion commands and feed-rates. It is possible to write the layer height values manually by using slicer software, such as Slic3r® or Simplify3D®. Although both 3D techniques, that is, FDM and PDM, use a stepper motor, they operate at different feed rates. As mentioned, PDM works using an air solenoid to push the filaments within a paste, and relies on the air solenoid and high-air pressure to control and deposit various pastes. Thus, as PDM is operated by a stepper motor, it requires fewer tools to deposit several paste forms.

Table 2.3: 3D printing system layer height examples

3D printing technology	Material type	Layer height (mm)
FDM	PLA, Nylon, elastic, ABS, CPE, PVA Filament	0.02-0.2
Selective laser sintering (SLS)	Polymer, metals like steel, titanium, nylon, glass, Powder	0.060-0.150
StereoLithography Apparatus (SLA)	ABS, polycarbonate, rubber, reinforced composites Resin	0.01-0.1
PDM	AgNW/CMC, silicone Paste	0.4-0.8

2.10.4 Infill patterns

Some FDM users have tried to develop an algorithm to partition a model into different samples to be printed with 0% infill density. However, 3D printing parts in PDM without any infill density is a relatively complicated process, and even with various infill patterns, it remains an unexplored research area. Each pattern has an advantage concerning material usage, printing time, strength, and other mechanical properties. As the perimeters in some applications were not adhering well to some infill patterns, Schunemann et al. (2015) designed a whole new type of infill pattern named T-bar, a tessellated pattern specifically designed for thick-walled parts. The tessellated infill was deposited successfully in silicone by using 3D pneumatic PDM. Nonetheless, an infill spacing and infill strategy are necessary to reduce deposition times and material use. In addition, the nozzle sizes play an important factor to avoid shrinkage and collapse the layers, especially in infill patterns that have large gaps. However, in some applications, the infill patterns produce a series of concentric rings forming concentric patterns, while the default rectilinear infill pattern tends to collapse at an angle of 45° and to clamp at 90°.

The mechanical performance of a printed object usually comes at the expense of quality. Indeed, the infill pattern is one of the key parameters that could influence the object quality. The mechanical properties, such as elongation, stress, rigidity, and

tensile strength, could increase as infill density increases. This also means that the cost of the 3D printed parts also increases. As shown in Figure 2.29, based on material paste properties, silicone, wax, and clay could be printed in some applications without any infill pattern in order to avoid hardness and roughness.

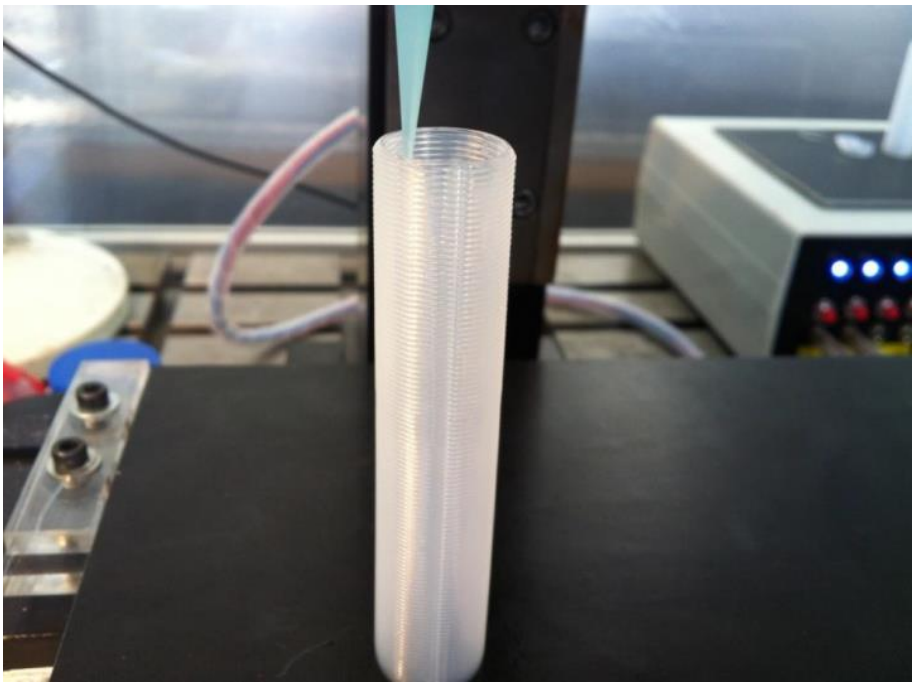

Figure 2.29: Hollow tube builds with two perimeters without infill; (Schunemann et al., 2015)

The process of manufacturing user-generated infill strategies and structures can be done through comprehensive software, such as Simplify3D®. However, this research has not explored the use of stacking to fabricate more complex infill patterns. To demonstrate the importance of having knowledge about an infill pattern for the built parts, the parts made with default rectilinear, grid, and honeycomb infill patterns are more efficient and much stronger. Thus, PDM displays opportunities for design by offering control of the tool paths and infill patterns with various properties of the paste materials. In conductive paste deposition, the high density of the infill pattern leads to high conductivity, as there are fewer gaps in the material. To demonstrate these patterns, the good attributes identified from the experiments were used to manufacture a final conductive print.

2.10.5 Support and build orientation

Support and build orientation play a significant role in the 3D printing process. They can enhance the part quality concerning accuracy and surface finish. Support structures are used with RP that employs a large liquid bath, such as the SLA technique while there is an FDM support material that dissolves when placed in a bath of chemicals. As mentioned earlier, 3D samples printed with parts overhanging by up to 45° need a support structure to avoid collapse. However, the use of a support material introduces a series of limitations, as it increases the volume, the manufacturing time, and the cost of material manufacturing and it affects the part strength. Therefore, several approaches have been proposed. For example, Leary et al. (2013) developed methods to achieve a reduction in the amount of material consumed and the cost. One method was to use only orientation module software (ORM) to determine the best orientation for complex geometries, so they can be printed without support materials. Likewise, Strano et al. (2013) claimed to have discovered a new approach to AM processes by using Matlab algorithms for the design and optimisation of support structures. However, they used their algorithms only for cellular support structures in the SLM process, while in some processes, such as in FDM, the purpose of the support material is to give a temporary mechanical support for the overhanging layers of the part. The support materials used in FDM were a water-soluble material, a modelling material, and a solvent soluble material. Recently, a polymeric composition material for use as a temporary support material in dual FDM extruder has become available. Nevertheless, for a single head, it would be difficult to use FDM for building parts, as it takes longer to change between build and support (polymeric composition) filaments, and 3D parameters.

The influence of the orientation in FDM is relatively small due to unclear layers. Furthermore, many options can help designers to minimise support materials in the FDM process. The paste deposition-based stepper motor process is quite different to FDM and SLM. It has not yet been demonstrated whether the support materials are needed for complex geometric parts or even for some printed parts in PDM, and if so, what types of support material can help PDM printed parts. Schunemann et al. (2015) demonstrated that PDM could produce samples based on silicone in seashell geometries without any support material being used. However, they were redesigning

their parts to avoid using support materials although silicone is viscous enough to be self-supporting (Figure 2.29). Hao et al. (2010) printed a Newtonian material, such as chocolate, where it is hard to understand the flow properties in simple and easy geometries. However, the 1.25 mm diameter tip nozzle did not meet the requirement for high accuracy, and they used ChocALM software with their simple parts so that no support structures were needed, as shown in Figure 2.30.

Figure 2.30: Simple square printed in chocolate (Hao et al., 2010)

The design of 3D food constructs relies on three factors: viscosity, applicability, and post-processing. In addition, 3D tools and parameters, such as nozzle diameter, tube size, and feed rate, also influence the 3D building of parts in most of the paste materials. Therefore, there are still many impediments to 3D PDM being used in place of conventional manufacturing fabrication processes. The various tasks faced by 3D paste deposition technology, especially in the field of electronic engineering, are referred to as process functionality.

2.10.6 G-code

The 3D PDM based on an extrusion tool installed in an FDM RepRap printer needs a user readable file format that specifies the print in order to manufacture parts. The PDM as an RP process manufactures parts in a layer-wise manner directly from 3D CAD models. Therefore, there are several slicing techniques available to slice the geometric model into layers and to produce a motion code, and one of most popular is the STL file format. Then, it is necessary to transfer these layers to the 3D open source printers using the programming language. The G-code of each layer can be generated by free and open-source software (FOSS), such as Slic3r (Wijnen et al., 2014), and PowerMILL software (Chang, 2004). Schunemann et al. (2015) used a trial version of software called Mach3, but this is limited to 499 lines of code, which means it is very limited when it comes to building 3D parts. A simple OpenScad that splits up a 3D file into separate layers for different materials has been developed. However, OpenScad does not focus on the artistic aspect of 3D modelling.

Hence, the paste material PDM was designed to replace the FDM extruder of open source printers, or it could be printed in both extrusions as dual-print. Therefore, the optimal parameters for layers of 3D PDM should be investigated. The advantages of using G-code and paste materials are that it is possible to change, adjust, and modify the size; to specify the amount of filament that should be deposited and where; and to take account of other critical parameters. This will leave many users free to prepare and edit the build material for the desired application. Nevertheless, material properties must be considered, as the paste material must be in a state of optimum viscosity and must be self-supporting to avoid the need for time to be left between the layers to allow the material to cure and harden compared with other processes.

2.11 3D Printed EDLCs Applications

An EDLC is used to support a smartphone battery, as it combines the high energy densities of batteries and the fast charge/discharge rates of EDLCs. It can provide enough energy to power a laptop battery, meaning that the EDLC can supply the power (laptop) if there is a lack of power due to a short or due to the power source shutting down. EDLCs have attracted considerable attention in recent years because of their possible application in electric cars. Based on different situations, some applications need the floating power source to have a high cycling capacity, supreme power, high reliability, and a range of functional temperatures. For example, in audio systems of standard power, the battery would supply power to long low current loads whereas the EDLCs would perform as a floating power source providing and taking powerful short-term pulses to start the device. Another promising application of 3D printed supercapacitors is for powering an electro chemiluminescent protein immunoassay for a voltage-driven biosensor as described by Kadimisetty et al. (2016). The electrolyte selection depends on the application of the EDLC. It is noteworthy that the polymer electrolytes with low values of activation energies are desirable for practical applications.

2.12 Chapter Summary

The previous literature on the fundamental function, the construction, the type and design, the flexible electrodes, the electrolytes, and the substrates of EDLCs were concluded in this chapter. Also, the research literature shows that there have been different methods for manufacturing flexible supercapacitors. Most of the recent manufacturing processes for flexible EDLCs pay more attention to the new active materials that can improve energy performance and flexibility. Furthermore, the 3D printing technology based on dual deposition heads is an established way of fabricating flexible EDLCs. 3D printing has the potential for a wide variety of electronic applications because of its simple process and low cost, and the broad range of material formats, such as paste or solid filament, that can be utilised.

2.13 Research Gap and Questions

Both previous and current literature have identified a gap in the manufacturing processes for flexible EDLCs. However, due to the material structures and the complexity of manufacturing processes involved, it would be beneficial to find a novel method of manufacture and to manipulate the fabricating parameters to make it possible to produce functional, flexible supercapacitors in a single manufacturing process. The materials used for 3D printers are not yet suitable and accessible for the manufacture of functional, flexible EDLCs because the electrical and electrochemical properties of available materials that could be deposited using 3D printers are so weak. Also, the mechanical properties, such as bending and twisting, are extremely limited. Therefore, it would be beneficial to prepare and design materials that are flexible and to control the process parameters to make it possible to deposit them with a 3D printer. This would be a substantial step forward, and flexible EDLCs could be manufactured with the proposed material.

With the 3D printer software Simplify3D®, there are several different patterns that the designer can choose to make the tool paths. Also, there is an option to modify the G-code for 3D printers, as it is complicated and gives various parameters. The EDLC printed parameters, for instance, layer height, part orientation, feed rate, and infill structure, are essential characteristics for the manufacturer, as the layer height and infill patterns of a tool path can have a significant effect on the final printed EDLC and

can determine how much material is used and how long it will take to build an entire working flexible EDLC. Therefore, it would be useful for the designer and electrochemist to already have basic information on how a 3D printer behaves and how it manufactures flexible EDLCs.

This research seeks to answer the following research questions, where original studies of the manufacturing process of flexible EDLC can take place:

- Can the flexible EDLC components be fabricated by a commercial AM process (3D printing) so that the designer is free to select how they are made and how they perform with a large range of parameters?
- Can flexible electrical double-layer capacitors based on AC slurry and gel electrolytes be manufactured in a single inexpensive manufacturing process?
- Can the conductive and active paste materials be used in the 3D printer to make flexible EDLCs that take advantage of the electrochemical properties of a paste material?
- Is it possible to manufacture flexible/wearable EDLCs using 3D printing technology?

Chapter 3 Methodology

3.1 Introduction

The research discussed in Chapter 2 has shown how to make use of FDM printing, and has highlighted the importance of the developments in 3D printing using conductive or active materials. There are several general approaches to making a conductive paste or conductive filaments. Printing with some conductive or active materials and user-created parameters can be difficult; this becomes especially challenging in AM technologies. It was believed that there were limited active and conductive materials that could be used with AM and the development of these materials is a key element in this thesis. The majority of this chapter is concerned with describing the materials and manufacturing processes used in this research, and the experimental methods used. It also discusses the measurement techniques, which are applied to the energy storage devices.

3.2 Experimental Design

Before the commencement of the research phase of this project, a review of established research methods was undertaken. The purpose of the work was to find out and select the most suitable research methods (Figure 3.1) that would yield the most significant knowledge and help to address the research questions outlined in Chapter 2. The research methods can be divided into three phases, according to Poggenpohl and Sato (2003, p.127).

The first phase involved preparing a literature review to support and to formulate research questions. Phase 2 worked with trial experiments to support and find method and to address the research question, and iterate to find the best method, as well as evaluating the equipment. Phase 3 used the knowledge obtained from previous phases to produce case studies that were undertaken to develop and be implemented to make suitable devices.

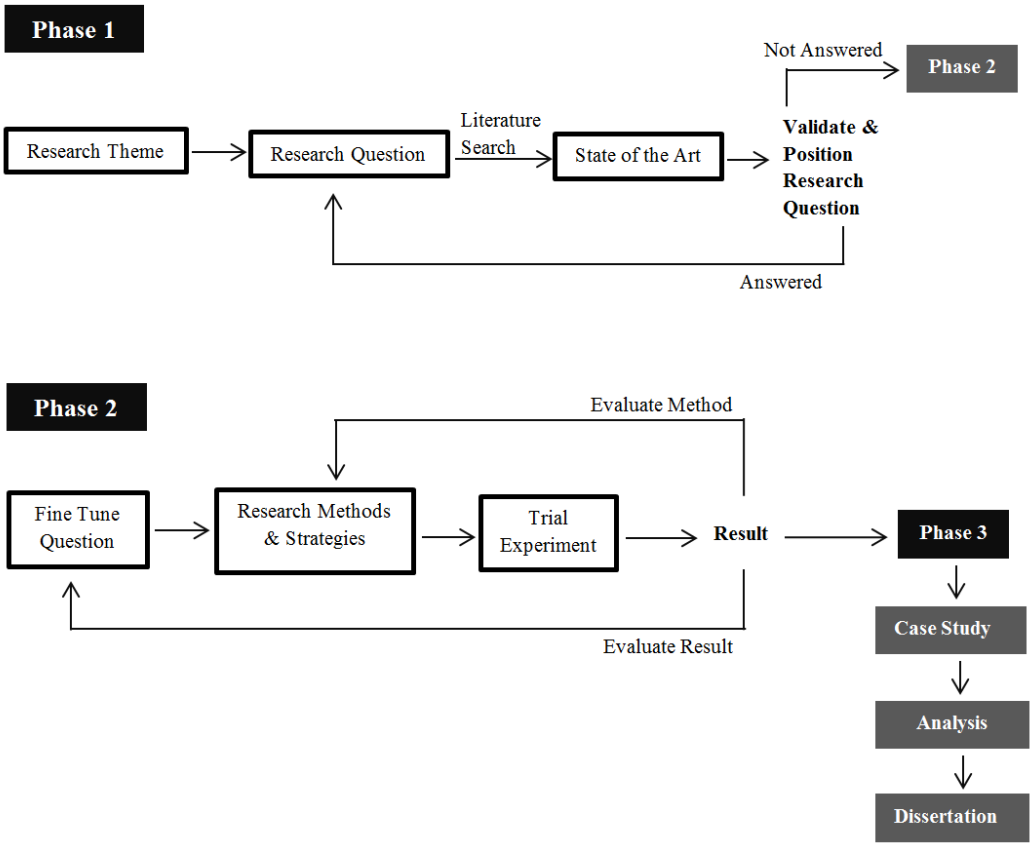

Figure 3.1: Experimental model used for the research project (Poggenpohl & Sato, 2003, p.127)

Figure 3.2 shows the development process used to manufacture the flexible energy storage device and how it was made. There are four main steps of the development process. The chart illustrates the first-step of the process for three main EDLC components and two forms of the substrate. The second step corresponds to the control of the 3D deposition printer. The AC slurry, gel electrolyte, and current collector paste are made and loaded into the syringe. Once the syringe is connected to the nozzle and tube, the 3D CAD file is sent to the printer and controlled by simplify3D®. It is now that a syringe manipulated with a stepper motor deposits the substrate continuously. The process is repeated for the electrode, and gel electrolyte until the EDLC part is complete. The two printed parts are sandwiched and then taken to the air vacuum container to remove any air, and finally the EDLC is tested using an electrochemical workstation, thereby allowing the determination of how the 3D process influences EDLC behaviour.

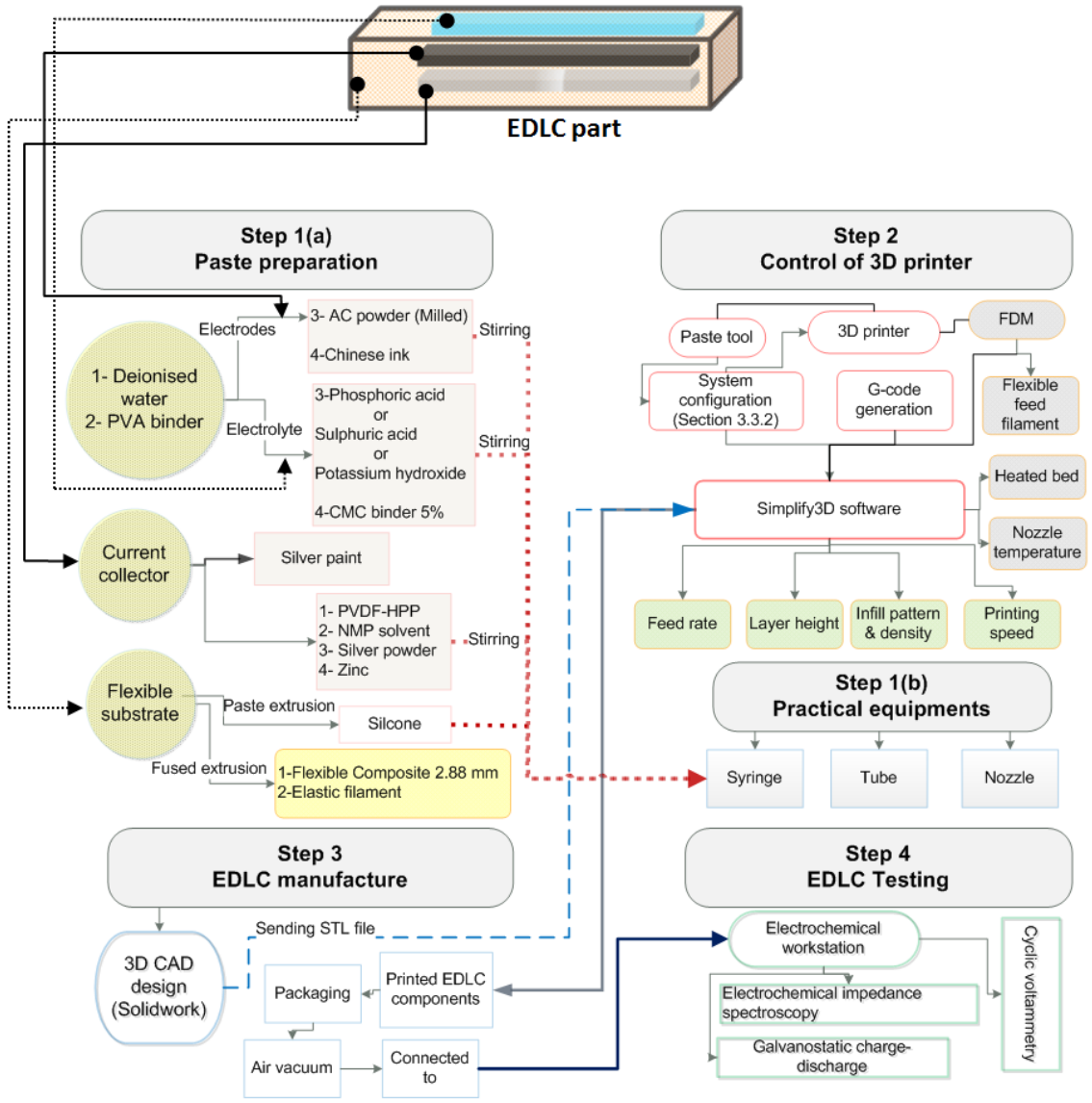

Figure 3.2: The structure of manufacturing process of flexible EDLC

3.3 Preliminary Test and Equipment

The way the equipment utilised changes is reliant upon the hardware. It is necessary to learn how various sorts of machines behave and to assess which parts to use for the investigation. Data collected during these tests showed how the configuration of the machine changed device properties and the functional parameters that were to be used in later phases of exploration. Hence, the next step included some tests with silicone materials and equipment to determine what paste materials structure and equipment were needed for the research since one of the targets of the research is to reduce the waste of paste materials that are prepared in the process.

3.3.1 Discov3ry paste extruder tool

Sections 2.9 and 2.10 discussed various processes for filament deposition, such as FDM extrusion that seems to be most used due to its low cost. The materials were limited to only materials those that could be heated. The extrusion process used by Schuneman et al. (2013) showed some advantages such as low-cost syringes which can be used changed quickly. Also, it would not require much maintenance with highly viscous materials. However, the drawback is that the feed rate pressure is manipulated manually by an air solenoid and this is makes the process more difficult. A direct drive such as a NEMA 17 stepper motor offers several advantages.

As shown in Figure 2.26, the Discov3ry paste extrusion operates at about 1:100 speed (RPM) to obtain the equivalent output flow rate. The specification can be found in Appendix C. Because of this ratio, a high-stress load is created on the stepper drivers when operating with higher viscosity pastes. However, 3D printed gears were added to this extrusion system to lower the cost for FDM printer users further. These are of double helix type to allow the gears to self-centre. This extruder head has the advantage that it can be mounted on FDM printers and offers different sizes of low-cost quick-change syringes (Structur3D®, 2014). Hence, the use of Discov3ry extrusion is good for the work described in this thesis.

3.3.2 System configuration

A Discov3ry extruder was connected to the main Ultimaker® machine. The frameware was installed by using software (CURA® 15.04.03) as resources for Ultimaker2-dual.hex and then transferred to the machine to work in a dual extrusion system. X Y and Z motor cables were attached to the corresponding connectors on the electronics board. The FDM extruder motor cable connects to the (E1) connector and the paste extruder motor at (E2). A high-temperature sensor model (PT100 B, Ultimaker®) should be connected to the electronic integration for paste extrusion set at 0°C i.e. cold extrusion, to avoid any error in the FDM printers. However, the extrusion was configured in the machine and the distance from the head nozzle to the bed plate was reset by using an ordinary white paper, which is already fixed at 0.8 mm. The nozzle tips of both extrusions were around 37 mm apart, and for the printed layer to line up,

a fixture offset was used by simplify3D®. To set up the fixture, the Discov3ry nozzle always had to be zeroed to the same point, as in Figure 3.3.

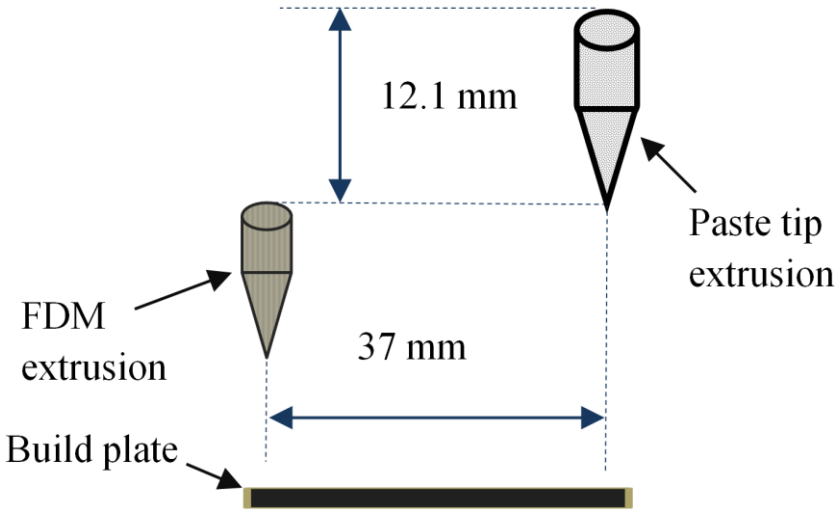

Figure 3.3: The nozzle tips of both extrusions

3.3.3 Paste deposition head and equipment

The deposition head parts were designed in Solidworks® and they were printed by an FDM printer in PLA filament material. First of all, one of the printer fans was removed to install a holding clamp for the paste extrusion nozzle. The syringe barrel hose was attached to the printer by an adaptor hose that attached to a printer head with a quick release fitting and to be connected to the nozzle hub; see Figure 3.4.

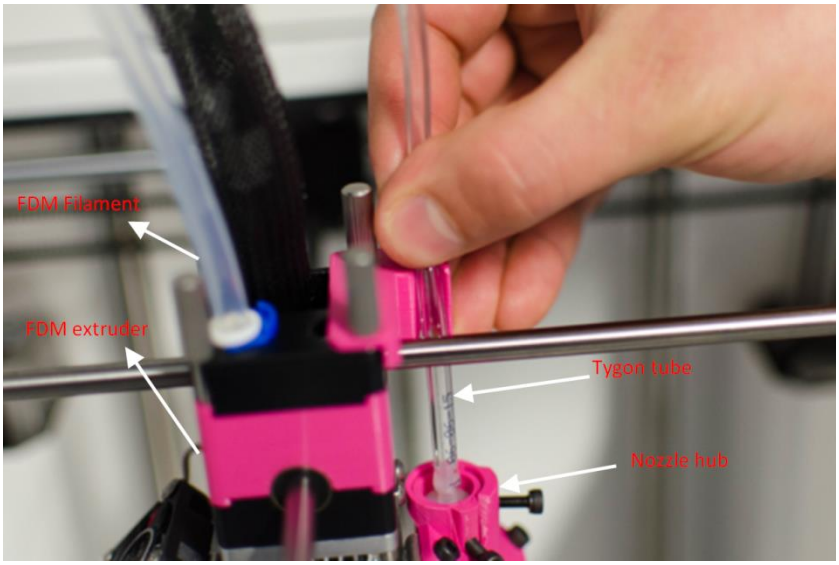

Figure 3.4: The quick release fitting

The parts were assembled and a Tygon tube, 45 cm in length, was connected to match the materials flow (see Appendix A). The syringe holder clamp, nozzle hub and adaptor, extruder line fixture, syringe barrel and piston were also connected. The Discov3ry extruder with a range of deposition nozzles and Ultimaker® hot end extruder were supplied. For several further tests, a 0.4 mm hot end nozzle and 0.4 mm and 0.6 mm tapered nozzles (Figure 3.5) were used for Discov3ry extrusion. Syringe barrels were used of several volume sizes; the barrels utilised for several tests were 50 cc, 30 cc and 20 cc, with an inner diameter of 26.67 mm, 22.63 mm and 18.28 mm, respectively (Adhesive Dispensing, 2005, A).

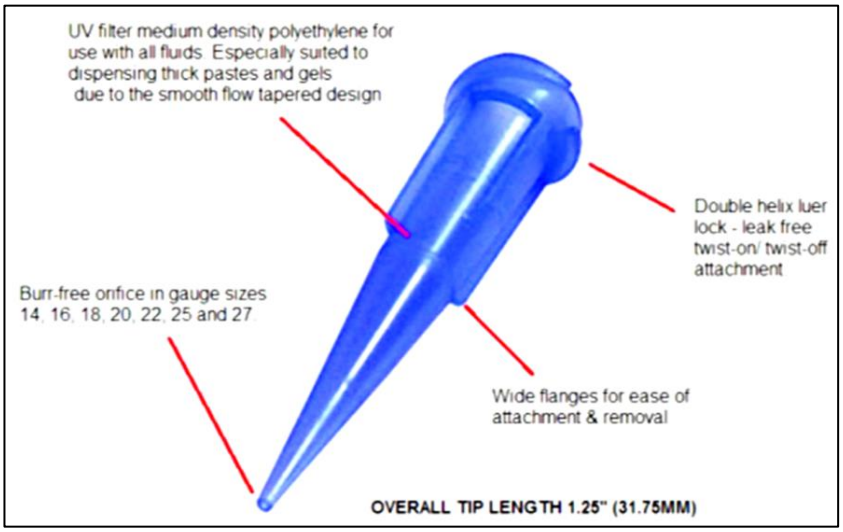

Figure 3.5: Tapered nozzle (Adhesive Dispensing, 2005, A)

3.3.4 Material selection

Combining the process and materials that were approved involved using a case study, which is making an electrical double-layer capacitor. Composite textiles, conductive material deposition, and inclusive G-code were developed. The functional components of a supercapacitor that are crucial to its operation are the electrodes, electrolyte, and current collectors. The most important material considerations would be the electrode material as it has a significant impact on specific capacitance (Chen et al., 2012). The material used for the first attempt was a commercial AC powder supplied by Sigma-Aldrich® (see Appendix E).

AC slurry was prepared at several concentrations to work as electrodes for EDLCs. Details of an optimum smooth flow AC slurry and more recipe details can be found in the next section. The choice of electrolyte in the EDLC is as important element as is the selection of electrode material. The maximum cell voltage of an EDLC will depend on the breakdown voltage of the electrolyte. However, there are two types of electrolyte in use in EDLCs: organic and aqueous, and because of the need to identify the research method, an aqueous gel electrolyte was selected. The process of preparing gel electrolytes is covered in the next section. To successfully create the supercapacitor, the frame part was designed and manufactured. The nature of the outside surface or 'shell' of the EDLC part is a major factor it seals the EDLC components from leakage or to losing efficiency by air attack. Hence, due to the aim of this research to print flexible

composite materials for the EDLC's parts, several materials were printed and investigated for manufacturing an energy storage device. The Laywoo-D3 FLEX created by Kai Parthy was chosen due to its design for FDM extrusion and its flexibility (3ders, 2015). NinjaFlex, a rubber-like elastomer material was selected due to its design for an FDM extruder, and it sticks well to the build platform and good bonding between layers, with optimum strength and elasticity. Dow Corning silicone sealant and 'Nonsense' sanitary silicones were chosen as they were designed for extrusion through nozzles, but issues arose during deposition (see Appendix D).

Chemicals and substances

Silver conductive paint with a volume resistivity of 0.001 Ω. cm was purchased from RS® Components Ltd. A flexible LAYWOO-FLEX 3 mm diameter filament created by Kai Parthy, and NinjaFlex 3 mm flexible material were used for EDLC substrates. Double face sticky tape was purchased from 3M® to be used on the 3D build plate. Silver powder was purchased from Gwent Group®, and Zinc metal powder (Zn, MW 65.38, SciChem®) were used for the current collector paste. Acetoxy silicone sealant clear (Dow Corning 781) was supplied by Screwfix®. All other materials including the AC powder (AC, AR grade, Cat. No. 05105, 1375 μΩ. cm, MW 12.01 g/mol), sodium carboxymethyl cellulose (CMC, MW 250,000), polyvinylidene fluoride-co-hexafluoropropylene (PVDF-HFP, MW 400,000~130,000), polyvinyl alcohol (PVA, MW 146,000~186,000, 99+% hydrolysed), 1-methyl-2-pyrrolidinone (NMP, 1.028 g/mol) sulfuric acid (H_2SO_4, 98.08 g/mol), and phosphoric acid (H_3PO_4, ≥85%, ACS grade) were supplied by Sigma-Aldrich®. The capability to use many different forms of materials made the 3D printing method useful for a large choice of applications.

Preparation of AC slurry electrode

To prepare various paste materials, a hot plate with a magnetic stirrer (JENWAY 1000, Bibby® Scientific) and oven with a maximum temperature of 300°C (Binder, Germany) were used for the entire project. It is believed that the AC paste is an effective material for a 3D paste deposition method as it is conductive, cheap, easy to prepare and frequently used for supercapacitors. A half gram of PVA was mixed with 10 ml of deionized water, and stirred by a stir bar at 50°C for 1 hour. 5 g of AC powder was heated at 80°C in an oven for 2 hours before using to ensure high capacity, then mixed continuously with the binder PVA solution and kept stirred for 24 hours. This made a

paste and was unsmooth since the AC powder was coarse. Therefore, the slurry needed pre-treatment before using because of the coarseness. However, several forms of AC slurry were prepared to obtain the smoothness of slurry necessary depending on the deposition parameters. The practical way to avoid any air bubbles and ensure an optimum deposition for most of the slurries was to use the front fill method throughout the project as shown below with AC slurry as shown in Figure 3.6.

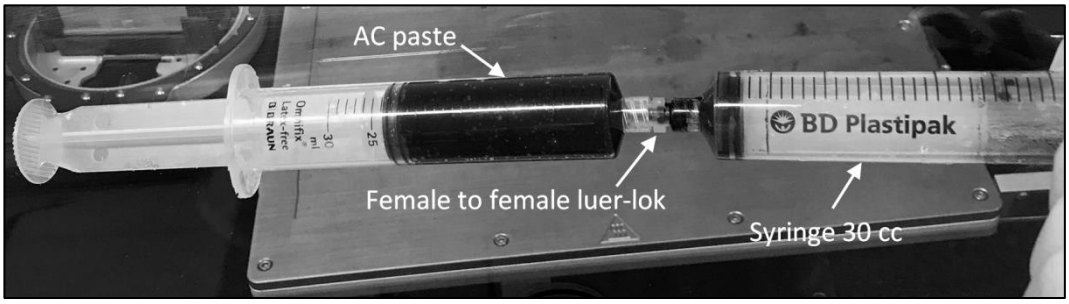

Figure 3.6: Filled syringe with 30 mL of AC, front fill method

Preparation of the gel electrolyte

The polymer gel electrolyte preparation was discussed by Zhang et al. (2015) and showed how effective it is when used as a separator in supercapacitor fabrication. It was used as it is a suitable gelling material having high dielectric strength, and excellent charge storage capacity with high ionic conductivity that can be obtained in amorphous polymers, as well as having a sufficiently flexible backbone (Sheha & El-Mansy, 2008). The gel electrolyte was prepared by the following method: 0.5 g of PVA powder was added to 10 mL of distilled water and was heated at 80°C for 1 hour. 0.5 g of CMC (5%) as a binder was then added, with constant stirring overnight, resulting in a clear gel. The electrolyte was sulfuric acid (H_2SO_4) allowed ionic transport in a separator between the electrodes of the supercapacitor. 1 mL of H_2SO_4 was then mixed with the above gel mixture. The gel electrolyte was prepared by adding the acid in a drop wise manner with magnetic stirring at 30°C for half an hour, and then with magnetic stirring overnight until it ultimately transformed into a homogeneous gel. Most of the gel electrolytes were loaded into syringes by the front filled method as shown in Figure 3.6.

Preparation of the current collector paste

It was difficult to prepare a conductive paste with a good bonding to the substrate used in 3D printing, especially when silicone was used as the substrate material. 1 g of PVDF-HFP pellets were dissolved in 15 mL of NMP at 40°C for an hour at first. After that, 4.5 g of zinc metal powder was mixed with 5 g of silver powder (Ag) and added to the solvent/polymer mixture and constantly stirred overnight. PVDF as a type of piezoelectric polymer that enhanced the bonding of silver and zinc particles, and therefore improved the conductivity of the current collector.

3.3.5 3D Deposition trials of silicone

The purpose of this test was to investigate the influence of deposition pressure on the deposited line. Acetoxy® silicone and nozzle sizes 0.8 mm were used to estimate the material flow rate. First of all, the syringe was filled with 50 mL of the silicone, mentioned above, by a front fill method from the applicator gun to avoid any air bubbles, as shown in Figure 3.7.

Figure 3.7: Front fill method

After the syringe was filled, the nozzle was modified, and the G-code command was setup to the 3D printer, as shown in Table 3.1. The G-code was generated by Simplify3D® software version 3.0 for printing with paste materials. There are several ways to prepare a G-code for a printer, such as Slic3r® or Skeinforge® to transfer a CAD model and slice it into layers, while in this case, the 3D printing machine that was used was a RepRap design with Arduino Mega 2560 chips. The G-code commands supported by Marlin 3D printing firmware are compatible with an Arduino controller. The first

process was to import the object (EDLC) into divided CAD parts as shown in Figure 3.8(a). The manufacturing process was divided based on EDLC CAD parts and requirements, and each part has individual parameters. As shown in Figure 3.8(b), based on the material rheology, the optimum layer height can be selected. The manufacturing process could be set up as single extrusion or dual extrusion, and an offset can be applied easily through the G-code option. Figure 3.8(c) shows how to write and use the G-code scripts in the software, the starting script, tool, and ending script of G-code. It was manually modified to contain different commands such as nozzle wipe and feed rates. Due to there being many part processes they were divided based on the EDLC structure, all the parameters were set up, and a printing button is pressed, sequential printing (object-by-object) can be selected or continuous printing (layer-by-layer) as shown in Figure 3.8(d).

Table 3.1: List of G-code commands

Command	Description
M302 S190	Set safe Ultimaker^2 extrude to 190 °C {IF NEWTOOL=0}
M92 E282	change steps per mm to default if using Ultimaker^2 extruder {IF NEWTOOL=0}
M92 E18000	change steps per mm to high if using Discov3ry extruder {IF NEWTOOL=1}
M302	set safe Discov3ry extrude to 0 °C {IF NEWTOOL=1}

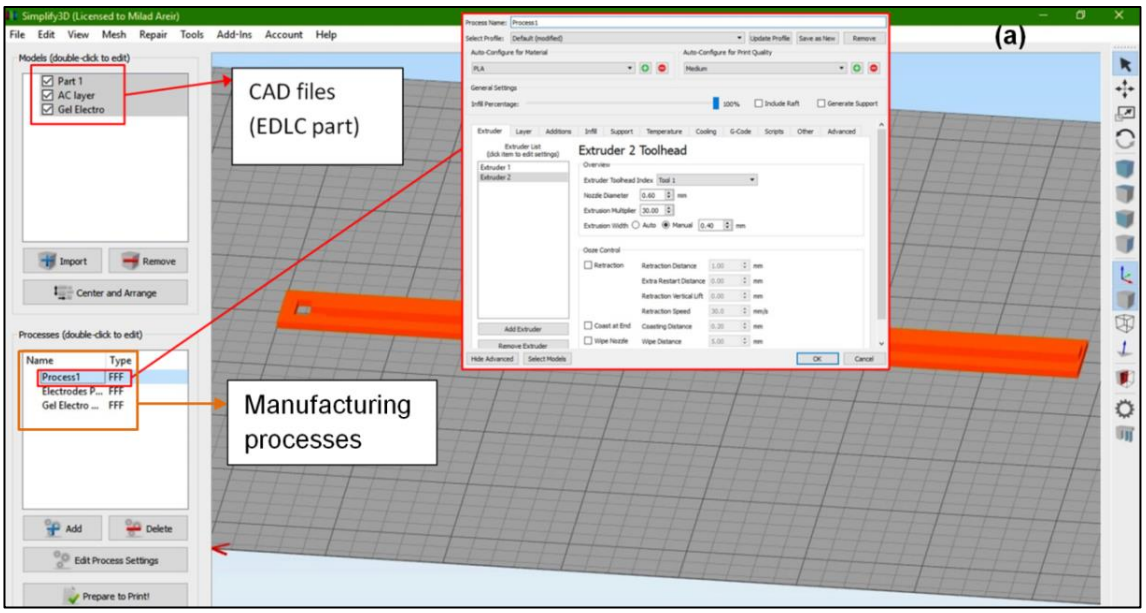
(a)
CAD files
(EDLC part)
Manufacturing
processes
Models (double-click to edit)
Part 1
AC layer
Gel Electro
Import
Remove
Center and Arrange
Processes (double-click to edit)
Name
Type
Process1
FFF
Add
Delete
Edit Process Settings
Prepare to Print!
Extruder 2 Toolhead

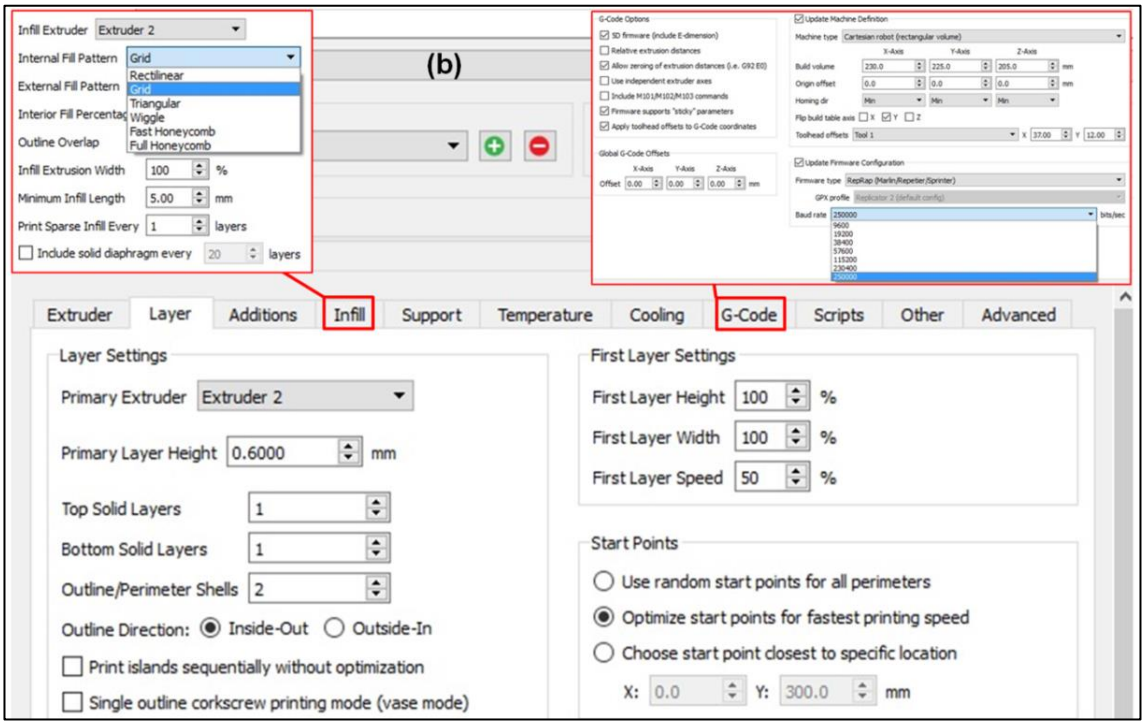
(b)
Infill Extruder
Extruder 2
Internal Fill Pattern
Grid
External Fill Pattern
Interior Fill Percentage
Outline Overlap
Infill Extrusion Width
100
%
Minimum Infill Length
5.00
mm
Print Sparse Infill Every
1
layers
Include solid diaphragm every
20
layers
Rectilinear
Grid
Triangular
Wiggle
Fast Honeycomb
Full Honeycomb
Extruder
Layer
Additions
Infill
Support
Temperature
Cooling
G-Code
Scripts
Other
Advanced
Layer Settings
Primary Extruder
Extruder 2
Primary Layer Height
0.6000
mm
Top Solid Layers
1
Bottom Solid Layers
1
Outline/Perimeter Shells
2
Outline Direction:
Inside-Out
Outside-In
Print islands sequentially without optimization
Single outline corkscrew printing mode (vase mode)
First Layer Settings
First Layer Height
100
%
First Layer Width
100
%
First Layer Speed
50
%
Start Points
Use random start points for all perimeters
Optimize start points for fastest printing speed
Choose start point closest to specific location
X:
0.0
Y:
300.0
mm

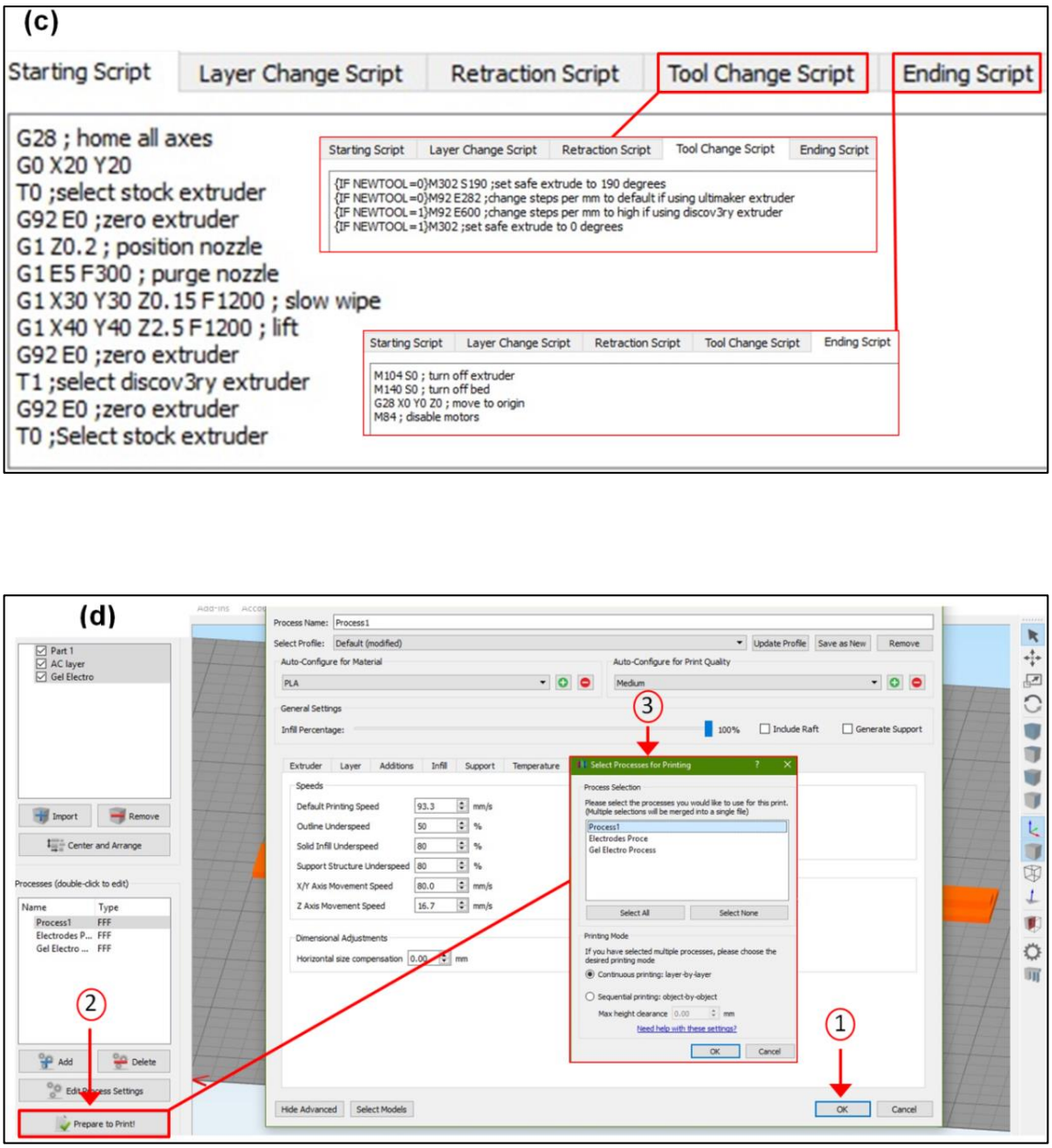

Figure 3.8: Screen shot of simplify3D software, (a) paste extrusion parameters; (b) layer height and patterns, (c) G-code script, and (d) layer-by-layer or object-by-object

The setting led to build failure. The mechanical backlash was enormous, and the extrusion did not start until 500 mm/min. The extrusion continued for over 20 min after the extruder stopped. Timing is imperative when switching materials and the extruder was too slow to deposit precisely as the retraction needs to be less than 1 second to avoid any mechanical issue.

To conclude, using retraction to equalize pressure was not practical as it would be very large; the backlash and the pressure had to build up in order to extrude. The Discov3ry extruder might be more suitable for constant extrusion rather than stopping and

starting when switching materials. Hence, the attempts failed to meet our requirements. To address this issue, the syringe size was changed from 50 mm to 30 mm. The extrusion multiplier was gradually increased from 20 to 30 and then to 40. The result was 1 cm ± 1 length deposited within 58 seconds. However, the main gear of the Discov3ry started bending, and the whole operation stopped to avoid damage as shown in Figure 3.9.

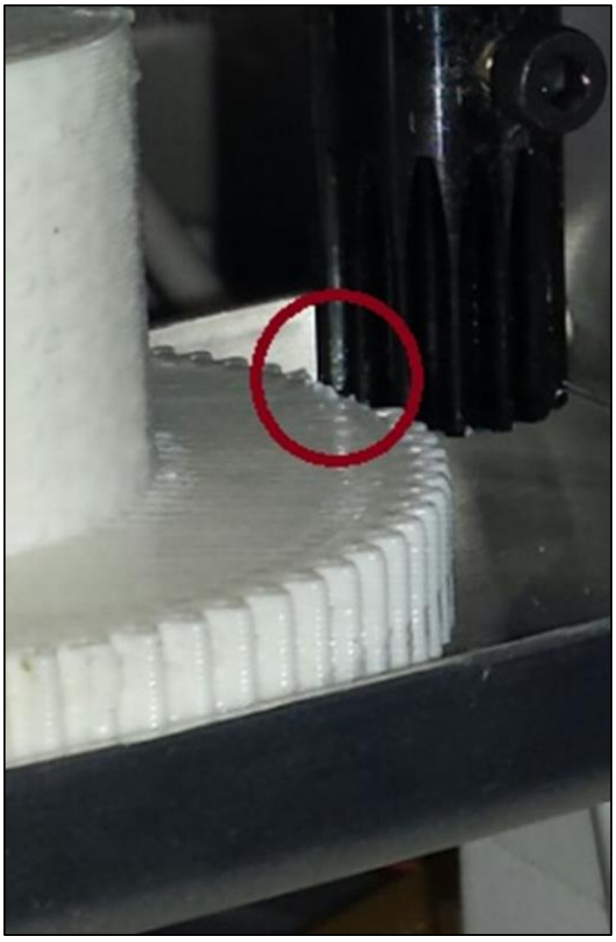

Figure 3.9: The main gear of the Discov3ry

However, another factor was probably that the material was not fresh or an inherent property of the material. Several different silicone materials might be good for deposition. Since the materials may have a different viscosity, different print quality outcomes can be expected. For example, the builds produced during the last test almost depleted the material in the 30 cc syringe; larger 55 cc syringes were sourced by (Adhesive Dispensing, 2005, B). Finally, the reverse loading method ensured that no air was introduced into the paste, but a few guidelines need to be considered to obtain longer life out of the paste extrusion are as follows:

- Using silicone with a minimum work time of 45 minutes.
- Using a print speed and/or multiplier that did not exceed 150 mm/s for the stepper motor.
- If using retraction, a few lines of retraction code were added into the G-code throughout the print (like e.g. 10-50 mm at one time).
- Using larger tip sizes for more viscous materials (this reduces the pressure build up in the system).
- Tygon tubing can also be used to enhance the material flow further.

3.4 Measurement Techniques

In a symmetrical two electrode cell, the electrode is a crucial component that determines an EDLC's capacity and how it behaves. There are different techniques for determining and evaluating the capacitance (*C*). Cyclic voltammetry (CV) is the most extensively method used for evaluating the capacitance but other methods: Galvanostatic charge-discharge (GCD) and electrochemical impedance spectroscopy (EIS) test were used for sophisticated investigation, for instance, to look at frequency effects and to measure corroding systems.

3.4.1 Cyclic voltammetry (CV)

CV is a test of potentiodynamic electrochemical measurement and used for analytical purposes. The most common of the CV curves is shown in Figure 3.10, where voltage (V) is plotted on the x-axis and current (A) on the y-axis. The charge passed measured in coulombs per area (Q) is a measure of the number of electrons used per unit area. The voltage in the x-axis is the electron potential. If an electron is added to the electrode that is called reduction or losing an electron called oxidation as the voltage turns more positive. When an oxidation or reduction occurred, the current in y-axis become a faradaic current and the voltage of the current peaks is determined by the redox voltage of the material. This allows observation of reactions on the surface of an electrode. Multiple CVs test should be applied at different scan rate (V/s) to understand the ion diffusion from the electrolyte through the porous of AC and give more information such as conductivity of electrolyte and porosity.

A Princeton Applied Research electrochemical workstation/VersaSTAT 3, within a potential range of 0 V to a given voltage (±0.8 to 1 V) at different scan rates, was used for preliminary characterisation of AC printed electrodes and was controlled by VersaStudio® software (v2.50.3). A CV test was used through the entire project and recorded for each EDLC sample for the evaluation and comparison of the effect of various parameters, for instance, thickness, infill pattern, and fill density on the EDLC electrical properties. Figure 3.10 shows an example of the CV measured of an expimental EDLC, and the broken line shows the behaviour of an ideal EDLC. The CV should be a symmetrical quasi-rectangular-shaped curve.

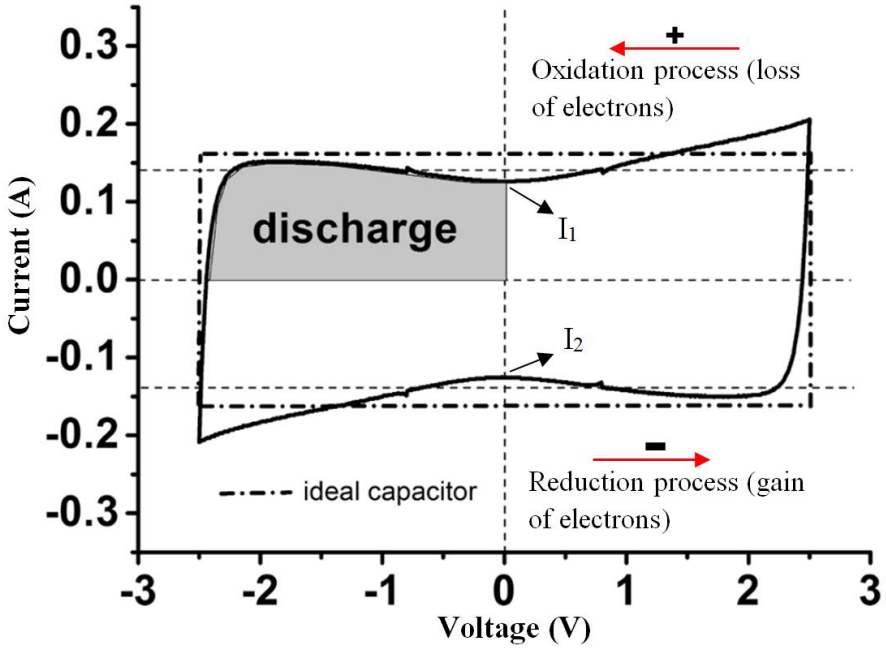

Figure 3.10: CV of the ideal electrochemical double layer capacitor (Lammel et al., 2013)

The primary purpose of the CV test is to use it to calculate and measure the capacitance (C) using:

$$C = \frac{\mathrm{Q_{total}/n}}{\Delta \mathrm{V}} \qquad (1)$$

Equation 1: where C is the Capacitance in farads (F), $\mathrm{Q_{total}}$ is the supercapacitor charge in coulombs (C), n is the number of electrodes, and ΔV is the change in voltage (V).

Also, we can calculate the capacitance from the CV test from the scan rate using the equation:

$$C = \frac{\mathrm{i}}{\Delta V/\Delta t} \qquad (2)$$

Equation 2: i is the current in Ampere (A), and ΔV/Δt is the scan rate (V/s).

The area-specific capacitance (C_a) of the supercapacitor can be calculated from the CV curves using:

$$C_a = \left({}^{1}\!/_{2\mathrm{A}(\Delta \mathrm{V}/\Delta \mathrm{t})(V_f - V_i)} \right) \int_{V_i}^{V_f} I(V)\Delta \mathrm{V} \qquad (3)$$

Equation 3: A is the area of the electrodes (cm^2), $\Delta \mathrm{V}/\Delta \mathrm{t}$ is the voltage scan rate (V/s), final voltage ($\mathrm{V_f}$) and initial voltage ($\mathrm{V_i}$) are the potential limits of the CV curve, and $\int_{V_i}^{V_f} I(V)\Delta \mathrm{V}$ is the numerically integrated area of the CV curve (Wang et al., 2017).

3.4.2 Galvanostatic charge-discharge (GCD)

The GCD technique seems to be the most useful and reliable technique for obtaining a large number of parameter values. The typical GCD method can be extended to characterise the electrochemical behaviour of EDLC materials. GCD technique is often used to evaluate the specific capacity, equivalent series resistance (ESR) and cycling stability of the EDLC. Also, the GCD was used to identify the charge and discharge time and how fast the EDLC can store energy. As shown in Figure 3.11(a), this measurement method moves a constant current through the current collector and measures its electrochemical behaviour as a function of time. The current is passed until a set voltage is reach on maximum possible for the particular electrolyte before faradaic reaction take place. The functional current can be set to change with time, instead of being kept constant. When the cell charged and reached a set voltage, the current is switched to the same amount in the opposite direction and this latter process is called discharge, as shown in Figure 3.11(a).

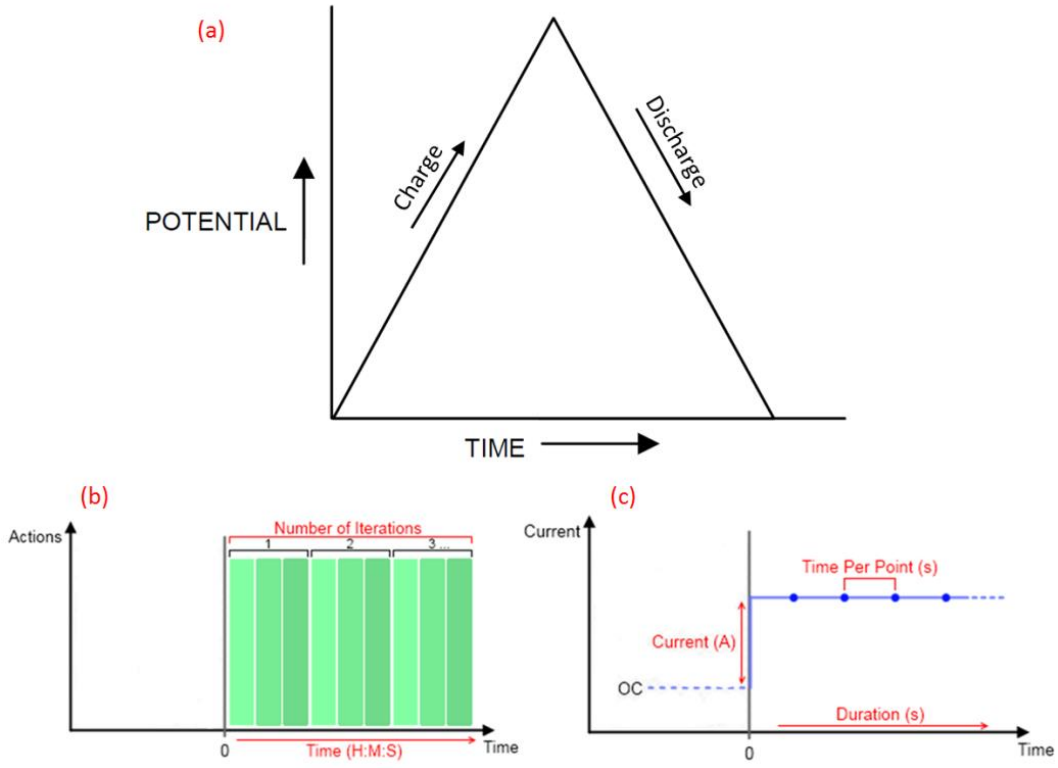

Figure 3.11: (a) GCD of the ideal electrochemical double layer capacitor, (b & c) properties for galvanic pulses curve (Ametek, 2015)

An important factor in GCD test is that when the current is moving in an electrochemical cell, and electron flow through a material, there is a voltage drop (iR drop) that occurs due to the two main factors: the distance between the two electrodes and gel electrolyte conductivity. GCD was carried out using an electrochemical workstation for the rest of the research project. Mostly, the cell properties applied through Versastudio® software were the current of 15 mA, and time per point of 0.025 s and total duration was 400 s, and the number of iterations between 5 to 10 cycles as shown in Figure 3.11(b & c). It was therefore advantageous at the initial stages of the project to understand an electrochemical performance and evaluate the energy efficiency. The capacitance can be calculated by:

$$C = \frac{\mathrm{i}.\ \Delta \mathrm{t}}{\Delta \mathrm{V}} \qquad (4)$$

Equation 4: C is the Capacitance in farads (F), i is the current in Ampere (A), and $\Delta \mathrm{t}$ is the discharging time (s) and $\Delta \mathrm{V}$ is the change in voltage (V).

The specific capacitance (C_s) of the supercapacitor device can be calculated as follows

$$C_s = \frac{\mathrm{i}.\ \Delta \mathrm{t}}{\mathrm{m}.\Delta \mathrm{V}} \quad (5)$$

Equation 5: C_s is the specific capacitance in (F/g), i is the current in Ampere (A), and $\Delta \mathrm{t}$ is the discharging time (s), m is the total mass of active materials of two electrodes (g) and $\Delta \mathrm{V}$ is the voltage of the discharge (V).

Also by:

$$C_s = \frac{2C}{\mathrm{m}} \quad (6)$$

Equation 6: C_s is the specific capacitance in (F/g), C is the capacitance calculated by equation (4), and m is the mass of a single electrode (g).

(ESR) is related to the attachment of the electrode particles to the current collector and shows some of the internal resistance of the electrodes. Also, ESR can be described as a sum of all serial resistances within the EDLC, and a higher ESR leads to higher potential drop and lower capacitance. The equation can calculate the ESR:

$$\mathrm{ESR} = \frac{\mathrm{V_{iR}}}{\mathrm{i}} \quad (7)$$

Equation 7: Equivalent series resistance (ESR), $\mathrm{V_{iR}}$ is the iR drop at charge and discharge (V) and i is current in amperes (A).

The energy density and power density are calculated from the GCD curves and equations (8) and (9).

$$\mathrm{E} = \frac{1}{2}\, C_s\, \mathrm{V}^2 \quad (8)$$

Equation 8: E is energy density, C_s is the specific capacitance, and V is the potential range.

$$\mathrm{P} = \frac{\mathrm{E}}{\Delta \mathrm{t}} \tag{9}$$

Equation 9: P is the power density, E is the energy density, and $\Delta \mathrm{t}$ is the discharging time.

The coulombic efficiency (η) is defined as the ratio of discharging time and charging time and calculated by:

$$\eta = \frac{\mathrm{t_d}}{\mathrm{t_c}} . 100\% \tag{10}$$

Equation 10: $\mathrm{t_d}$ is the discharge time (s) and $\mathrm{t_c}$ is the charging time (s).

The energy efficiency (η_{eff}) is affected by the equivalent series resistance (Ω) and C is the capacitance (F) calculated from the GCD curve.

$$\eta_{\mathrm{eff}} = \mathrm{e}^{-2\ (\mathrm{ESR}.\ C)/\mathrm{t_d}} \tag{11}$$

Equation 11: ESR (Ω), C is the capacitance (F), and $\mathrm{t_d}$ is the discharge (s).

3.4.3 Electrochemical impedance spectroscopy (EIS)

EIS or often called a Nyquist plot and is the most complex and sophisticated characterisation technique described in the thesis. It was used to monitor the charge transfer and capacitive behaviour of EDLC. It evaluates impedance (Z) by applying a small sinusoidal (ac) current across a cell and measuring the resulting ac potential (Galvanostatic EIS) or ac (Potentiostatic EIS) along with phase shifts between the ac voltage and current to measure impedance (Z). EIS does not need to apply any voltage or current. It is carried out the measurement over a certain frequency range. The electrochemical workstation performed the EIS (Potentiostatic), and EIS properties were used through this entire thesis used a frequency range from 100 kHz to end 0.01 Hz, and the sine wave (ac) amplitude was 4 mV RMS for AC properties, 10 points per decade for scan properties and 0 V for DC properties. Shown in Figure 3.12, is the typical Nyquist plot for a cell with mixed kinetic and charge transfer control. The ESR of the cell and solution resistance of the electrolyte (R_s), including the resistance of the electrode itself and the ion charge transfer resistance (R_{ct}) can be obtained from the Nyquist plot. An important factor in determining ESR is the strong bonding of the carbon paste material to the conductive current collector.

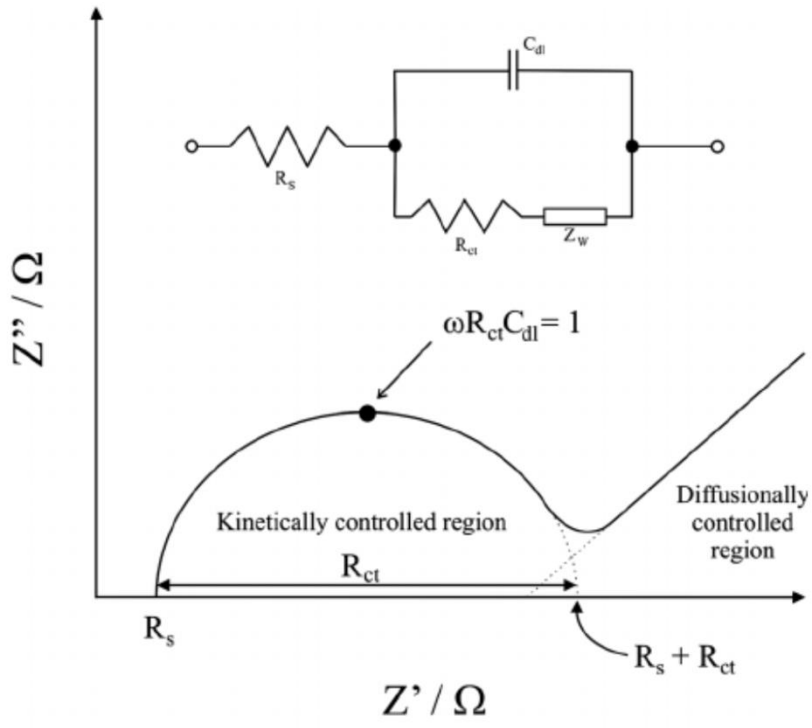

Figure 3.12: Ideal Nyquist plot (Randviir & Banks, 2013)

3.4.4 iR determination (Ω)

The manufacture of a flexible supercapacitor by 3D printing technology is a great challenge, and needs materials' consideration. The conductivity of deposited materials should be high. Also, the geometry of the flexible EDLC should be an ideal to avoid a high resistance. The best way to measure resistance as mentioned in section 3.4.2 is by GCD, but it needs mathematical calculation. Therefore, the iR compensation (iR_{comp}) technique as a current interrupt was applied by the electrochemical workstation to measure and correct the internal resistance. We can calculate the voltage drop (V_{iR}) or iR drop by the iR_{comp} values, using the equation

$$V_{iR} = iR_{comp} \times i_{cell} \quad (12)$$

Equation 12: V_{iR} is the iR drop (V), iR_{comp} is the cell resistance (Ω), and i_{cell} is current in amperes (A).

3.5 Chapter summary

This chapter has outlined the research area and methodology. It presents the versatility of the dual printing deposition process through the use of EDLC component materials. The EDLC electrode pastes and gel electrolyte have been prepared with a PVA binder for the demonstration of 3D printed energy storage device. The desired paste resolution was determined by the nozzle and syringe size. The G-code has been generated and modified using the simplify3D software throughout the research work. The electrochemical measurement techniques were presented in this chapter. All the electrochemical measurements in this thesis were performed at room temperature using a VersaSTAT 3 workstation. The next chapter will show the experimental method for printing a multilayer AC for electrodes by using 3D printing technology. Furthermore, electrochemical investigations will be carried out by taking into consideration the AC deposited layer.

Chapter 4 Initial Investigation of the Manufacturing Process for Electrochemical Double-Layer Capacitors by Dual Printing Extrusion

4.1 Introduction

This chapter describes an initial Investigation of the manufacturing process for electrochemical double-layer capacitors by dual printing extrusion. It describes the development of novel paste materials for electrodes and electrolytes. The 3D printing process parameters and electrochemical performance of the EDLCs are explored.

The details of equipment's, tools, and measurement methods were given in the methodology chapter. The major contribution of this chapter is developing an approach for printing multilayer activated carbon (AC) paste as electrodes by using 3D printing technology. Several forms of AC slurry were difficult to deposit because of the carbon particle size and acid concentration, and required iterative development to overcome these problems. This work investigates how the supercapacitor behaves in relation to the printed AC layers. The 3D printing technology also allows the manufacture of complex internal patterns accurately, and the use of these patterns is explored in this chapter

4.2 Experiment and Manufacture of Flexible EDLCs

4.2.1 Materials

Silver conductive paint with the volume resistivity of 0.001 Ω. cm was purchased from RS® Components Ltd. and was used due to its strong adhesion onto flexible composite substrates and its ability to provide high conductivity when fully hardened. Flexible LAYWOO-FLEX 3 mm diameter filament was used. Double face tape was purchased from 3M®. All other materials including AC powder, etc., were supplied and mentioned in section 0.

4.2.2 Machine process

To extrude several forms of material, the machine was changed from only one extrusion to dual extrusion. The FDM system by the 3D printer was used with a 0.4 mm nozzle able to produce layer heights of 0.02 mm (Bellini et al., 2005; Li et al., 2002). A single syringe tool was installed in the printer firmware and controlled by simplify3D software. The double head calibration was setup using simplify3D software for a tool head offset. To set up the modified fixture, the nozzle tip had to be zeroed to the same

tip dot and therefore the offset was measured manually for the nozzle tips of both heads for FDM and Discov3ry as shown in Figure 3.3. The Discov3ry extrusion takes time for building up enough pressure to achieve a steady state of extrusion for printing; the retraction will take a similar time to propagate through the length of tubing. Marlin G codes are preparatory functions which set the mode for the rest of the commands. M codes are machine specific miscellaneous functions (Reprap, 2015). Once a syringe has been filled, the G-code commands are sent to the Ultimaker® machine as shown in Table 3.1.

4.2.3 Fabrication technique

Designs were first drawn using Solid Works software. The electrodes were then fabricated using a paste extrusion Discov3ry syringe tool with an open source 3D printer Ultimaker. The FDM 3D printer uses a spool of filament drawn through a 0.4 mm heated nozzle. The materials were deposited by the FDM process using a layer by layer technique. The EDLC frame was printed using a flexible composite material, LAYWOO-FLEX. This flexible composite material was created with 65% co-polyesters and 35% recycled wood and has a comparatively lower tensile strength and high degree elasticity with no warping. Filament deposition of this material with a 0.4 mm nozzle was found to be possible using high temperatures, based on experimental work. Table 4.1 shows the process parameters used for this work. The fill density was set at 20%, wall line width was set at 0.6 mm, the travel speed was 150 mm/s, and the build plate was cooled to 10°C. The layer height was initially set at 0.4 mm for the first layer and double face tape 3M® was used on the build plate to help the object stick. The samples were printed on flexible composite substrates with the same size of electrodes for three capacitors with the length of 40 mm, the width of 2 mm, and same thickness sizes. During these tests, there were no issues with clogged nozzles or material jams. To successfully print 2 mm width of AC layers and with geometries, the height of the attached Discov3ry nozzle was set at 1 mm using a 0.6 mm diameter smooth flow tapered tip. The primary layer height was set at 0.6 mm for the first layer in rectilinear infill pattern, and extrusion multiplier was fixed at 30. During this test, there were no issues with clogged nozzles or air bubbles.

Table 4.1: 3D process parameters used for manufacturing of EDLCs

Material	Nozzle diameter (mm)	Layer height (mm)	Extrusion temperature (°C)	Printing speed (mm/s)	Feed-rate
LAYWOO-FLEX	0.4	0.4	255	40	1.5 mm/s
AC paste	0.6	0.6	0	67	700 steps/mm

4.2.4 Preparations of 3D AC electrode

Table 4.2 shows different kinds of AC slurries. To provide a printable slurry matrix for the EDLCs, the AC slurry 2 is made as following method: 2 g of PVA were dissolved in 40 mL distilled water at 50°C with 1 hour stirring, and then this PVA solution was mixed with 2 g AC powder that had been already pre-heated to 100°C for 1 hour, all the mixing materials were kept stirring overnight to make a homogenous slurry. AC 2 has been selected as electrode paste because of its optimum viscosity. Table 4.2 summarizes the differences between each slurry formulation. The viscosity of the AC slurry must be suitable to allow deposition under the optimum feed-rate while considering the filament shape. It can be seen from the table that the AC slurry 1 does not contain electrolyte acid and needs an increased pre-treatment temperature and process time for the PVA binder. It displayed a wrinkled morphology especially when air was entrained during the syringe filling procedure leading to a variation in viscosity. AC slurry viscosity is a property arising from collisions between particles. When the AC slurry does not mix well with the acid and is then forced through a tube, the PVA liquid which composes part of the slurry generally moves faster through the Tygon tube and AC powder remains in the syringe as shown in Figure 4.1.

Table 4.2: List of AC slurries

AC slurry	AC (g)	PVA binder (Wt/vol %)	Stirring time (h)	Electrolyte (ml)	Viscosity
AC 1	1.6	8% at 90°C	3	N/A	Low
AC 2	2	5% at 50°C	1	N/A	Optimum
AC 3	2.3	8% at 80°C	1.5	10 H_3PO_4	Low
AC 4	2.5	9% at 60°C	3/4	13 H_3PO_4	Optimum
AC 5	2.5	8.7% at 60°C	1	8 H_2SO_4	Optimum
AC 6	3	9% at 60°C	1	10 H_3PO_4	High

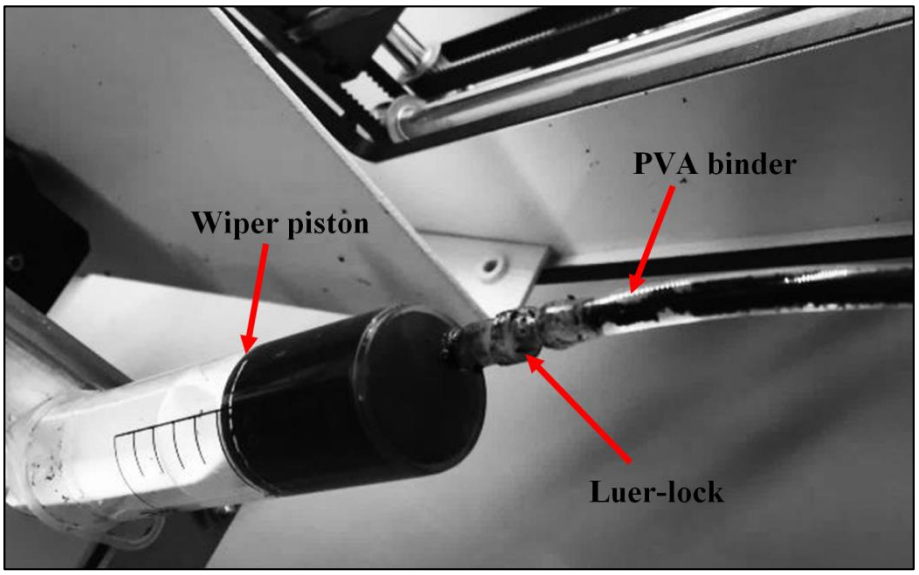

Figure 4.1: AC slurry depositions

To reduce the pressure building up in the system larger tip sizes could be used for more viscous materials. The problem was alleviated by eliminating all agglomerates. The particle size of AC powder was reduced by ball-milling. In addition, the tube size was increased from 3.17 mm (ID) to 4 mm (ID) with the same tube length of 38 cm, and this seemed to solve the issue. To ensure that no air was included in the AC paste, the AC was loaded into the 30 cc barrel with a female to female luer-lock coupling. Wiper pistons were used with paste materials due to their low-medium viscosity. As shown in Figure 4.2, AC slurry 2 could be deposited with a 0.6 mm diameter tapered nozzle because of the lower concentration of PVA binder. Treatment temperature and time have been decreased. The particle size of the AC powder was decreased in order

to avoid blocking between the tip of the nozzle and barbed male locking nut (see Appendix 0B).

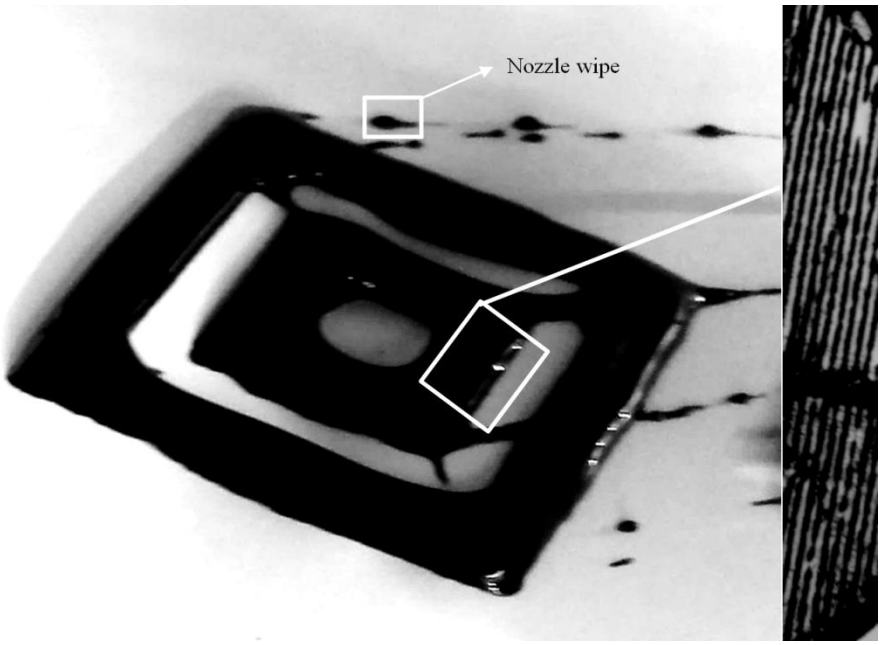

Figure 4.2: AC 2 slurry depositions left and close-up view showing the rectilinear pattern right

To achieve a working electrolyte in the electrode structures with 3D deposition, the AC 4 has been prepared in 13 mL of phosphoric acid (H_3PO_4) to serve as a source of ions and a promoter of ion conductivity for EDLCs. In addition, maximize the minimum layer heights of the AC filament without loss of geometry. It has been observed that AC 4 can be deposited with a blunt end tapered nozzle 0.6 mm diameter and its viscosity allows consecutive layers to be built up at a feed-rate of 800 steps per mm. The extrusion multiplier was also fixed at 30. In comparison, deposition of AC 6 becomes increasingly difficult, as the viscosity is higher. The rheology of the slurries needed to be controlled especially when aqueous electrolytes were added. AC 5 is an example. It has been discovered that an AC slurry containing sulfuric acid (H_2SO_4) forms oily structures which stick well when printed onto the substrate. In addition, the layers bond and drag other previously printed layers at the same feed-rate, even at a layer height of 1 mm as shown in Figure 4.3. However, after being disappointed with previous tests with this material structure, the sulfuric acid mixed AC was not used because the filaments were broken up at several points on the first layer during

deposition and the deposited layers connected to each other like other elastic materials.

Figure 4.3: AC 5 slurry depositions

4.2.5 Preparations of 3D gel electrolyte

The gel electrolyte was prepared from 1 g PVA powder in 20 mL distilled water stirred at 50°C for 1 hour to work as binder. 2 mL (95 wt %) aqueous solution of sulfuric acid H_2SO_4 was added to the aforementioned solvent mixture. To tailor the rheology 0.8 g of 5% CMC binder was added and followed by magnetic stirring overnight.

4.2.6 Fabrication of EDLCs

The flexible composite EDLC designed has two electrodes, a gel electrolyte as a separator, and current collector layers as shown in Figure 2.3. After printing the frame part, two layers of silver paint were brushed on to work as current collectors, followed by a connected 20 mm length of conductive copper tape, and then we deposited a 2 mm thickness of AC slurry and H_2SO_4/PVA gel electrolyte sequentially. The cell components were then packaged by pushing the two halves together, and sealed by depositing 1 mm of silicone layer to work as a gasket to prevent the two main components electrodes and gel electrolyte leaking out. Boos (1970) declared that the principal function of the gasket is to confine the electrodes.

4.3 Results and Discussion

4.3.1 3D process characterization

To successfully fabricate the supercapacitor, the main frame part (the case) was designed and manufactured. The outside surface or 'shell' of the EDLC part is an important factor, due to its job saving the EDLCs components from leakage or losing efficiency by air attack. Therefore, to address this issue the fill density should be approximately higher than 20% to enhance the strength and quality, and in addition, a value of 0.6 mm wall thickness may ensure that all gaps are closed completely. This can reduce the chance of leaks. The EDLC was made by combining the process and materials. We have shown that it is possible to build a 3D layer with the AC slurry using thread patterns of electrodes. The AC slurry needs to have appropriate rheological properties to be printable and to avoid distortion. An optimum balance should be pursued between AC powder, PVA binder, and electrolyte. The materials chosen for the flexible composite EDLC were AC slurry 2 and a H_2SO_4/PVA gel electrolyte. These materials were chosen as they were designed for extrusion through the 0.6 mm diameter nozzle. The deposition density of several layers in rectilinear patterns of the AC electrode (2 mm × 40 mm) with the layer height of 0.6 mm and density of 20%, excluding the gel electrolyte, was 1.37 g/cm^3. In order to avoid any contacts between two electrodes, the fill density of the gel electrolyte has to serve as a separator and an ion conductor. The fill density was fixed to 20% to obtain 1.37 g/cm^3, the same as that for the AC electrodes. It is difficult to predict the shrinkage from the printed particles; time is needed to let the material between layers cure and dry.

4.3.2 Electrochemical measurements

The functional components of an EDLC that are crucial to its operation are the electrodes, the electrolyte, and the separator. It is believed that the performance of the EDLCs manufactured by the 3D printing method is limited by the viscosities of both the AC paste and gel electrolyte due to the consideration of flow rate. The CV curves were recorded using a potential window range of 1 V at different scan rates of 20, 50, and 100 mV/s as shown in Figure 4.4. The maximum capacitance we achieved was 68.7 mF at a scan rate 20 mV/s by using equation (1). It was found that the capacitance of the flexible EDLC in H_2SO_4/PVA reached was 68.7 mF at the scan rate of 20 mV/s. At

scan rates, 50 and 100 mV/s a lower capacitance was obtained with 59.8 and 49.7 mF respectively. EDLCs take advantage of the electro-ionic charge storage induced in the electrochemical double-layer of high-surface area carbons by diffusion and adsorption of ions. The capacitance decreases with the increase of the scan rate because the ions cannot diffuse as effectively into the surface.

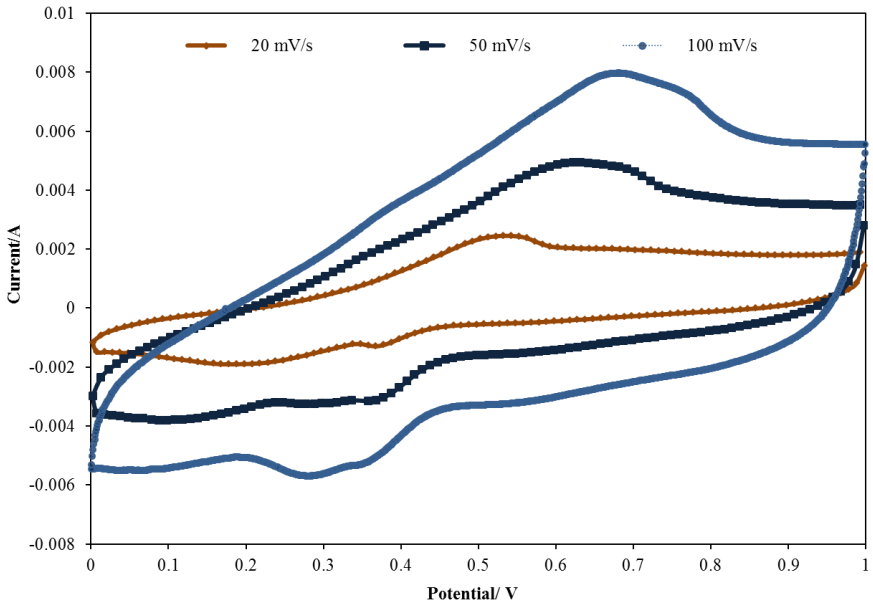

Figure 4.4: CV curves recorded at different scan rates of 20, 50 and 100 mV/s for a flexible composite EDLC

It can be seen that there is an oxidation or reduction profile on the CV curve. However, the CV curves are not perfectly rectangular as would be expected from a perfect capacitor. This might be explained by the high resistance of the gel electrolyte and the AC paste electrodes. In addition, it could be that the layer height needs to be reduced to less than 0.6 mm to press the filament of AC paste into the current collector layer to promote layer adhesion. There may also be some corrosion of the current collector. Another important method to characterise the performance of supercapacitors, the GCD test, was also used. Figure 4.5 shows the typical GCD curve of a flexible composite supercapacitor recorded with a charging potential of 1 V at the charging current of 15 mA. It shows symmetric charge and discharge processes and the capacitance can be calculated by equation (4).

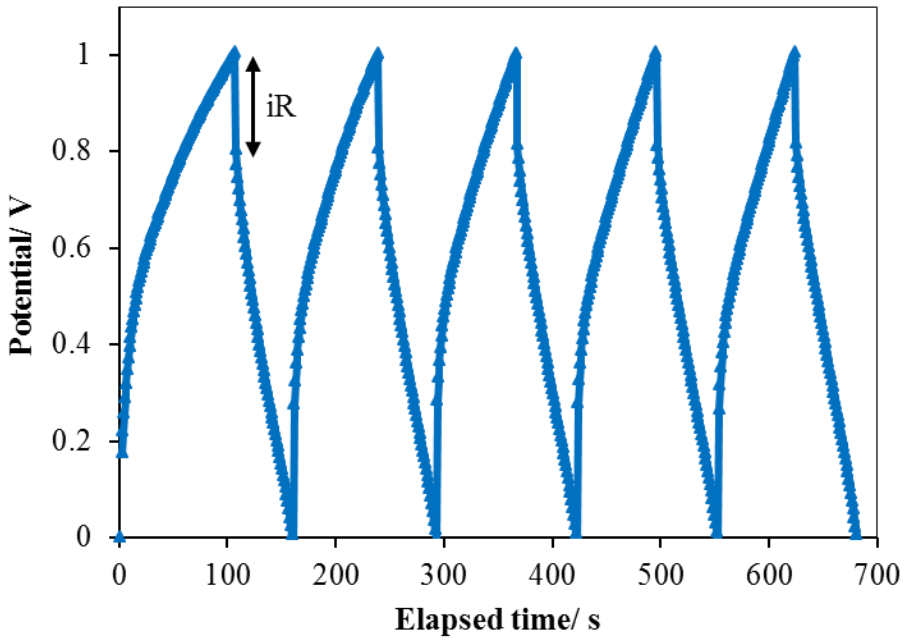

Figure 4.5: GCD curve recorded at a charging current of 15 mA

The fifth cycle charge-discharge had an ideal EDLC behaviour with a short charge/discharge period of less than 1.3 s. The capacitance value of 24.37 mF calculated by equation (1), is nearly half of the total capacitance obtained from CV curve at 100 mV/s. The specific capacitance (C_s) of the supercapacitor device was calculated by equation (5). The specific capacitance of the flexible EDLC calculated from the GCD curve based on the mass of the AC slurry was 0.121 F/g. ESR is related to the attachment of the carbon particles to the current collector as represents some of the internal resistance in the electrodes and was calculated by equation (7). One of the important factors of the AC slurry and gel electrolyte used for EDLCs is to allow the thickness and infill patterns structures of the AC slurry and gel electrolyte to be easily controlled in the 3D printing process. Therefore, in order to study the contact between components in this EDLC, the ESR was calculated to be 13.3 Ω.

4.4 Chapter Summary

FDM/Paste deposition is a very versatile, cost effective, and open source printing technique, allowing many materials in forms of paste/solid to be printed. The work in this Chapter has demonstrated the possibility of AC application to make EDLCs by using inexpensive equipment. AC slurry in various concentrations was used for active materials to produce EDLCs by 3D printing method. There are limitations on the usable range of AC slurry rheology for 3D FDM/Paste printing. The 3D flexible composite EDLCs were manufactured successfully and characterized in this work. The AC slurry and gel electrolyte were printed successfully in a rectilinear infill pattern. H_2SO_4/PVA gel electrolyte was printed onto flexible composite EDLCs as an efficient separator. A silicone layer was printed as well to form a gasket to prevent EDLC components leaking or drying out. The specific capacitance and ESR of these electrodes in the gel electrolyte of H_2SO_4/PVA were evaluated at a current density of 4.5 mA/cm^2 and found to be 0.121 F/g and 13.3 Ω. The outcomes observed for the process efficiency could be optimised by further improvement and reduction of the layer height of the filament to avoid layer breaks. Therefore, it was decided that the next chapter, is to look at the areas of control needed to make EDLC components with different layer thickness.

Chapter 5 Optimisation of EDLC Structural Parameters: Electrode and Electrolyte Thickness

5.1 Introduction

This chapter presents an approach for optimising the performance of printed multilayer EDLC components using 3D printing technology. It describes the energy storage performance of the printed supercapacitors in relation to the differences in thickness of the AC printed layers and the differences in density of gel electrolyte. EDLCs were designed and manufactured; the electrochemical behaviour of the EDLC made with a 3D printed AC electrode using H_2SO_4 based gel electrolytes was investigated. The performance of the flexible EDLCs manufactured by 3D printing in a rectilinear infill pattern has also been investigated. A supercapacitor based on printed AC and composite materials displayed a specific capacitance of 38.5 mF/g when measured at a potential rate change of 20 mV/s and a current density of 0.136 A/g. The highest energy density value for the flexible EDLC was 0.019 Wh/kg and power density of 165.0 W/kg in 1.6 M H_2SO_4/PVA gel electrolyte. This gel electrolyte was chosen because of its low cost and non-flammability when compared to organic electrolytes. The main research work reported in this chapter is to look at the areas of control needed to make EDLC components with different layer thicknesses. This is an important factor as it affects the electrolyte ions being transported between the layers of the two electrodes.

5.2 Materials and Methods

5.2.1 AC slurry electrode preparation

This AC slurry was the most challenging material to deposit. It is relatively inexpensive and of high chemical stability. The electrodes were printed using an AC, which was made into a paste with a small amount of PVA to act as a binder with a high dielectric strength in water. Higher binding strengths between the individual particles lead to considerably higher shape stability of the 3D part (Shen, 2015). To provide a printable paste matrix for the EDLCs, the AC slurry was made with 2 g of PVA, which was dissolved in 40 mL distilled water to give 5% wt/vol at 50°C with 1 hour of stirring. This was mixed with 2 g of AC powder that had been already preheated to 100°C for 1 hour to ensure max capacity. This mixture was stirred overnight to make a homogenous slurry.

5.2.2 H_2SO_4/PVA gel electrolyte preparation

The H_2SO_4/PVA gel electrolyte was synthesized by dissolving 1 g of PVA powder in 20 mL of distilled water stirred at 50°C for 1 hour. An aqueous solution of H_2SO_4 of 1.6 M concentration was mixed with the above solution. In order to tailor the rheology, 0.8 g of 5% wt/vol CMC binder was added. The mixture was magnetically stirred overnight. These materials were chosen for extrusion through a 0.6 mm diameter nozzle. The issues that arose during deposition were alleviated by material reformulation.

5.2.3 Manufacture method of EDLCs

Deposition of patterned structures of AC slurry and printing new composites allowed the use of a wide number of different materials and processes. The main goal was to reduce manufacturing time and reduce waste material during extrusion printing and filament formation. The Ultimaker® FDM process deposits the filament in a layer-by-layer technique. The EDLC frame parts were printed as shown in Figure 5.1 step (1) using a flexible composite material LAYWOO-FLEX. Table 5.1 shows the FDM process parameters used for this work. The fill density was set at 30%, wall line width was set at 0.6 mm, the travel speed was 150 mm/s, the build plate was cooled to 10°C and double face tape 3M® was used on the build plate to help the object stick. After printing the frame parts, a 20 mm length of conductive copper tape was connected to

the electrode bottom for electrical contact to two layers of silver paint applied with a brush, which served as current collectors.

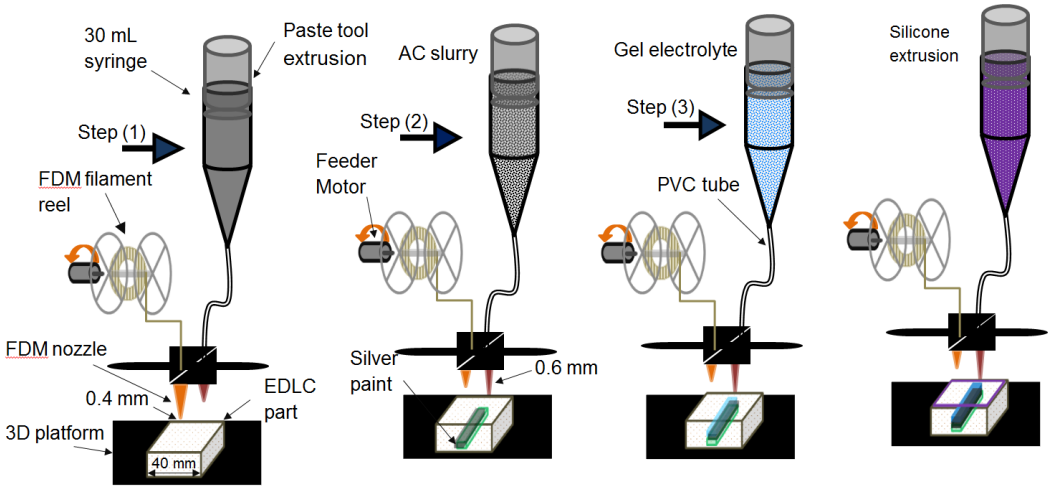

Figure 5.1: Schematic illustrations of EDLC fabrication

Table 5.1: FDM process parameters used for manufacturing of the EDLC frame parts

Material	Extrusion temperature (°C)	Layer height (mm)	Nozzle diameter (mm)	Printing speed (mm/s)	Feed-rate (mm/s)
LAYWOO-FLEX	250	0.4	0.4	50	1.5

The part was returned to the build plate for step (2) to deposit several thicknesses of AC slurry by Discov3ry® tool extrusion of a 0.6 mm layer height in a rectilinear infill pattern structure at a feed-rate of 21000 steps/mm. The extrusion used a linear stepper motor with a 100:1 planetary gear ratio pushing on a 30 cc syringe and a 3 mm inner diameter of PVC tube to obtain the speed that gives the right output flow rate. The AC and gel electrolyte must be viscous enough to be extruded from a syringe at room temperature yet hold its shape once extruded. The AC filaments deposited were exactly parallel on the consecutive layers. This was repeated with the same parameters for the gel electrolyte layer as shown in Figure 5.1 step (3). As shown in Table 5.2, in order to demonstrate the prevention of any contact between the two AC electrodes,

the fill density of gel electrolytes that serve as a separator and ion conductor were fixed to 100%, 60% and 30% for model A, B and C, respectively. Finally, the top surface outline perimeters were sealed by depositing a 1 mm of silicone layer that acted as a rubber gasket to ensure an excellent adhesion between the two parts of the EDLCs. The assembled EDLCs as shown in Figure 5.2 were sandwiched and kept for half hour under vacuum at room temperature to give the volumetric capacitances as shown in *Table 5.3*.

Table 5.2: EDLCs Parameters

	Model A	Model B	Model C
Thickness (mm)	1	2	3
Layer height (mm)	0.6	0.6	0.6
AC mass (g)	0.11	0.22	0.33
AC density (g/cm^3)	1.375	1.375	1.375
Fill density (%)	100	60	30
H_2SO_4/PVA density (g/cm^3)	6.75	2.68	1.58

Table 5.3: EDLCs performance

	Model A	Model B	Model C
Discharging time (s)	0.4	0.3	0.2
Capacitance at 20 mV/s (mF)	25.6	29.4	25.4
Capacitance at 50 mV/s (mF)	18.5	25.3	16.4
Capacitance at 100 mV/s (mF)	14.3	21.9	14.5
GCD capacitance (mF)	7.3	5.9	3.9
Specific Capacitance (mF/g)	38.5	26.9	11.9

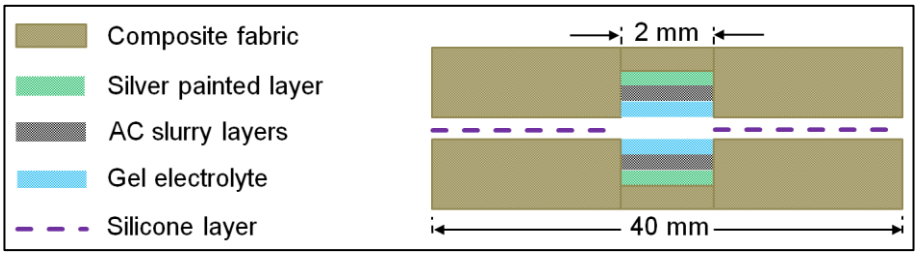

Figure 5.2: Schematic structure of an EDLC

5.3 Results and Discussion

5.3.1 3D process characterizations

The results from this experiment are shown in Table 5.3. This summarizes the relationship between the AC and gel electrolyte laydown. It can be seen that the thickness of the electrode also had effect on the energy storage of the samples. Many factors influence the performance of AC printed electrodes. The conductivity of the AC electrode was deteriorated by the increase of its thickness as the electrode mass increased and the specific capacity decreased. The type of AC including particle size, surface composition, heat treatment, and the permeability of PVA binder, 3D printing fill density, infill pattern structures, and filament substrate such as Laywoo-Flex is important. The particle size of the porous AC is important (Saeidi & Lotfollahi, 2016), as is the shape in the 3D deposition process to prevent clogging of the printing nozzles; AC has been milled for up to 72 hours at ambient temperature by ball milling to enhance the flow and reduce the internal friction when extruded. In addition, the distribution of carbon particle size could affect the electrochemical capacitance (Welham et al., 2002). The AC slurry used in this work has particles with approximately 100 nm in diameter.

Fill density is an important factor in 3D printed electronics since the quantity of printed materials directly affects the cell capacity and it should be higher than 20%. For example, less than 20% of fill density of the electrode or electrolyte layer will cause holes and therefore shorts. In addition, the structure of the AC electrode will affect the microstructure of gel electrolyte and the current collector, and subsequently affect the performance of the supercapacitor. It could be the effect of the air permittivity of the frames and the airflow affects the conductive materials. This might affect the activated materials that have been tested in the capacitors. After 24 hours using the electrochemical workstation, the energy storage disappears. In addition, the gel electrolyte leaks through the infill structures. Therefore, the higher the fill density of printed materials, the higher the lifetime of the energy storage. The gel electrolyte contained corrosive strong H_2SO_4 presenting oily structures that stick well when printed onto the electrode surface. It is not advisable to use this gel with a 3D open

frame machine as the acid presents a hazard and might cause serious burns to a user in comparison to a gel electrolyte based on phosphoric acid (H_3PO_4).

5.3.2 Flexible composite EDLC characterization

A supercapacitor has been fabricated using the prepared AC slurry, which was sized to make volumes of 0.08, 0.16, and 0.24 cm^3 for model A, B and C, respectively. The cell was assembled as shown in Figure 5.3 by placing the two AC electrodes parallel to each other, the gel electrolyte was between and sealed by silicone to avoid electrolyte leakage.

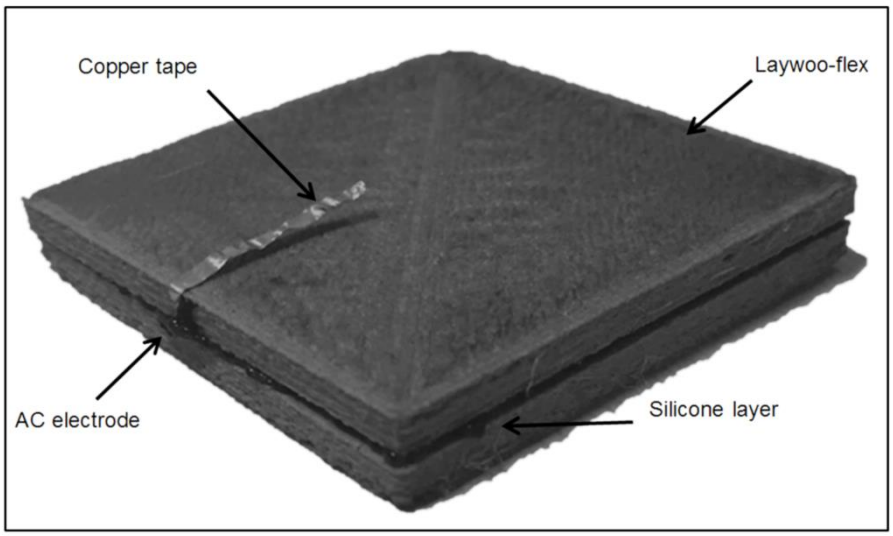

Figure 5.3: Assembled flexible composite EDLC

CV profiles of AC slurry at 20 mV/s using H_2SO_4/PVA as gel electrolyte with a 1V potential window for the three supercapacitors of model A, B and C are shown in Figure 5.4. The outcomes show typical shaped curves at 20 mV/s. It can be seen that there is an initial oxidation on the CV curve. It might be due to the current flow from electrode to electrolyte. This shows that the EDLCs performance is not the same for material with different thickness. It is easier to achieve an ideal rectangular shape of testing result for the 1 mm EDLC than that for the 3 mm EDLC. This might be due to the series resistances of 100% fill density for gel electrolyte in 1 mm EDLC, or the copper tape resistance and electrical resistance of the porous carbon. It has been noticed that the 20 mm length conductive copper tape with 5 mm underneath the AC electrodes loses its structure and breaks within 48 hours. This could be because of the high acid

density. H_2SO_4 was used in the gel electrolyte, in comparison with a gel electrolyte based on H_3PO_4 where the copper tape remains connected for a longer time. The capacitance of the EDLC may depend on the total electrolyte-accessible surface area (EASA) of the AC material that they are proportional to each other because the AC electrodes are electrochemically active in storing charges (Zhou et al., 2015). Faradaic behaviour was observed for model B and A in comparison with model C. This could be generated by reduction in model B and by oxidation in model A. The electrode is corroding which demonstrated the instability of the silver painted layer. Faradaic reaction is competing with the capacitor surface reaction. The capacitances of the model A, B, and C supercapacitors were calculated to be 25.6, 29.4, and 25.4 mF at 20 mV/s, respectively. Table 5.2 shows that the AC electrodes should be of comparable thicknesses.The optimum thickness of the electrode layer contains very little amount of the electrolyte material. It can be seen from Table 5.3 that Model B electrodes with an optimum fill density of gel electrolyte (2.68 g/cm^3) showed a better electrochemical capacitance compared Model A that has a higher fill density of 6.75 g/cm^3. It has been found that these devices had a lower capacitance after 24 hours. This anomaly could be for many reasons. One reason could be that the composite material filament structure becomes easy to break if the filament is kept unsealed in an air environment for some time before printing. In this case, it can be difficult to print the filament, and the feeder motor cannot push it to the hot end for extrusion. It is not recommended to print any filament material after a change in its properties during storage.

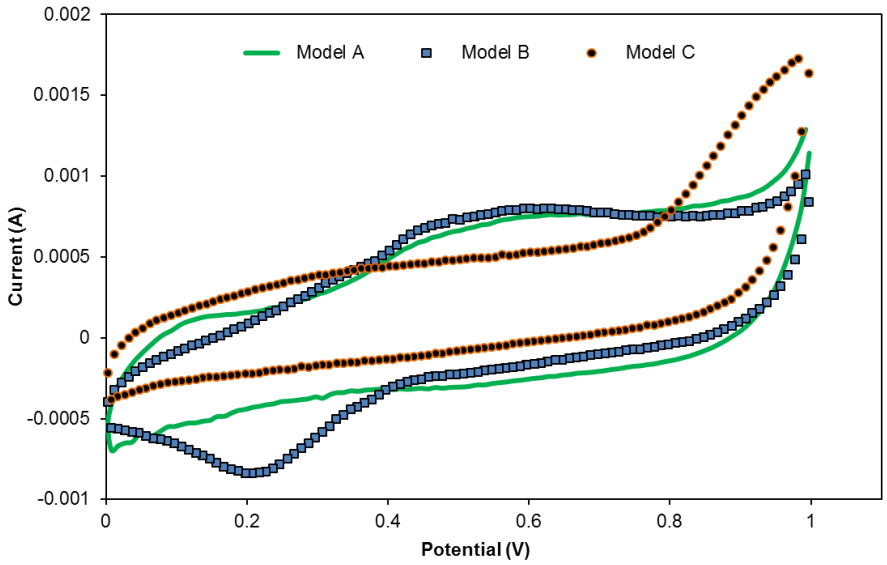

Figure 5.4: CV curve of 3D flexible EDLC recoded at different scan rate of 20, 50, 100 mV/s

The capacitance value of model A was 14.3 mF based on the CV curve obtained by equation (1) under the scanning rate of 100 mV/s. While using GCD testing, this showed that the capacitance decreased dramatically to half, 7.3 mF, when calculated by equation (4). The fifth cycle GCD curves run at charging current of 15 mA for the three supercapacitors are shown in Figure 5.5. If compared with the result obtained from the GCD curve and equation (4), it can be seen that the value of the capacitances increased with decreasing AC thickness. Figure 5.4 shows the CV curves and it can be seen that the capacitance decreases with the increase of the thickness of the AC layer. Also, from *Table 5.3* we can see that the capacitance value decreases when the thickness of the AC and H_2SO_4/PVA gel electrolyte laydown increases.

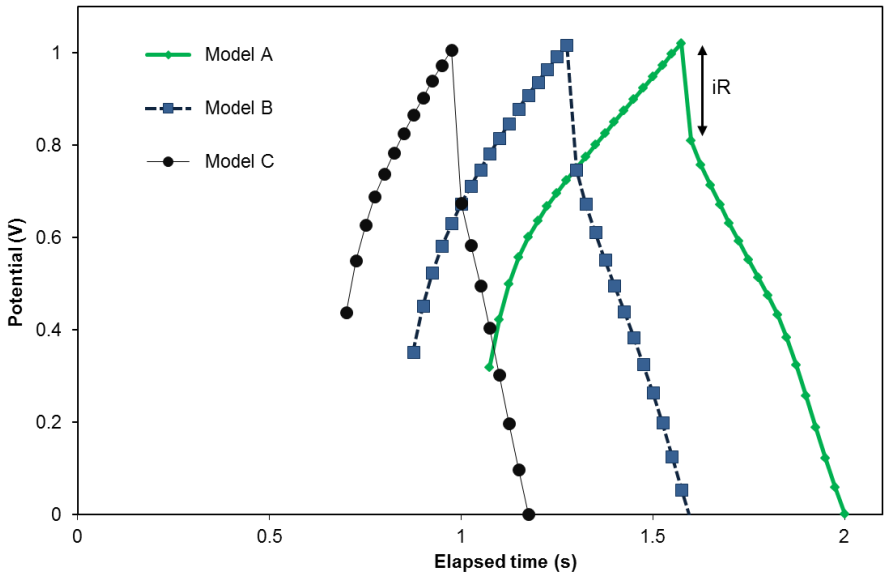

Figure 5.5: GCD curves obtained from the capacitors with different AC electrodes thicknesses at a charging current of 15 mA

The iR is a potential drop at the beginning of each discharge curve shown in Figure 5.5. From equation (5), the assembled EDLC showed a specific capacitance of 38.5, 26.9 and 11.9 mF/g for 1, 2, and 3 mm thickness, respectively. The comparison of the results for the composite supercapacitors with three different electrode thicknesses in 1.6 M H_2SO_4/PVA gel electrolyte is shown in Figure 5.6. It was expected that an increase in the thickness of AC layers might lead to an increase in the specific energy stored. However, it has been noticed in the samples that as the AC thickness increased from 1 mm to 2 mm the specific capacitance decreased approximately 30% from 38.5 mF/g to 26.9 mF/g and dramatically decreased in the 3 mm capacitor to 11.9 mF/g. The electrode mass might be expected to contribute to the further energy storage as increased about 100% from 0.11 g to 0.22 g and increased a further 50% in 3 mm capacitor to reach 0.33 g. This was mainly due to the sample sizes of the electrode. There seems to be little correlation between the mass of AC and the thickness of gel electrolyte. The increase of the specific capacitance of the composite EDLCs may increase proportionally with the decrease of the AC thickness. It could be due to the time of the electrolyte diffusion processes, as ions cannot move faster through the high viscosity of the 3D printed AC.

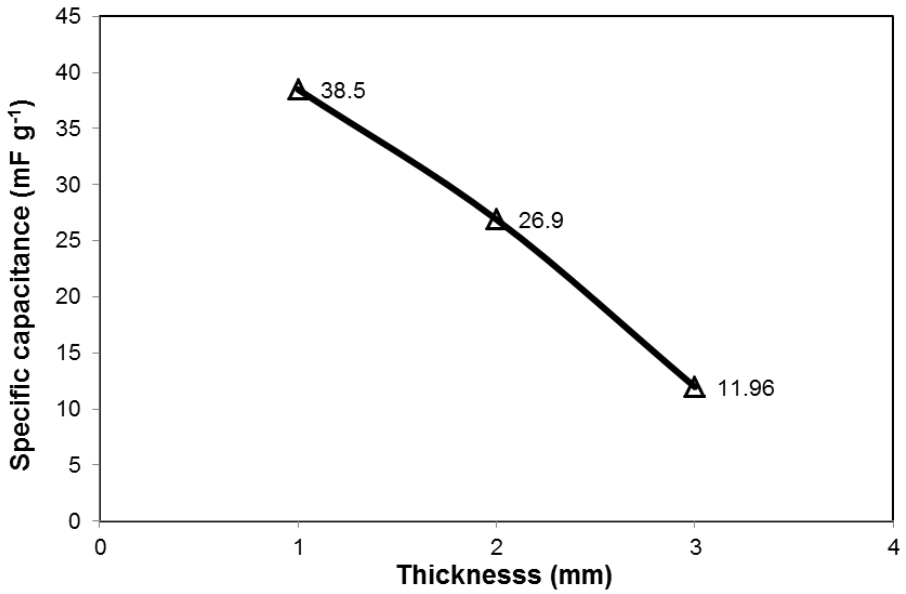

Figure 5.6: Specific capacitance curve for several AC electrodes thickness

It can be seen from Figure 5.7 that the discharging time slightly decreased as the AC electrodes thickness increased, (the experiment was achieved at a current of 15 mA and 1V). This is illustrated by the 1 mm thickness composite electrodes having an ideal EDLCs behaviour with a short charge-discharge duration below 0.4 s. In addition, it had long lifetime storage at 0.3 mF in comparison with the GCD curves of model B and C, which were overlapping. Gel electrolyte ion concentration may be effective in separating the two electrodes. As shown in Table 5.2, with an optimum density 2.68 g/cm^3 laydown percentage of H_2SO_4/PVA gel electrolyte with 2 mm thickness of AC slurry, the capacity value was higher measured by a CV curve. With an approximate 73% increase of gel electrolyte laydown, the AC slurry discharging time was 0.3 s. Sa'adu et al. (2014) have enhanced the quality of the polymer electrolyte and reduced the thickness of the electrode to increase the capacitance. The energy density and power density are calculated from the GCD curves and equation (8) and (9).

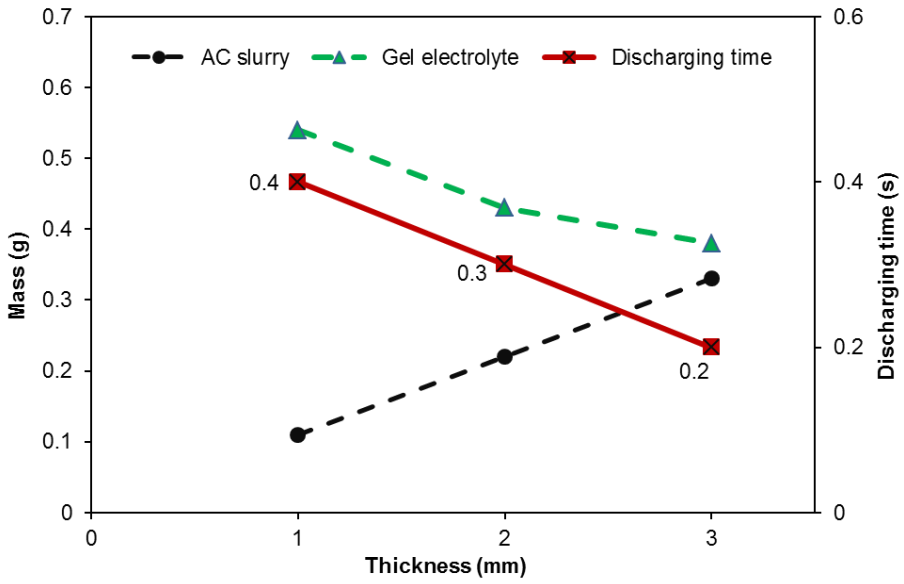

Figure 5.7: The discharging time (s) vs AC and gel electrolyte (g) curve for several AC electrodes thickness (mm)

The highest energy density of the AC supercapacitor was obtained in model A reaching 0.019 Wh/kg with a corresponding power density of 165.0 W/kg with 1.6 M H_2SO_4/PVA gel electrolyte. While model B and C have energy densities of 0.013 Wh/kg and 0.006 Wh/kg with a corresponding power densities of 124.1 W/kg and 55.4 W/kg, respectively. Thus, AC based EDLCs generally have the disadvantage of lower energy density when operated with gel electrolytes compared to organic electrolytes (Chen et al., 2015; Zhang et al., 2012). High dielectric constants are used to increase an energy density for EDLCs. As shown in Figure 5.8, the smaller equivalent series resistance (ESR) might lead a larger power density. An ESR difference can be explained in terms of the conductivity of gel electrolyte, using the electrochemical impedance spectroscopy technique between the frequency of 0.01 Hz-100 kHz.

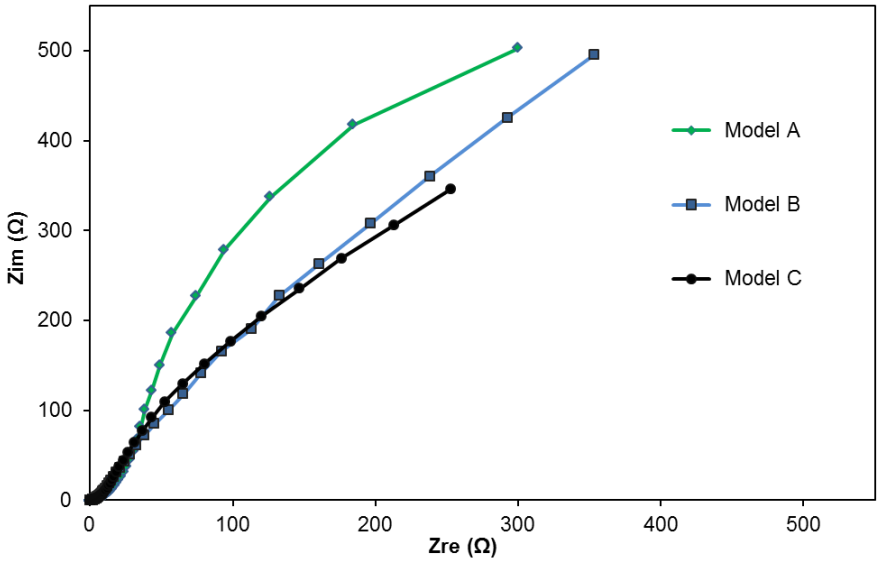

Figure 5.8: Nyquist plot performed at 0 V with frequency range from 100 kHz to 0.01 Hz

The iR drop of model A in the GCD curve for 1.6 M H_2SO_4/PVA electrolyte was approximately 0.13 V due to its 100% fill density. While for model B and C the iR drops were about 0.23 V. Slightly similar values of the iR drop for potassium nitrate (KNO_3) and H_3PO_4/PVA electrolytes have been reported (Bae et al., 2011). ESR were measured at the start frequency 100 kHz going to 0.01 Hz and were calculated by equation (7) and are 8.6, 13.3 and 15.3 Ω for model A, B and C, respectively. It can be seen from Figure 5.8 that ESR curves for model B and C are quite similar but different from model A which has a different slope. It is valuable to see that the semicircle nearly vanishes in the Nyquist plot for model B and C. It might be due to the value of a different contact resistance, leading to less hindering of ion transfer and high frequency could lead the current leakage. Water separation from H_2SO_4/PVA gel electrolyte during 3D deposition process played a dominant role in ESR value. The layer height was 0.6 mm and that may increase ESR in comparison with other processes. A sufficient time to let electrodes dry could have helped AC layers adhere well onto the current collectors, which decreased the ESR. Also extra amounts of binder content will increase the electrode resistance (Zhang et al., 2016). But 5% wt/vol PVA binder content was found to help the flow deposition with a 0.6 mm diameter tapered nozzle.

5.4 Chapter Summary

The results obtained from this research study revealed several interesting features of the FDM and paste deposition processes. The following are the main conclusions:

- The deposition with a 0.6 mm tapered nozzle was optimized for AC ball milled for up to 72 hours, to obtain a feed rate of 21000 steps/mm with a layer height of 0.6 mm. This approach resulted in a relatively low printing time of less than 2 minutes for each AC and gel electrolyte fill structures.
- The results showed that the AC thickness had an effect on the capacitance; when the thickness of AC layer increased from 1 mm to 3 mm, the specific capacitance decreased from 38.5 mF/g to 11.9 mF/g.

Chapter 6 Highly Flexible EDLCs

6.1 Introduction

This chapter aims to investigate the performance of the flexible EDLCs manufactured by 3D printing in a honeycomb pattern. The EDLC cells were fabricated using a slurry made from commercial AC and a gel electrolyte deposited on a transparent silicone substrate. The flexible EDLCs structures can be used in flexible electronics with different patterns and sizes using 3D printer and can be applied to many applications such as wearable technology. A honeycomb pattern was used due to less material and less time being consumed than with other patterns. The electrochemical testing of six and twelve AC electrodes of 2 mm thickness using 2.4 M concentration of H_3PO_4 was investigated. Mechanical bending tests were carried out to prove the stability of the electrochemical performance and flexibility of the 3D printed supercapacitors

6.2 Experimental

6.2.1 Preparation of AC slurry

In order to reduce the size of the activated carbon (AC) particles and to ensure a uniform deposition of AC slurry through a tiny 0.6 mm tapered nozzle, a ball-milling process was used. 100 g of AC powder was added into 50 mL of carbon-based Chinese ink, and 100 mL of distilled water, and milled for 72 hours. The average particle diameter is 0.4 µm. Then 5 g of the milled AC powder was heated at 150°C in an oven to allow the solvent, mostly water, to evaporate. 2.6 g PVA powder was dissolved in 20 ml distilled water at 50°C for 1 hour under magnetic stirring. The dry AC power was mixed with the PVA gel solution under stirring at room temperature for 24 hours. To ensure the homogeneity of the AC slurry 8 mL H_3PO_4 and 1 g of 5% CMC was added.

6.2.2 Preparation of PVA/H_3PO_4 gel electrolyte

The PVA gel electrolyte used in this study was an important component for flexible EDLCs and its properties significantly affected the EDLC's electrochemical performance. To prepare an aqueous solution of PVA, 2.5 g PVA powder was mixed with 30 mL distilled water and was stirred at 50°C for 1 hour until fully dissolved. To avoid a rough layer and to get more sticky 1.5 g CMC of 5% was then mixed with the PVA solution followed by 18 mL 6 M H_3PO_4 with magnetic stirring overnight until completely homogeneous.

6.2.3 Current collector paste preparation

It was critical to prepare a conductive paste with a good bonding to the substrate in 3D printing, especially as silicone was used as the substrate material. 1 g PVDF-HFP pellets were dissolved in 15 mL NMP at 40°C for 1 hour first. After that, 4.5 g zinc metal powder was mixed with 5 g silver powder (Ag) and added to the solvent/polymer mixture and kept stirring overnight. PVDF as a type of piezoelectric polymer enhanced the bonding of silver and zinc particles therefore improving the conductivity of the current collector.

6.2.4 Fabrication process

Figure 6.1 shows the practical 3D fabrication technique of the flexible EDLCs. The 3D printer setting for the heated platform was set to 10°C and the extruder temperature was 0°C. A 30 mL BD luer-lock syringe was used. A 3.5 mm inner diameter of PVC rubber tube with length of 38 cm was used. To reduce the amount of the three materials used in this work they were deposited in a 20% honeycomb infill pattern. A 0.6 mm diameter tapered nozzle and a 0.6 mm layer height were used. The feed-rate was fixed at 21000 steps per mm at a printing speed of 67 mm/s. To avoid trapping any air bubbles, the silicone was filled into the syringe without any purification using an applicator gun and other pastes by female-to-female luer-lock coupling. The retraction function in the software was disabled to avoid hardware mechanical issues. A non-stick Teflon sheet was used on the printing platform.

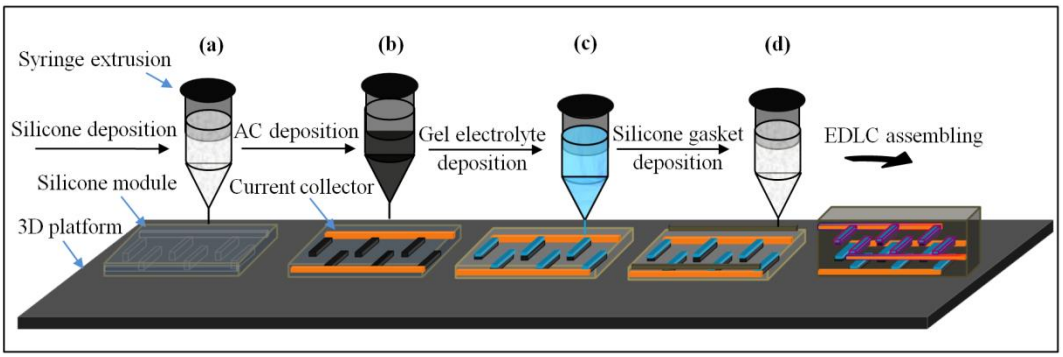

Figure 6.1: Schematic illustration of the 3D fabrication procedures of flexible EDLCs

6.3 Fabrication of Flexible 12-Electrodes EDLCs

A computer aided design (CAD) was created with Solid Works® and converted to 3D printer instructions in a layer by layer using simplify3D® software. Each layer was fabricated in sequence by 3D paste extrusion as shown in Figure 6.1(a).

A silicone layer thickness of 0.6 mm was used throughout. Two layers of current collector were applied with a brush, which served as current collectors. Electrode layer thicknesses of 0.6 mm were used throughout with dimension 38 mm length x 2 mm width Figure 6.1(b). The gel electrolyte dimensions were similar to the electrodes and this gel electrolyte layer was used as the separator. As shown in Figure 6.1(c) the same 3D parameters for the PVA/H_3PO_4 gel electrolyte layer were used for deposition to reach weight for the six electrodes of 1.3 g. It has been demonstrated that various structures can be manufactured using silicone based 3D paste extrusion. The rheology of the paste materials needed to be controlled to allow deposition maintaining the filament shape. Pastes that have solvents such as NMP or acetone need to be printed at a low temperature to avoid evaporation. To minimize gel electrolyte leakage during the sandwiching of the two halves a 1 mm silicone layer was deposited around the edge Figure 6.1(d). The EDLC cells were printed without any metal current collector (see section 6.2.3), and kept in a vacuum desiccator for an hour to allow the infiltration into the carbon of the PVA/H_3PO_4 electrolyte.

6.4 Result and Discussion

In this section, we present three EDLCs produced by a novel manufacturing process in a single module part. The schematic illustration of series connection without a combination circuit involved in the structure of the highly flexible EDLC is shown in Figure 6.2. The stability of the EDLCs performance and its flexibility is mainly based on two factors, the vapour pressure of the solvent and the strength properties of the binders. Adhesive, common, cheap, and environmentally safe binders were used in the EDLCs. However, they tended to block a large part of the conductive particles, the carbon's surface area, and the electrolytes. The adhesion between the current collector based on PVDF-HFP and the silicone substrate is weaker than that between other substrate elastic materials. The current collector based on PVDF-HFP showed a low resistance in comparison with current collector that had a CMC binder but the

current collector paste based on CMC showed good flexibility in comparison with PVDF-HFP. The current collector based on PVDF-HFP was used as conducting layer in this work due to its high conductivity.

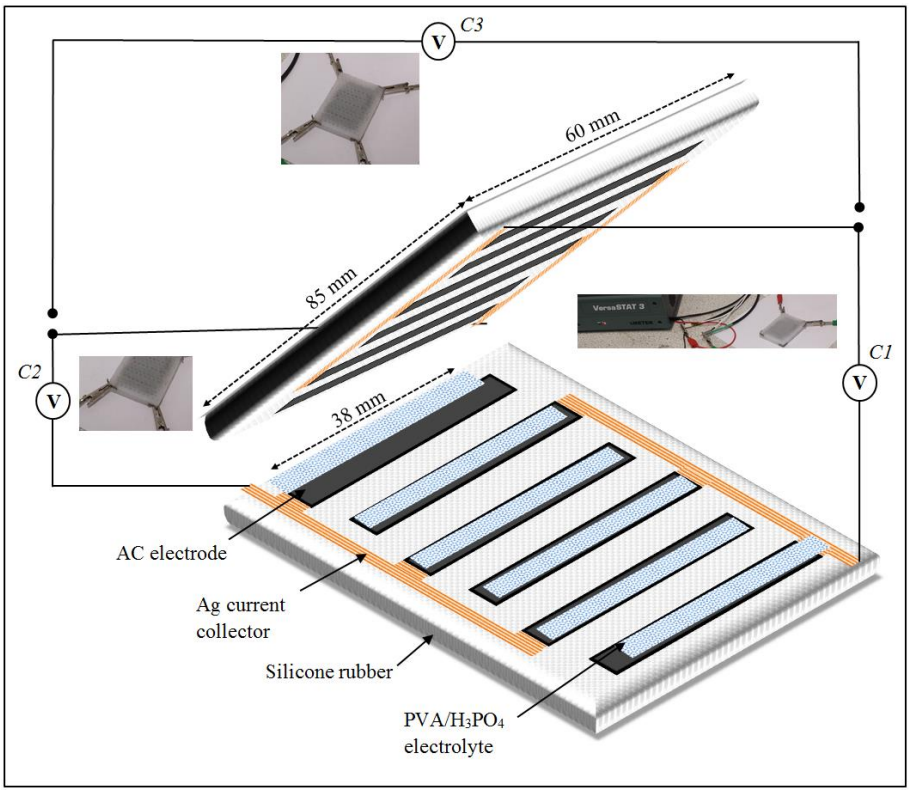

Figure 6.2: Schematic showing the steps used to connect the circuits of flexible EDLC

One of the fundamental challenges of 3D paste printing is that it is limited by syringe loading and the extrusion pressure required. The EDLC material was very challenging to deposit because it was prepared from powder and water leaving entrained air bubbles. This will cause breaks in the filament deposition leading to gaps and the structure to collapse. To optimise the structure, each layer must maintain its shape when printed. It is difficult to predict the shrinkage of EDLC materials components with low viscosity, as they spread after being deposited from the nozzle. Some acids and solvents are quick to evaporate during deposition, therefore; it is an important to select an appropriate acid and solvent. The rheological suspension properties of EDLC components are important in 3D printing processes and need to be controlled. The viscosity, surface tension, and AC particle content were adjusted to the requirements of the 0.6 mm tapered print nozzle. As shown in Figure 6.3, the two layers with 0.6 mm of top shell thickness in 20% honeycomb infill pattern lead to silicone layer shrinkage

and distortion. To avoid an unsmooth skin surface on the honeycomb infill pattern it was necessary to increase the fill density above 20%. It is very important to obtain excellent printed layers of silicone substrate and avoid formation of large gaps. This will reduce the defects within the current collector and AC layers and will lead to a uniform thickness and a stable electrochemical performance.

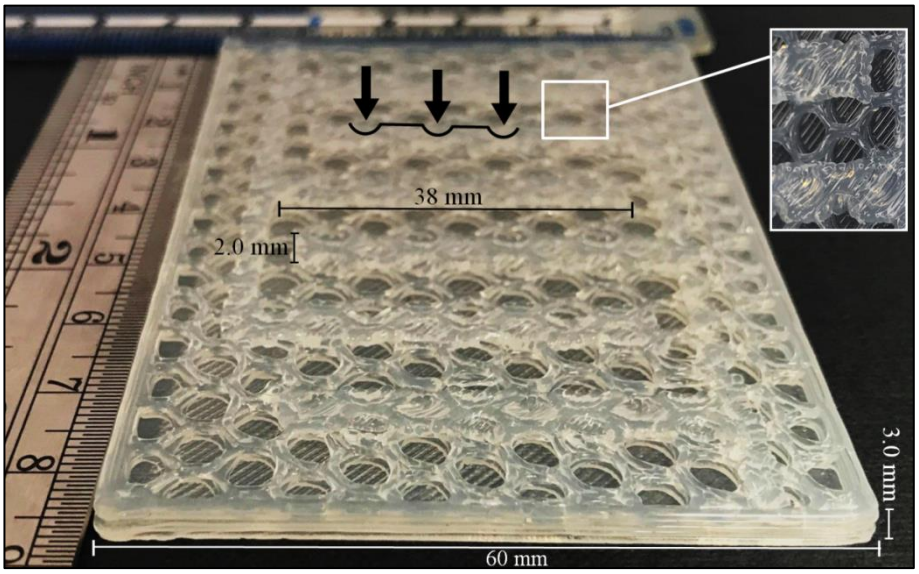

Figure 6.3: Silicone honeycomb infill pattern exhibiting shrinkage layer noted by the lines

6.4.1 Cyclic voltammetry

To determine the electrochemical properties of the AC printed onto silicone, it is highly important to take measurements at a sufficient scan rate by using CV, the most widely used method for determining the capacitance. CV was performed in the potential range from 0 V to 0.8 V to prevent the decomposition of water. The CVs were recorded in the aqueous 2.4 M PVA/H_3PO_4 to determine *C1*, *C2,* and *C3*. The mass of each electrode was 0.2 g and the total mass was 2.4 g. The capacitance of *C1* and *C2* were calculated by equation (1) and n was 6 to be 264 mF, and 244.5 mF at 5 mV/s, respectively. The capacitance of *C3* was calculated by equation (1) and n was 12 to be 158.7 mF. The electrodes for *C1* delivered capacitance of 151.49, 83.98, 37.79, 20.15 and 10.8 mF when the scan rates rise to 10, 20, 50, 100, 200 mV/s, respectively. At very slow charge rates, the ions can travel deeper inside the AC leading to a better surface coverage reaction. As shown in Figure 6.4(a), it can be clearly seen that the capacitance decreases because of the increase of the scan rate as the ions cannot get

to the electrode surfaces quick enough. Other processes are also seen. A little reduction current was observed in *C2* at scan rate 200 mV/s, which shows a faradaic (reaction) current. It is seen from Figure 6.4(b) that the three EDLCs display a relatively good rectangular behaviour and the *C1* and *C2* showed the largest current at scan rate of 5 mV/s in comparison with *C3*. However, the shrinkage of silicon surface in honeycomb pattern plays a role in changing dimensions and should be avoided because of their negative effect on EDLCs performance.

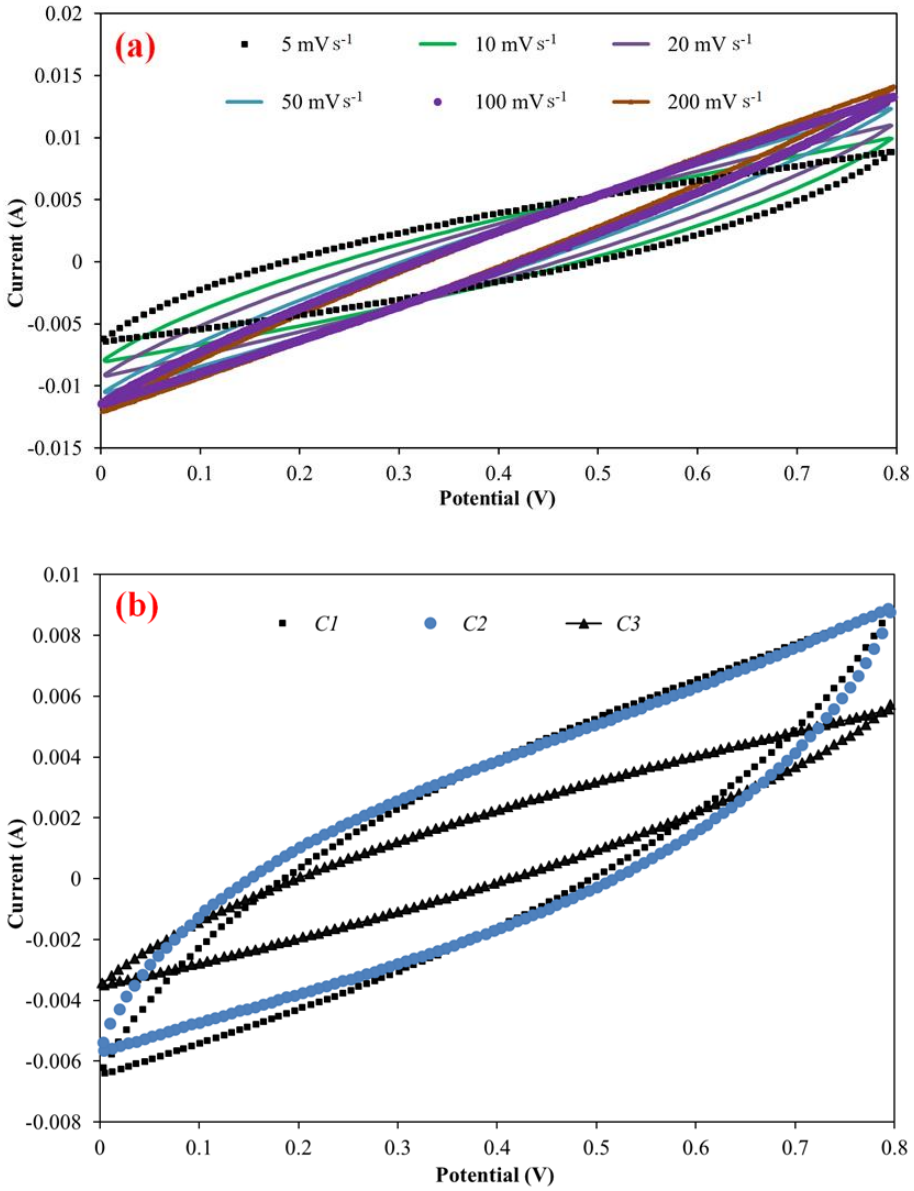

Figure 6.4: (a) CV curves obtained from the *C1* at different scan rate, and (b) CV curves obtained from the three EDLCs at a scan rate of 5 mV/s

6.4.2 Galvanostatic charge-discharge

The GCD test was carried out for *C1* and *C2* at a current density of 11.5 mA/g and 5.7 mA/g for *C3* in the potential range 0 V to 0.8 V. Figure 6.5 shows a typical fifth cycle charge-discharge curve for each EDLC. The capacitance for *C1* calculated from the GCD curve using equation (4), is 11.2 mF, nearly half to that calculated from the CV at scan rate 100 mV/s. There is little effect of current value and it can clearly show that the potential error (V_{error}) was extremely high in *C3* GCD curve. Uncompensated resistance might generate this error. The iR drop at the beginning of each discharge curve was increased due to the high resistance and high voltage error. It was difficult to measure the iR drop and discharge time in *C3*. Kampouris et al. (2015) have considered the electrode to be polarized when the potential of an electrode is forced away from its open circuit. Similar negative slope trends of GCD curves for EDLC devices have been reported previously (Zhang et al., 2016; Ramachandran et al., 2014). Because of uncompensated resistance, the impact of high iR drop on measurement is crucial. PVDF-HFP dissolved in NMP as binder is believed to be responsible for the scanning voltage going into the negative range during discharge process in GCD curves and away from the logical value of zero of aqueous electrolyte. Non-linear GCD curves are features of battery behaviour, which should not be used for measurement of capacitance values (Guan et al., 2016).

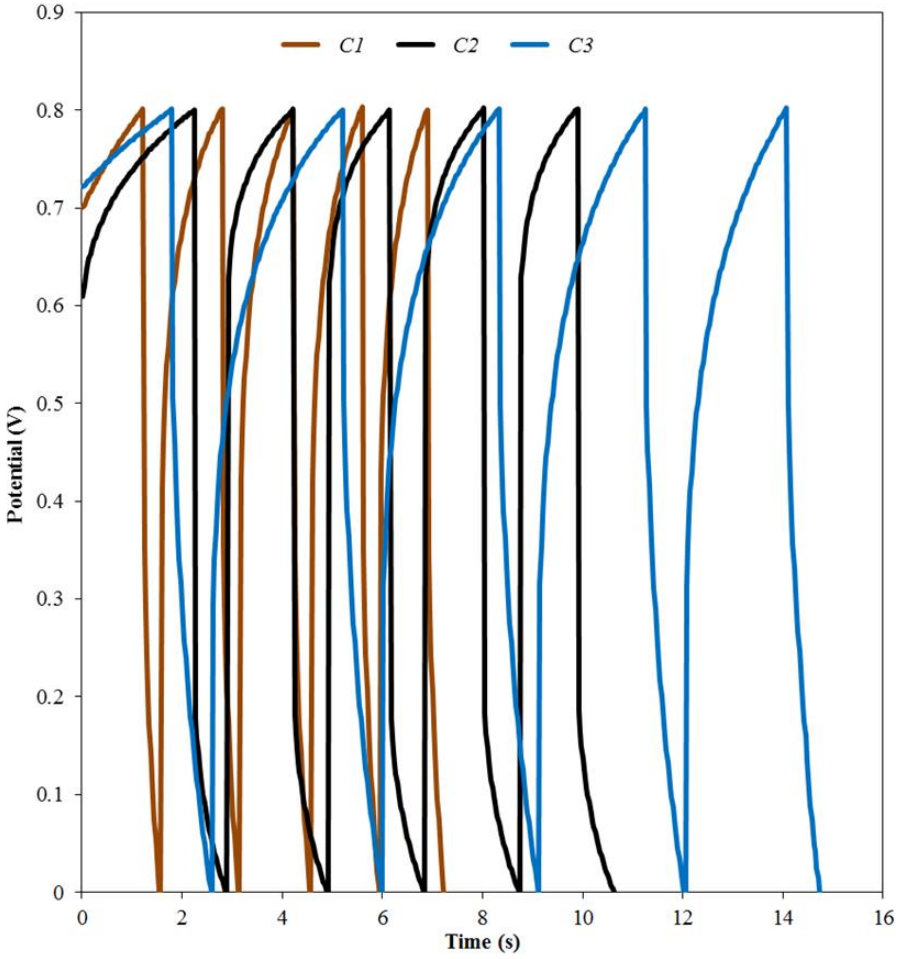

Figure 6.5: GCD curves of the first five cycles of each EDLC at 0.8 V recorded at a charging current of 15 mA

The values of specific capacitance were continually compared. The highest specific capacitance calculated by equation (5) was that reached at 7 mF/g for *C1*. A minimum specific capacitance of 1 mF/g was observed for *C3* at a current density of 5.7 mA/g. At a similar density for PVA/H_3PO_4, the specific capacitance values of the flexible EDLC decreased when the charge/discharge current decreased. The energy density and power density are calculated from the GCD curves and equations (8) and (9).The highest energy density of the *C1* was obtained to be 2.24 Ws/g with a corresponding power density of 3.18 W/g. While the *C3* has lower energy density of 0.32 Ws/g with a corresponding power density of 1.6 W/g.

6.4.3 Effect of piezoelectric binder on the GCD curves

We investigate the effects of PVDF-HFP and its ferroelectric properties in EDLCs galvanostaic performance as shown in the schematic diagram of the fabrication process of the flexible EDLCs (Figure 6.1). Six EDLCs samples were fabricated based on a two-AC electrode system with 2 mm thickness and 0.6 mm layer height in 1.6 M of PVA/sulfuric acid (H_2SO_4) gel electrolyte. Both AC electrodes and current collector contained 20 wt/vol % of PVDF-HFP binder. Electrochemical measurements were performed using a VersaSTAT 3.0 electrochemical workstation. For reliable measurements, all GCD curves were measured at 15 mA. The first EDLC was with 1.6 M of PVA/H_2SO_4 gel electrolyte and the GCD slope trend at a charging potential 1 V showed negative potential at -0.2 V as shown in Figure 6.6(a). The GCD result was compared with the similar electrodes parameters fabricated with the same current collectors and concentration of the PVDF-HFP binder but with 2.4 M of PVA/H_3PO_4 gel electrolyte. The GCD curve for this experiment at a charging potential 0.8 V is showed in negative voltage and decreased dramatically to -1.4 V on discharge as shown in Figure 6.6(b). This suggests that PVA/H_2SO_4 gel electrolyte at charging potential 1 V has a little effect and behaves significantly better than the electrodes in PVA/H_3PO_4 electrolyte at charging potential 0.8 V.

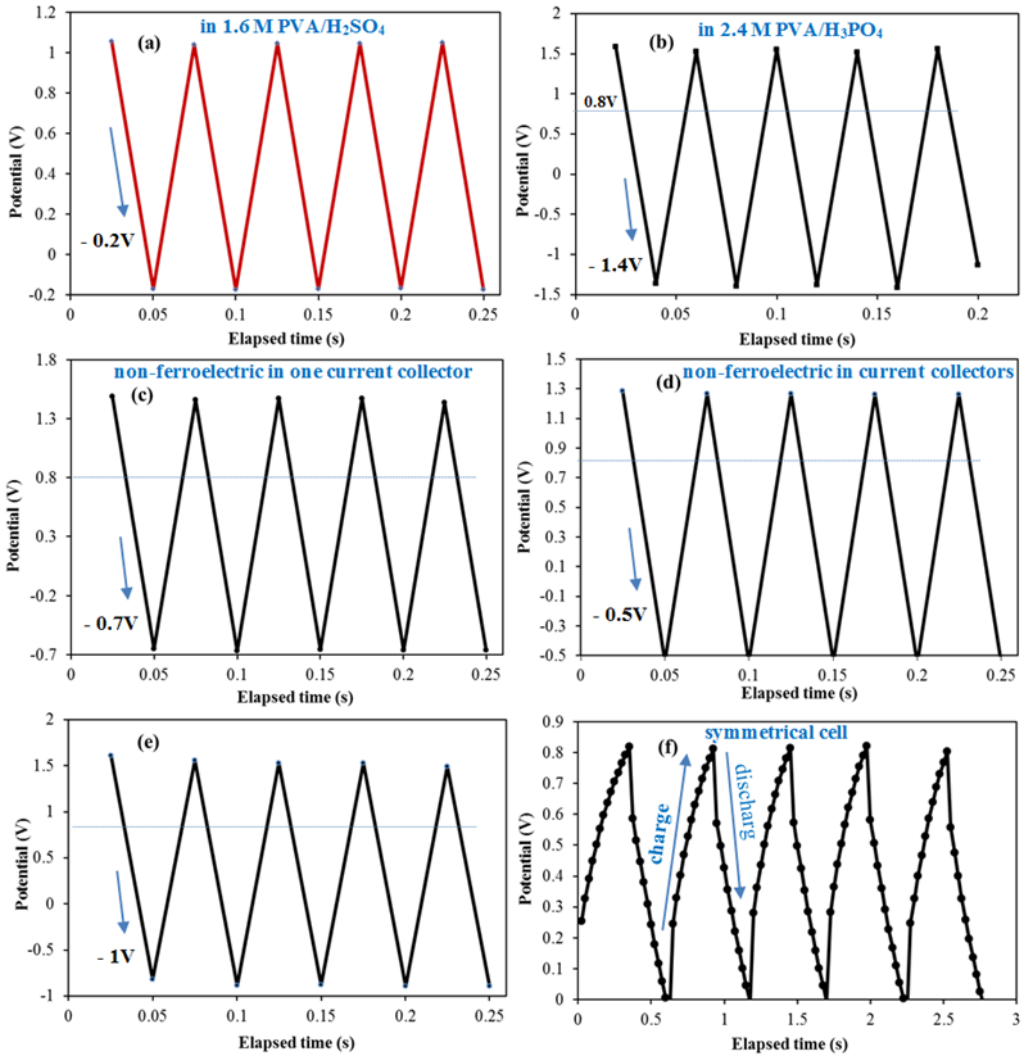

Figure 6.6: Effect of piezoelectric binder modified AC electrode and current collector on the GCD curves

One of the current collectors in the EDLC based on PVA/H_3PO_4 used silver paint while the other current collector and two AC electrodes are prepared using PVDF-HFP binder. It can be seen that the GCD curve of this structure as shown in Figure 6.6(c), the negative voltage range in the same gel electrolyte concentration is -0.7 V, and is -0.5 V when two current collectors were replaced by silver paint as shown in Figure 6.6(d). The material with a more negative potential range should not be chosen as the positive or negative electrode. It can be seen from Figure 6.6(e), that GCD curve for two AC electrodes based on PVA binder with two current collectors based on ferroelectric binder in PVA/H_3PO_4 response is in high negative potential range at approximately -1 V. Probably, the effect of PVDF-HFP as a binder of EDLC electrodes and current collectors is responsible for nonlinear voltage-time relation during the GCD

test. The current collectors based on ferroelectric material have a high negative potential range on discharge compared to an AC electrode, which consisted of ferroelectric material. Figure 6.6(f) Show a symmetrical cell scanned from 0 V to 0.8 V at the same charging current 15 mA based on non-ferroelectric binder for AC electrodes and current collectors. Scanning the voltage into the negative range results in an increase of ESR and potential error and there is a loss of the energy.

6.4.4 Electrochemical impedance spectroscopy (EIS)

The ESR difference is explained in terms of the conductivity of PVA/H_3PO_4. Other various factors may influence ESR such as electrode thickness and its attachment to the current collector, layer height, cell size, infill pattern and fill density. The ESR can be easily determined by obtaining a symmetrical GCD curve. An asymmetrical GCD curve is often difficult to measure due to the nonlinear slope. No noisy process was observed in any of the GCD curves. Thus, iR drop can be determined more reliably from the iR_{comp} using the electrochemical workstation in auto-ranged experiment. The iR_{comp} were 14.9 Ω and 18.86 Ω for *C1* and *C2*, respectively. *C3* displays a higher iR_{comp} was 41.37 Ω because it might have been affected by remaining ionic resistance produced during the charging of *C1* and *C2*. From the iR_{comp} values, we can calculate Vir using the equation (12). The values of V_{ir} are 0.22, 0.28, and 0.62 V for *C1*, *C2*, and *C3*, respectively.

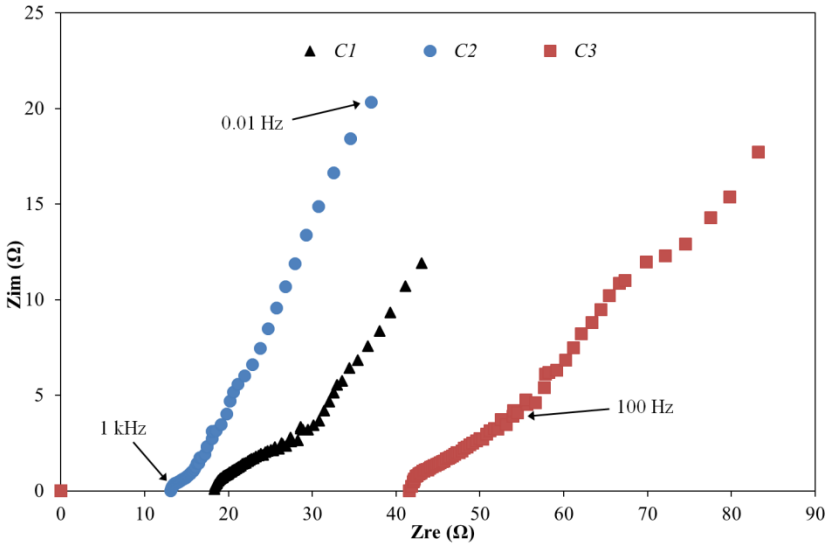

Figure 6.7: Nyquist plot recorded at potential of 0 V for a frequency ranged from 100 kHz to 0.01 Hz

As shown in Figure 6.7, ESR can be estimated for each EDLC from the intersection between the low frequency and more straight section of the Nyquist plot and the X-axis (Lei et al., 2013). The height of the 3D printed layer is 0.6 mm for AC electrodes and generally showed a weak adhesive force between electrodes and current collector resulting in poor cycle stability and high ESR. In addition, PVA/H_3PO_4 aqueous gel electrolyte could not permeate quickly in comparison with the organic electrolyte. The AC based on PVDF-HFP binder showed a weight loss due to a loss of solvent leading to change in the layer thicknesses of electrode. The ion charge resistance is inversely proportional to the electrode area at 2 mm thickness. The expected semicircle cannot be seen in the higher frequency range due to the low contact resistance and the charge transfer resistance was low. It was unexpected that the bulk solution resistance of the PVA/H_3PO_4 in *C2* was higher than *C1* and *C3*. The plot is horizontal at low frequency because of losing a quantity of electrons by Faradaic reactions or at 15 mA of charging current there has been an increase in the iR drop. The reduction of ESR and iR drop allows flexible EDLCs to achieve high power density. The main contribution of this work that a new approach to manufacture EDLC in a single process with various types of materials has been developed, which means EDLC can be manufactured to be the same or different form without the requirement for a mould pattern. AC, gel electrolyte, and silicone deposition by 3D printing process not only reduces the transferring pattern process and waste it also controls the layers and weight. The EDLCs were sealed as an integral part of this process without the need of additional laminating.

6.5 Design of the structure of printable wearable EDLC

Figure 6.8 shows the schematic diagram of an EDLC designed for this study. Due to the working mechanisms, there are four layers of materials on each side of an EDLC, i.e. silicon substrate, current collector, AC material, and gel electrolyte. This EDLC was also designed as a wearable device, i.e. a bracelet, thus the structure of the supercapacitor designed for this study included a locking mechanism to allow the complete product to be worn around the wrist as a bracelet.

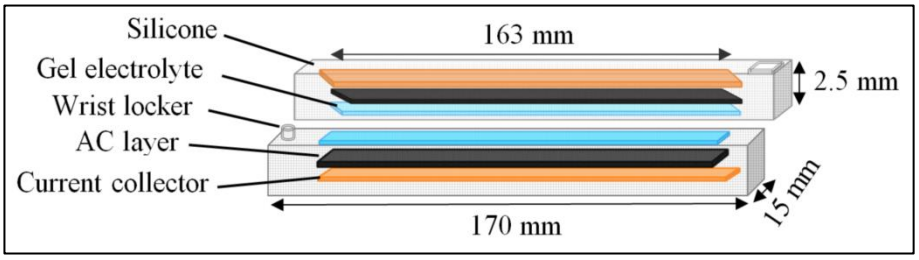

Figure 6.8: Schematic of the structure of printable wearable EDLC

Figure 6.1 shows the manufacture processes of a flexible EDLC, and Table 6.1 lists the manufacturing process parameters. The EDLCs components were deposited in a 100% fill density in grid patterns to make the device robust. The frame part of an EDLC printed by depositing acetoxy silicone material on a build platform covered with Teflon paper, which was used for easy removal when the wet silicone is dried. Subsequently, the frame part printed was left to cure for 2 hours. In addition, 5% CMC binder was coated by spreading method on surface of the silicone substrate in order to help the current collector layer stick onto the silicone substrate better. The current collector material to be deposited on silicone layer, and kept for 2 hours to fully cure and adhere to the silicone substrate. Next, the AC electrode layer of 0.6 mm thickness was deposited with a dimension of 163 mm x 5 mm as shown in Figure 6.8. Following this, the gel electrolyte of PVA/H_3PO_4 was deposited onto the electrodes and they were kept in a vacuum desiccator for an hour to allow the infiltration of the PVA/H_3PO_4 electrolyte into the carbon particle porous fully.

Table 6.1: 3D process parameters used for manufacturing a wearable EDLC

Pastes	Layer height (mm)	Nozzle diameter (mm)	Printing speed (mm/s)	Feed-rate (steps/mm)
Silicone & AC	0.6	0.6	90	18,000
Electrolyte & conductive paste	0.6	0.6	60	15,000

The components already built and fully dried were then returned to the platform of the 3D printer to deposit another layer of silicone around the edge to act as a gasket. The other side of the EDLC was printed the same as described above. Finally, the two sides were sealed together as a complete EDLC, as revealed in Figure 6.9.

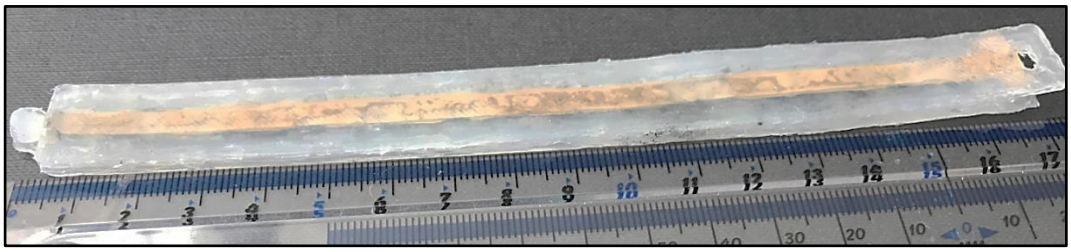

Figure 6.9: Image of flexible wearable EDLC

In total four EDLCs (designated as *C1*, *C2*, *C3* and *C4*) have been manufactured under the same conditions in this study to investigate the reproducibility of the manufacturing process and the stability of the electrochemical performance of the EDLCs. *C1* was selected as a sample for assessing the electrochemical performance of a single supercapacitor designed and manufactured in this section. *C1* and *C2* were selected for evaluating the combined electrical circuit.

6.5.1 Evaluation of the 3D printing process

Figure 6.10 shows a half (one side) of the EDLC successfully printed with 2 layers on 2.5 mm thick silicon substrate, each layer of the material printed was about 0.6 mm thick and the total printing time spent was approximately 8 minutes. The total mass of

printed AC electrode was 2 g for both EDLC frames at 100% fill density. Overall, the 3D printed flexible EDLC showed that the adhesion between different material layers was strong and there was no leakage. The grid pattern selected for different layers of materials displayed a solid structure and robust final product. The disadvantage of the paste extruder driven by a stepper motor was that it was difficult to have a consistent deposition rate when the material's viscosity was too high with the tiny 0.6 mm diameter tapered printing nozzle. Therefore, the silicone and AC slurry had to be fresh material, with a low viscosity, in order to obtain a consistent deposition and an accurate dimension for each layer of the material (see Appendix D). The PVA/H_3PO_4 gel electrolyte and its viscosity and smooth flow could be manipulated by adding H_3PO_4 acid if necessary.

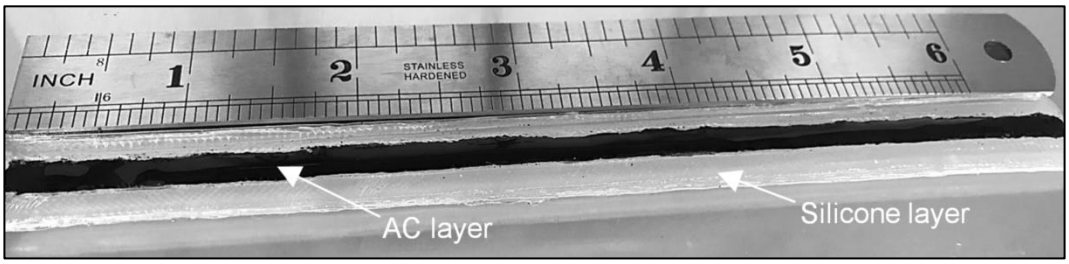

Figure 6.10: 3D printed EDLC part of the silicone substrate and AC layers

The scanning electron microscopy (SEM) of the surface morphology of the 3D printed AC slurry electrode is shown in Figure 6.11. It was measured on a Zeiss (Model SUPRA 35 VP), and operated at an acceleration voltage of 20 kV. It reveals that the AC slurry consists of PVA binder and has a porous structure that was impregnated with H_3PO_4 electrolyte. The small number of holes is intriguing. It might be due to the trapped air when the paste was extruded or the front filling method of the AC paste has entrapped some air.

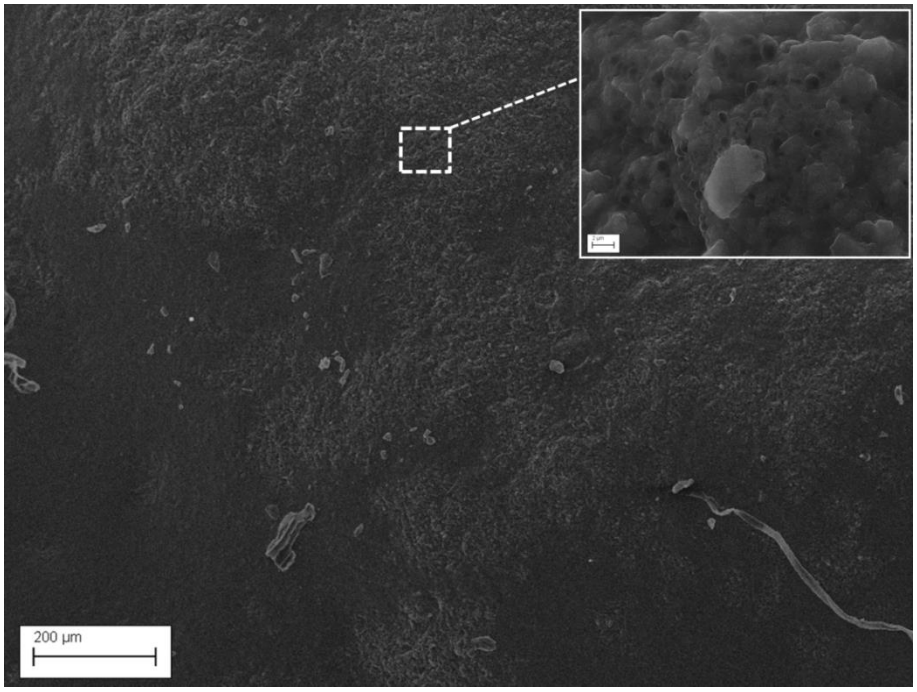

Figure 6.11: SEM image of 3D printed AC electrode layers

6.5.2 CV characterization

CV tests were performed to determine the capacitance of the printed AC electrodes. All CV curves were recorded with an applied potential from 0 to 0.8 V. Figure 6.11 shows the typical charge-discharge profile of the flexible EDLC (*C1*). *C1* delivered a capacitance of 1.4, 0.7, and 0.2 F at the scan rate of 20, 50, and 100 mV/s, respectively, calculated by equation (1). It can be seen that the charging current decreases with the decrease of scan rate, which leads to an increase of the capacitance. The Ca of the flexible EDLC based on both electrolytes calculated from the CV curves by equation (3) were 1.48, 0.45, and 0.13 F/cm^2 at scan rate of 20, 50, and 100 mV/s, respectively. The specific capacitance of the EDLC depends on the specific surface area of AC electrode in contact with the electrolyte. The Chinese ink used in the AC material may also provide an extra accessible specific surface area in this case. The capacitance increased with the decrease of the scan rate because at the lower scan rate the ions could travel deeper inside the AC material leading to a better surface coverage reaction.

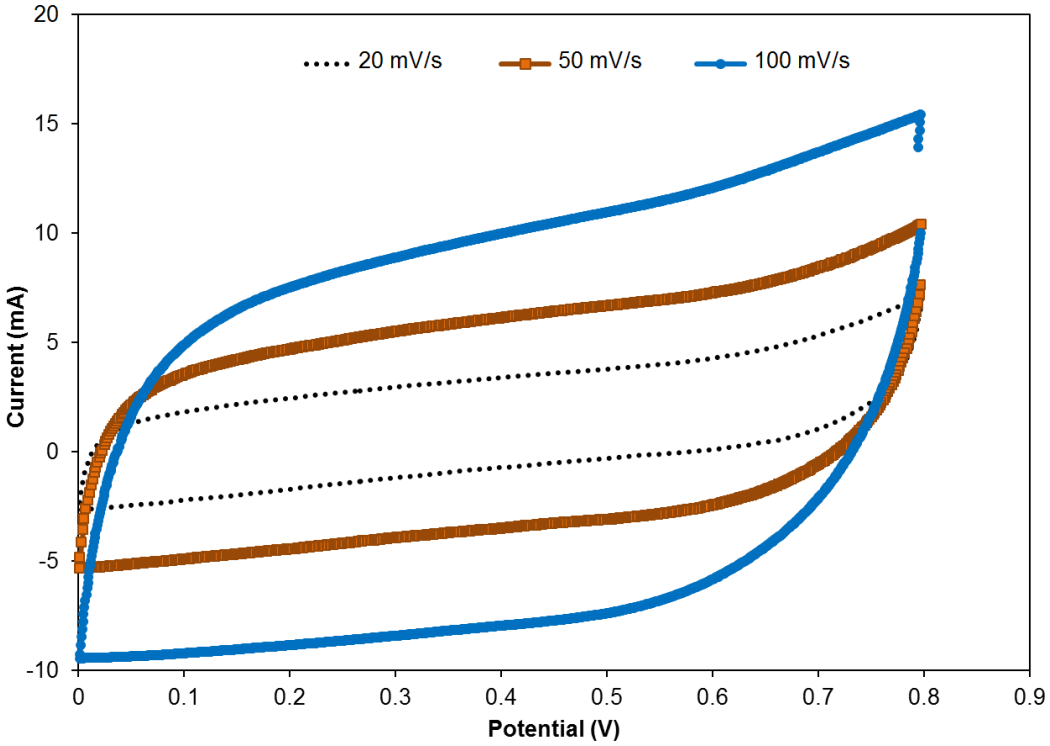

Figure 6.12: CV curves of printed flexible EDLC recoded at different scan rates of 20, 50, 100 mV/s

6.5.3 GCD characterization

Figure 6.13(a) shows five cyclic charge-discharge curves measured for *C1* at a constant current of 15 mA. By applying the potential to the electrodes, ions were pulled to the surface of the electrical double layer and supercapacitor was charged. Inversely, they moved far away when discharging the supercapacitor and the dielectric material (PVA/H_3PO_4) was responsible for preventing the two AC electrodes from contacting or shorting. The curve is almost linear within the whole potential range, which shows an excellent supercapacitor performance. There was an iR drop because of the equivalent series resistance (ESR) of the EDLC and discharge current, which is the voltage drop (V_{iR}) at the beginning of each discharge curve, as shown in Figure 6.13(a). The iR drop for the electrolyte was about 0.12 V. The iR compensation technique (iR_{comp}) using the electrochemical workstation in an auto-ranged experiment showed the resistance to be 5.5 Ω. The minimum iR_{comp} (1.96 Ω), is similar to the ESR and shows a good contact between printed AC and current collector and there was no corrosion on current collector caused by PVA/H_3PO_4. The discharging time of the GCD process was 4 s. The

capacitance can be directly calculated by GCD using equation (4), which was 0.1 F and almost half of the capacitance value calculated by CV at the scan rate of 100 mV/s. This is because the high current of 15 mA was applied constantly during the GCD test at 0.8 V, whereas the maximum current observed from the CV test was 15 mA at the scan rate of 100 mV/s (shown in Figure 6.12). It has been proved above that the higher current applied the lower the capacitance that can be obtained. It is considered that the high current of 15 mA and the thickness of 0.6 mm of the AC electrodes lead to a low operation of kinetic movement of ions. In addition, the low iR_{comp} and the maximum current of 15 mA at the scan rate 100 mV/s may lead to some energy loss. Figure 6.13(b) shows that the iR increased when the current increased, the capacitance calculated by the GCD using equation (4), was 4.13, 2.65, 1.93, 0.45, and 0.1 F at currents of 4, 6, 8, 10, and 15 mA, respectively. The specific capacitance (C_s) of the flexible EDLC based on the mass of each AC electrode calculated by equation (6) was 0.2 F/g. The coulombic efficiency (η) of *C2* was calculated by using equation (10), to be 59.91%. The energy efficiency (η_{eff}) of *C2* was calculated by using equation (11), to be 60.1% at the same current value of 15 mA.

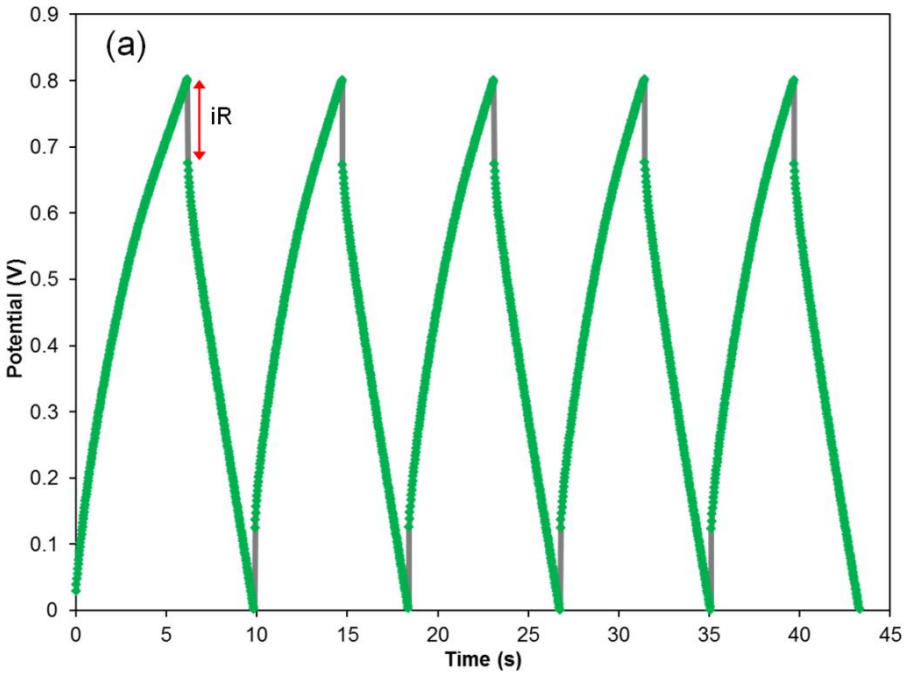

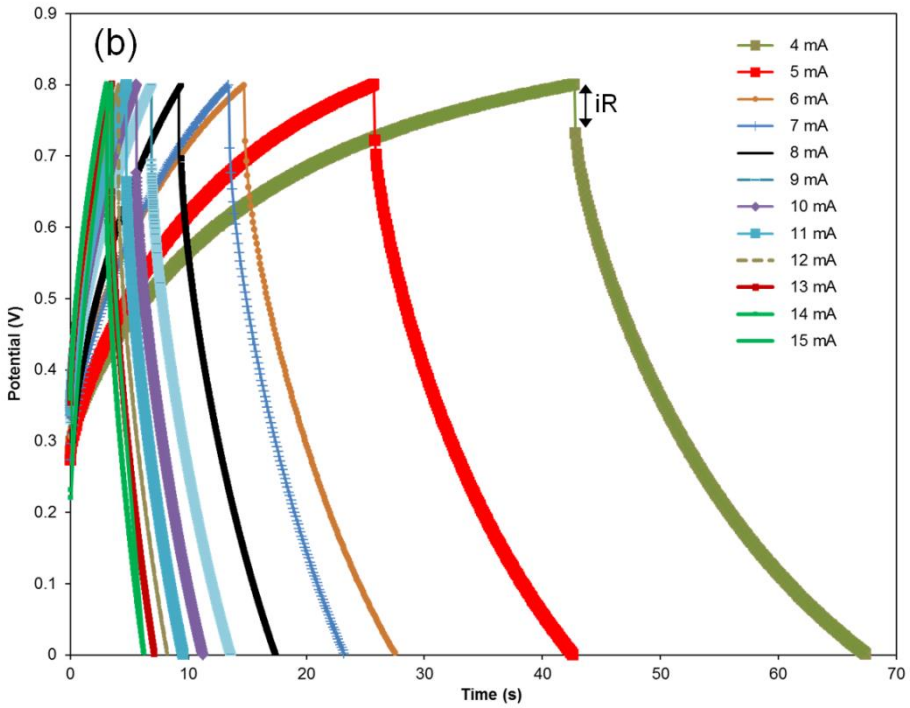

Figure 6.13: (a) Constant current GCD curve of flexible electrodes at current of 15 mA, and (b) GCD curve recorded at different charge currents

The specific energy density of the EDLC printed was 0.064 Wh/kg, and specific power was 57.60 W/kg. AC based EDLCs have the unique advantage of higher power and energy density when used with organic electrolytes (Chen et al., 2012). The specific energy of the flexible EDLC in PVA/H_3PO_4 gel electrolytes developed in this study was not comparable with organic electrolyte based EDLCs. Table 6.2 shows a comparison of the supercapacitor based on a 3D paste process and the supercapacitors made using other 3D printing methods. Each type of the 3D printing method has its specific advantages and disadvantages (Sun et al., 2015; Zhu et al., 2016; Li et al., 2016; Wang et al., 2017; Zho et al., 2014; Foster et al., 2017). The specific capacitance of 3D flexible supercapacitors was 1.48 F/cm^2 which is much higher in comparison with that manufactured by 3D laser direct writing (which was 3.8 mF/cm^2) (Li et al., 2016), or manufactured by micromachining technique (Sun et al., 2009).

Table 6.2: 3D printing techniques for fabrication of supercapacitors

Fabrication process	Electrode/ Electrolyte	Performance				Ref.
		Specific capacitance	Energy density	Power density	Cycling stability	
3D printing direct-ink writing	Graphene aerogel/KOH	63.6 F/g	0.14 mWh/cm^3	49.4 mW/cm^3	95.5% after 10,000 cycles	Zhu et al., (2016)
3D laser direct writing	rGO/Au/PVA-H_2SO_4	3.8 mF/cm^2	n/a	n/a	50% after 10,000 cycles	Li et al., (2016)
3D micro extrusion	rGO/PVA-H_2SO_4	41.8 F/cm^3	7.6 mWh/cm^2	29.2 mW/cm^2	41% after 10,000 cycles	Sun et al., (2015)
3D laser direct writing	Polyimide/PVA-H_2SO_4	2.3 mF/cm^3	n/a	n/a	96% after 2000 cycles	Wang et al., (2017)
3D printing selective laser melting	PPy/PVA-H_3PO_4	2.4 F/cm^3	213.5 Wh/m^3	15.0 kW/m^3	78% after 1000 cycles	Zhao et al., (2014)
3D printing (FDM)	Graphene PLA/PVA-H_2SO_4	485.4 µF/g[1]	n/a	n/a	33% after 200 cycles	Foster et al., (2017)
Micromachining technique (LIGA-like)	PPy/ $LiClO_4$-H_2O-PVA	0.03 F/cm^2	n/a	2.2 mW/cm^2	n/a	Sun et al., (2009)
3D paste process	AC/PVA-H_3PO_4	1.48 F/cm^2	0.064 Wh/kg	57.6 W/kg	56% after 500 cycles	This work

6.5.4 Test of combination circuits of printed flexible EDLCs

The applications of flexible EDLCs strongly depend on operating voltage. However, the maximum voltage that can be applied on a single aqueous electrolyte based EDLC is low (< 0.8 V), therefore, they often need to be connected to each other in series or parallel combinations to achieve desired operating voltage and capacitance as shown in Figure 6.14(a, b). In order to demonstrate the electrical functionality of the flexible EDLCs manufactured in this study, the tests of electrical performance of two EDLCs in the form of series and parallel connection were carried out. Figure 6.14(c) shows the CV curves of two individual flexible EDLCs (*C1* and *C2*) and their series and parallel combination circuits. It can be seen from curves at scan rate 20 mV/s that there is a very little reduction and oxidation at around 0.5 V in *C1*, *C2* and parallel circuits. The area of the CV curve decreased significantly for series circuits at the operating voltage of 1.6 V. It is noticed that the area of *C1* or *C2* is approximately equal to double of the area for the series circuits whereas the total area of *C1* and *C2* is equal to the area in the parallel circuit, which implies that the ELDCs behave as a normal energy storage device. Table 6.3 gives the relationship between the capacitance values at the scan rate of 20 mV/s and iR_{comp}. It can be seen that the flexible EDLCs made in this study behave strictly like the normal energy storage, i.e. the theoretical values are very close to the experimental values. In addition, the relationship between the capacitance values of individual EDLCs and their series and parallel circuits measured by CV and GCD tests strictly comply with the principle of energy storage. The fact that the capacitance value for series circuit (0.7/0.034 F) being lower than that for parallel circuit (2.6/0.17 F) as is expected.

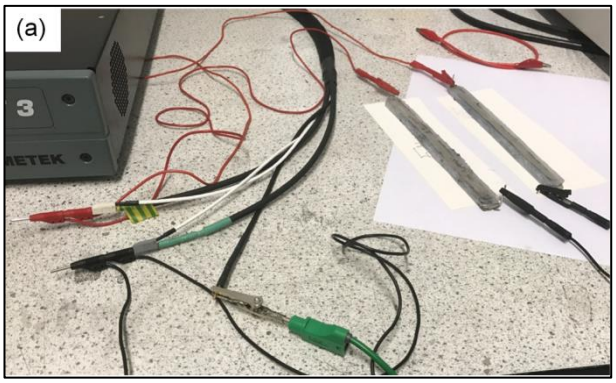

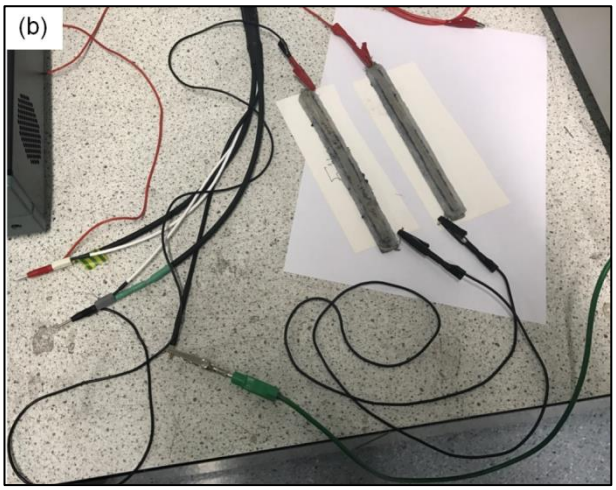

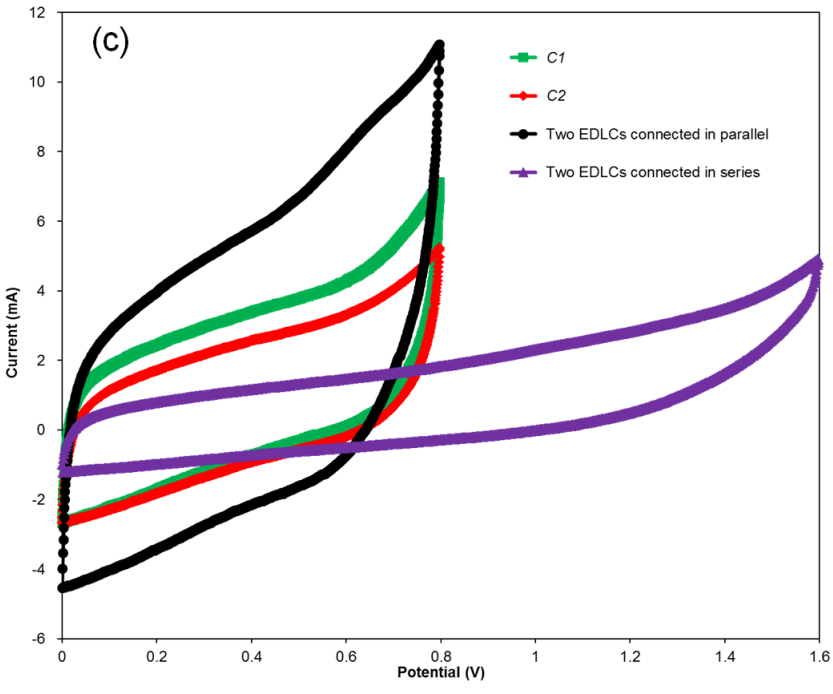

Figure 6.14: (a) Photograph of two EDLCs in parallel, (b) in series, and (c) CV recorded at 20 mV/s for two single EDLCs and their electrical combinations in series and parallel

Table 6.3: All circuits calculated capacitances from CV at 20 mV/s and GCD with iR compensation

	Capacitance (F)				iR_{comp} (Ω)
	by (CV)		by (GCD)		
	Experiment	Theory	Experiment	Theory	
C1	1.4		0.1		5.5
C2	1.5		0.07		3
Parallel	2.6	2.9	0.17	0.17	1.96
Series	0.7	0.72	0.034	0.04	8.69

The GCD plots in Figure 6.15 shows a comparison of the first cycle charge-discharge curve for each type of circuit, i.e. two individual EDLCs and their series and parallel connection. The capacitances for *C1* and *C2* calculated from the GCD curve using eqation (4) are 0.1 and 0.07 F, respectively. The capacitance calculated from the GCD tests for parallel circuit is 0.17 F, which is the same as the sum of *C1* and *C2* calculated by GCD. It can be seen obviously that the iR drop significantly decreases in parallel circuit, which was 0.08 V at 15 mA, in comparison with 0.36 V at the operating voltage of 1.6 V in the series circuit. The iR drop observed is larger with the series circuit due to the high value of ESR. The maximum current that can be applied in the parallel circuit at 0.8 V was identified to be 19 mA, i.e. under 19 mA and 0.8 V the parallel circuit behaves appropriately, and the iR drop increased to 0.11 V accordingly. The specific energy density of flexible EDLCs in PVA/H_3PO_4 gel electrolyte in parallel and series circuits was 0.11 Wh/kg, 0.087 Wh/kg, with power densities of 55 W/kg, 110 W/kg, respectively.

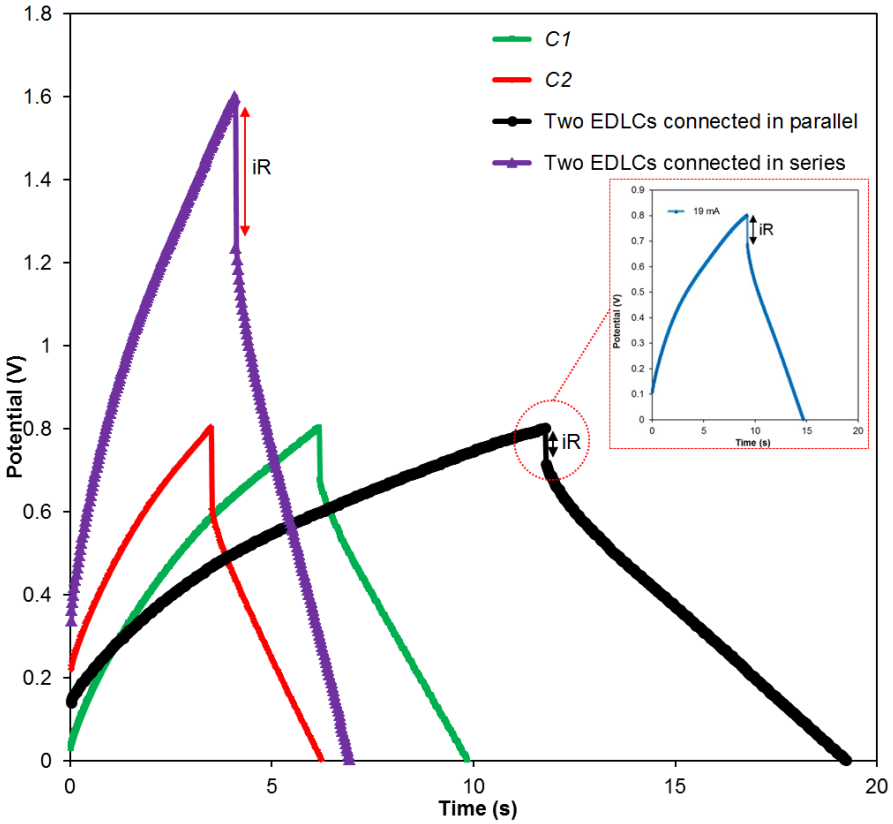

Figure 6.15: GCD curve of the first cycle for each circuit and enlarged view of parallel circuit at 19 mA

Figure 6.16 shows that the results correspond well with the impedance performances of *C1*, *C2* and their electrical combinations in series and parallel at the frequency range of 100 kHz to 0.01 Hz. It shows a good capacitive performance even at a high frequency, e.g. 100 kHz. The semicircle cannot be seen from the graph because of the low contact resistance and highly accessible surface of the printed AC electrode; and the charge transfer resistance was low due to the electrolyte concentration. The ESR can be estimated for each circuit from the intersection between the straight section of the Nyquist plot at low frequency and the X-axis (Lei et al., 2013). In addition, the iR_{comp} can be estimated by the same approach, but can be measured more accurately when using the auto range function in an electrochemical workstation.

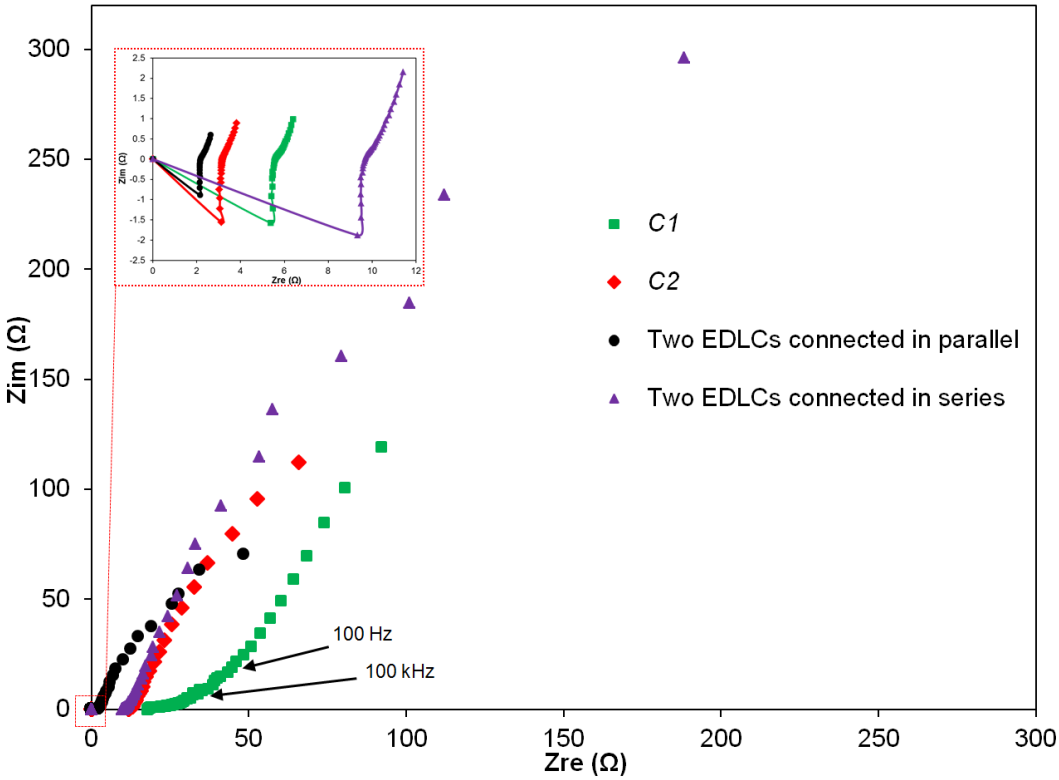

Figure 6.16: Complex plane plot of the impedance for each circuit using a 0V and the enlarged view in the area of high frequencies

6.5.5 Flexibility of the EDLCs

An important requirement for an energy storage device nowadays is its flexibility as conventional supercapacitors can be too bulky, heavy, and rigid. Highly flexible EDLCs that can be bent without affecting the performance are desired. Mechanical bending tests were carried out in this study to investigate the flexibility of the EDLCs printed. *C2* was chosen for the bending tests with radius (r) of 15 and 35 mm. The CV curves in Figure 6.17 show no obvious oxidation or reduction when the current was 15 mA and the operating voltage of 0.8 V at the scan rate 50 mV/s under the conditions of being flat and with a bend radius of 35 and 15 mm. The capacitance of *C2* under those conditions was 0.68, 0.37, and 0.4 F, respectively, i.e. 54 ~ 58% of capacitance was retained under the bending conditions when compared with the original flat status. It is believed that this deterioration of capacitance was due to the adhesion between the AC electrodes and the current collector of the EDLC becoming worse under the bending condition, which caused higher resistance of the EDLC. This result is in good agreement with the findings from the results described by other researchers (Zhang et al., 2016).

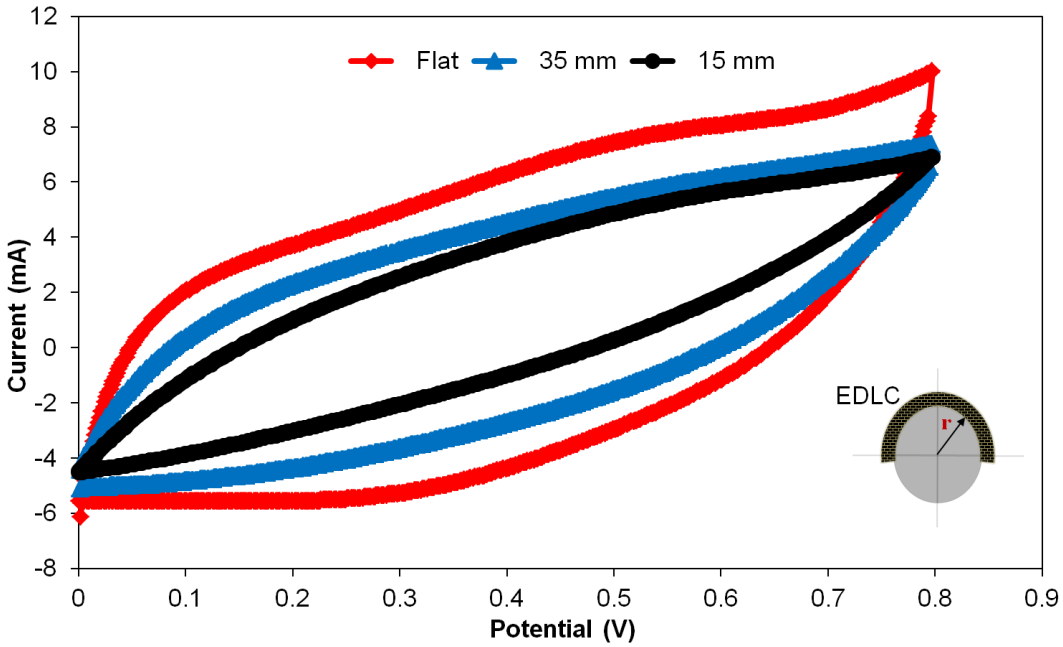

Figure 6.17: CV curve of 3D flexible EDLC recoded at 50 mV/s under flat, bent radius of 35 and 15 mm conditions

The GCD behaviour was also investigated at the bending radius of 35 mm and 15 mm at 0.8 V and current of 15 mA, as shown in Figure 6.18. It can be clearly seen that the iR drop significantly increases in the bent condition in comparison with the flat EDLC. The iR_{comp} also increases to 17.3 Ω at 35 mm bending radius in contrast with 13.5 Ω when the bending radius was 15 mm and 3 Ω when it was flat. Hence, the result shows that the iR_{comp} at the bending radius of 15 mm is approximately 21% less than the iR_{comp} for a radius of 35 mm, which is the reason for the slight increase of the capacitance as revealed by the CV measurement discussed above. The reason for iR drop change under the bending tests could be the conductivity decrease caused by the contact area change of each layer. At high bending, the iR drop decreases because of compression of the EDLC components particles.

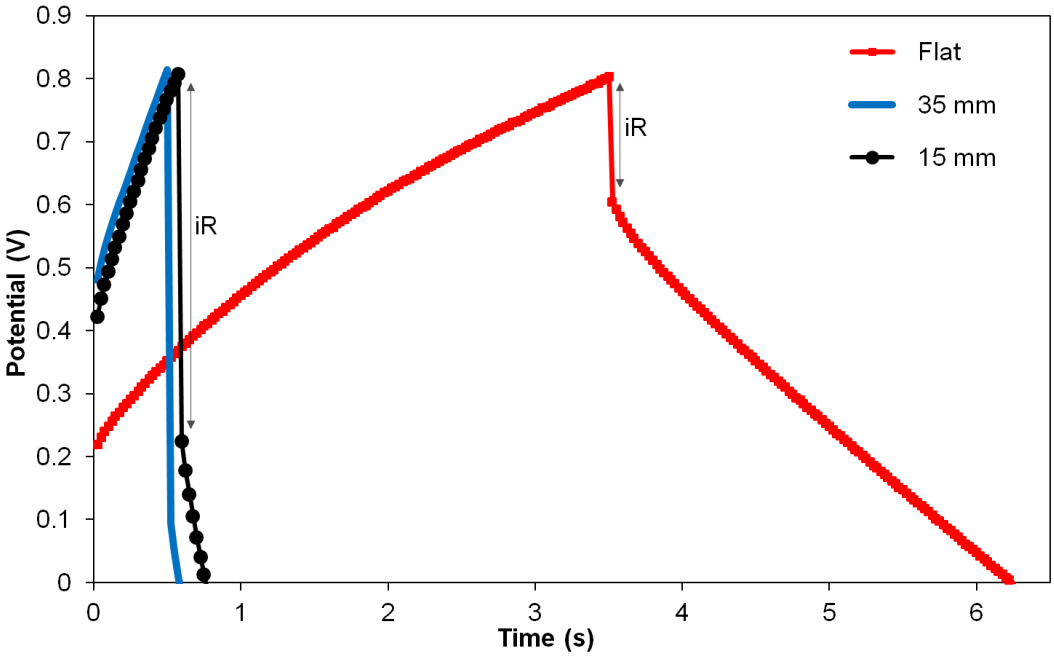

Figure 6.18: GCD curves of flexible EDLCs with bending and flat status at current of 15 mA

Figure 6.19: Digital image of flexible EDLC

6.5.6 Cycling stability

Figure 6.20 shows the CV curves of *C2* for different cycles recorded at a scan rate of 80 mV/s. It can be seen that the capacitance decreases gradually when the cycling number increases. After few cycles, the contact force between electrode and PVA/H_3PO_4 gel electrolyte was changed and this suggests that the ion diffusion in the PVA/H_3PO_4 decreased as the water had evaporated. The capacitance of *C2* was calculated by equation (1). Figure 6.21 shows the corresponding capacitance with respect to the CV cycle number. Capacitance decreased significantly to 80% of that initial capacitance at the 50^{th} cycles, the capacitance was 56% compared to the capacitance at 5^{th} cycle after 500 cycles.

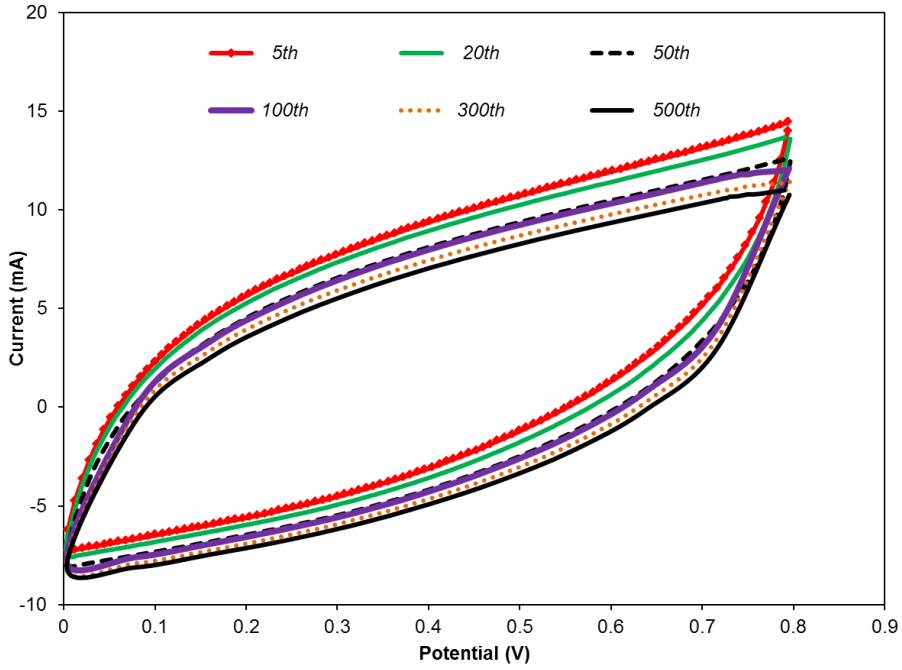

Figure 6.20: CV curves of the EDLC under cyclic test

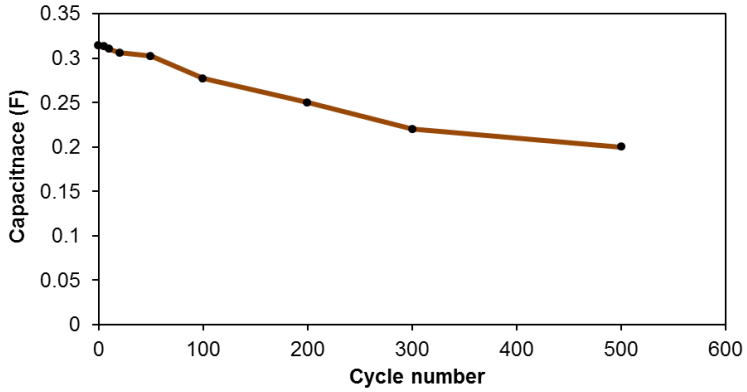

Figure 6.21: Capacitance decay curve of the EDLC during 500 cycles

6.5.7 Reproducibility of the EDLC

The other two EDLCs (*C3* and *C4*) fabricated with the same manufacturing processes and conditions as *C1* and *C2* were evaluated by the same method to investigate the reproducibility of the 3D printing method. The performance of all four EDLCs has been compared and is shown in Figure 6.22. It shows the typical shape of CV curves at the scan rate of 100 mV/s. The area of the CV charge and discharge curves is quite similar suggesting the stability and reproducibility of the 3D printed process for flexible EDLCs. The capacitances of all samples made are very similar at the scan rate of 20 mV/s, i.e. *C1* 1.4 F, *C2* 1.5 F, *C3* 1.4 F, and *C4* 1.2 F, respectively.

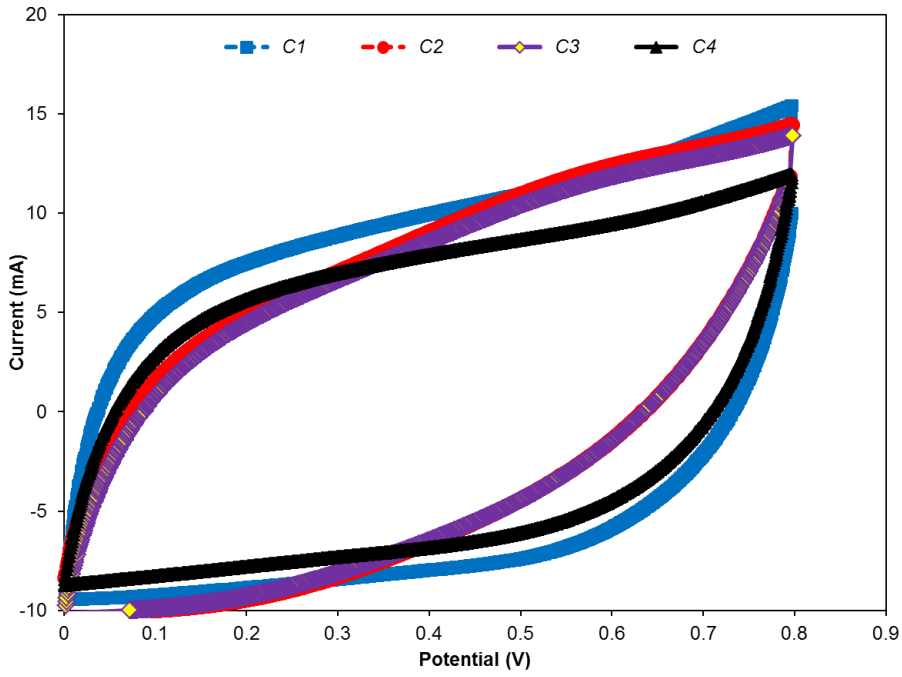

Figure 6.22: CV curves of four EDLCs under the same 3D parameters and conditions

6.5.8 Integrating with energy harvesting devise

Energy harvesting is the process by which energy is derived from external sources such as solar energy and piezoelectric devices. A flexible 3D supercapacitor was investigated in a practical application to see how it would charge by harvesting energy. As shown in Figure 6.23, we have integrated the circuit, with a piezo buzzer of 27 mm diameter, driven by a frequency of 4.6 kHz. A piezo buzzer generates energy when it is stuck on a working speaker therefore; we have run the circuit for 1 hour and our flexible EDLC was charged to reach 0.6 V.

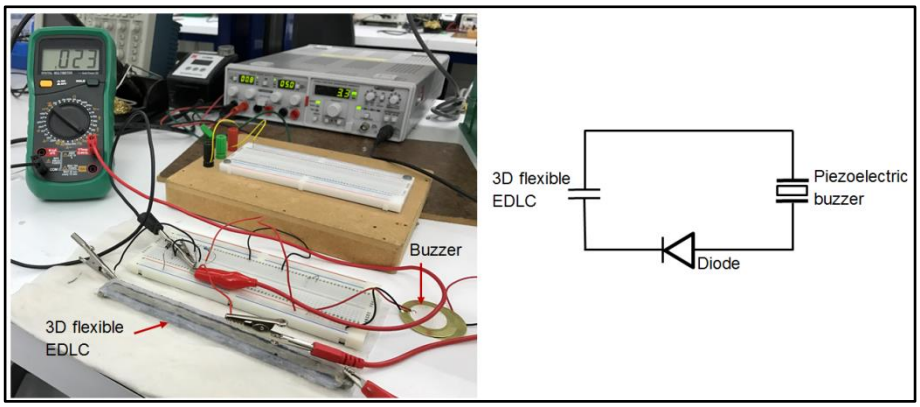

Figure 6.23: Integrated 3D flexible EDLC, the piezoelectric buzzer and diode circuit

6.6 Chapter Summary

Flexible EDLCs with a silicone rubber-like substrate were fabricated successfully by 3D printing technology. It has been shown that 3D printing is a promising technique to make various patterns and accurate shaped structures using multiple materials that have different mechanical properties. Only one single extrusion device was responsible for building the structure described in this work. Three cells have been deposited in one module in a honeycomb pattern at a feed rate of 21,000 steps per mm. The reversing of the electrode polarity on discharge has been investigated and the electrochemical performances were tested at a potential of 0.8 V with a 2.4 M PVA/H_3PO_4 gel electrolyte. The reduction of internal resistance has been shown to be dependent on the binder strength and thickness, pattern structure and the fill density of electrodes, gel electrolyte, and current collector. The various materials that are needed to compose an EDLC can be applied in one extrusion system. Moreover, in section 6.5, four EDLC samples were fabricated successfully with grid patterns by 3D printing onto flexible silicone substrate. A typical structure of an EDLC was created by depositing current collectors, AC electrodes, and PVA/H_3PO_4 gel electrolyte onto silicone rubber as promising flexible materials for various applications of energy storage devices. The 3D printed EDLCs exhibited an excellent electrical capacitance performance for different combination circuits. The mechanical bending of the 3D EDLC was tested and exhibited a good flexibility and retention of 54 ~ 58% of its initial capacitance at a scan rate of 50 mV/s. The 3D printing process had a good reproducibility and this suggests that 3D printing based on paste extrusion may be used to develop more sophisticated electronic devices with various forms of paste materials. The integration of a flexible EDLC with an energy harvesting device has also been demonstrated.

Chapter 7 Conclusions and Suggestions for Future Work

7.1 Findings and Results

Returning to the original research questions, we consider how far these have been answered:

- Can the flexible EDLC components be fabricated by a commercial AM process (3D printing) so that the designer is free to select how they are made and how they perform with a large range of parameters?

  - The work in Chapter 4 has shown that this is possible.

- Can flexible electrical double-layer capacitors based on AC slurry and gel electrolytes be manufactured in a single inexpensive manufacturing process?

  - The work in Chapter 5 has shown this is possible and studied and optimised the electrode particle size and thicknesses, and electrolyte fill densities.

- Can the conductive and active paste materials be used in the 3D printer to make flexible EDLCs that take advantage of the electrochemical properties of a paste material?

  - The possibility to achieve a good electrochemical performance of 3D flexible EDLC is depending on the properties of paste materials proposed in Chapter 6.

- Is it possible to manufacture flexible/wearable EDLCs using 3D printing technology?

  - The work in Chapter 6 has revealed/enabled the manufacturing of lightweight and highly flexible 3D wearable EDLCs.

Here, brief findings are provided, and results are summarised as follows:

1. The bending test was joined with the electrochemical workstation to test the performance of the flexible EDLCs based on bending conditions. The flexible EDLCs bracelet shaped based on the silicon substrate was functional under bending tests with radius (r) of 15 and 35 mm. 54 ~ 58% of capacitance was retained under the bending conditions when compared with the original flat status. Moreover, the relationship between the capacitance, iR_{comp} and iR drop was clarified. It was found that the capacitance decreased when the resistance and voltage drop changes under bending tests. The reason is that the conductivity decrease was caused by the contact area change of each layer.

2. To meet the requirements of various applications, EDLCs are usually connected in parallel or series due to the limited voltage on a single EDLC based on gel electrolyte. The combination circuit of two flexible EDLCs was connected and tested. It showed that EDLCs behave like a typical energy storage device in parallel and series combinations.

3. The life cycle is an essential concern in the durability of EDLC performance; it will influence its suitability in different applications such as electric vehicles. The flexible EDLC based silicone substrate was able to retain 56% of capacitance after 500 CV cycles. The energy and coulombic efficiencies of the flexible EDLC were achieved to be 59.91% and 60.1%, respectively.

4. The procedure for the manufacture of 3D flexible EDLC is reproducible, and the capacitance results showed that there was a little difference between four values of flexible EDLC samples.

7.2 Summary of Contribution to Knowledge

The academic contribution made by thesis summarised as follows:

7.2.1 Deposition of activated carbon paste

The AC paste developed in this work is conductive and it would be difficult to claim that AC deposition is not a requirement of future work. To date, there has been little research work available in the AM arena with AC paste. It could be due to the limitation of slicing software, as most are operated with particular material, mostly thermoplastic, not precisely AC slurry. The process provides no waste material, only depositing material additively where it is required in the supercapacitor structure. Although potentially this could also be achieved by inkjet printing, the viscosity of the AC materials makes them unsuitable for this approach. The 3D manufacturing process for the AC electrode has established. The purpose of using 3D printing to deposit AC paste is not only to reduce the transferring pattern method, but it also controls the layers and weight. Three different patterns (rectilinear, grid and honeycomb), and thicknesses of 1, 2, 3 mm were deposited and investigated. The optimum deposition of the AC was investigated and optimised using the ball-milling method, and binder, and electrolyte acid content.

7.2.2 Deposition of gel electrolytes

One unique aspect of the design of this 3D printed supercapacitor is that only layers of gel electrolyte separate the two electrodes; there is no added filter paper separator as is conventionally used. Two types of the gel electrolyte H_3PO_4 based PVA binder, and H_2SO_4 based gel electrolytes have been deposited and evaluated for the application of the 3D printed flexible supercapacitor. In addition, three different patterns (rectilinear, grid and honeycomb), and various infill densities were deposited and investigated. Manufacturing and evaluation of PVA/H_3PO_4 and PVA/H_2SO_4 electrolytes along with 3D printable supercapacitors have been accomplished.

7.2.3 Manufacture of flexible supercapacitor by dual head extrusions

Regarding the originality of the manufacturing process, the use of a combination of two 3D printing processes, FDM and paste extrusion to fabricate a supercapacitor is

also unique. The manufacturing of flexible EDLCs by using 3D printing process is not just to reduce the two or three step process of manufacturing flexibles EDLCs to a single process. The digital 3D printing process makes it easy to change the 3D form of the printed supercapacitor due to it being digitally controlled compared to roll-to-roll methods, which require screens or plates to be made to reproduce the image. It also allows for the manufacture of a group of individual EDLCs samples, which means that it can manufacture the same or different to each other without the requirement for a mould pattern. However, Flexible EDLCs were successfully designed and made using a flexible compositefilament as a substrate, AC paste as the active electrode material, and gel electrolyte by 3D dual extrusions. The flexible EDLC showed a good electrochemical performance.

7.2.4 Manufacture of flexible supercapacitor by single head extrusion

It is still a challenge to manufacture by 3D single head extrusion and to achieve a good and stable electrochmeical performance, particularly under mechanical bending conditions. 3D single head paste extrusionallows a wide selection of composite materials to be deposited by quickly changing syringes in comparing to FDM. 3D paste printing does not need complicated post-processing such as thermal sintering, a mask to transfer patterns or heat to laminate EDLCs. The use of 3D paste printing has been found to be simple, and allows more rapid prototyping of EDLCs and achieves end properties of 3D EDLCs. Different flexible EDLCs were successfully designed and manufactured using silicone material as the substrate and showed good electrochemical behaviour.

7.3 Suggestions for Future Work

The analyses conducted in this thesis have given growth to many possible further studies that might allow for better understanding of the 3D dual printing process of manufacture flexible supercapacitors. This work covered multi 3D parameters related to the manufacture of the flexible energy storage devices and their influence on the electrochemical performance. It can be recommended expanding this process to other electronics products, such as a diode, battery, and transformer, and wherever 3D printing is becoming involved in different sectors. Several consequences reported here need further investigation. The study of the influence of layer geometry has revealed

some questions for instance, how 3D printed material characteristics at lower layer height (≥0.6 mm) would be, especially their conductivity and electrochemical performance. The effectiveness of 3D printing process for saving the time of manufacture, waste, and printed in three different infill patterns have been demonstrated. Further experimental work for 3D printing flexible supercapacitor in user-generated infill patterns could be alternative option to be compared with the present findings. This will help to identify which infill pattern can behave better in quality and electrochemical performance. Due to the unlimited shapes that the 3D printing process can achieve in compared with the conventional method, it would be interesting to manufacture flexible supercapacitors in a more complex shape to fully work particularly with wearable electronic devices.

Another promising way for the future work is to develop and design conductive slurries that can be deposited for the development of wearable technology. Further investigation of the composite materials properties and rheology of the deposit slurries would be strongly interested. It would also be of interest, with performing standard tests on those conductive slurries to test their suitability. It is difficult to deposit with higher viscosity slurries because of the paste extrusion tool consists a weak metal unit that holds a 20 to 50 cc syringe, as well as used a low torque stepper motor with a 100:1 planetary gear ratio. Therefore, it can be redesigned to enhance the flow rate and to avoid high pressure on the stepper motor.

With further improvements of the AC slurry, gel electrolyte, and print parameters, the resolution of less than 0.6 mm should be achievable to maintain electrochemically stable flexible EDLCs. Decreasing the layer height of a 3D paste process could result in significant improvement in bonding between the layers and thus increase in electrochemical performance. To satisfy the needs of flexible electronic devices, the performance of the flexible EDLCs under stretching and twisting will be examined in future work. The optimised parameters can be applied to other devices and the manufacturing of 3D electronic structures for users.

X. References

3ders., (2015). Laywoo-D3 FLEX filament. [online] Available at: http://www.3ders.org/articles/20150513-kai-parthy-is-back-with-laywood-flex-a-flexible-version-of-laywood-3d-printer-filament.html [Accessed January 2016].

Adhesivedispensing, (2005, A). Tapered nozzles. [online] Available at: http://www.adhesivedispensers.co.uk/tapertips.htm. [Accessed April 2015].

Adhesivedispensing, (2005, B). Syringes. [online] Available at: http://www.adhesivedispensers.co.uk/7300LL1NPK.htm. [Accessed April 2015].

Ametek scientific instruments (n.d.). VersaStudio software. [online] Available at: http://www.ameteksi.com/products/software/versastudio-software. [Accessed Aug 2015].

Bae, J., Song, M. K., Park, Y. J., Kim, J. M., Liu, M. and Wang, Z. L. (2011) 'Fiber Supercapacitors Made of Nanowire-Fiber Hybrid Structures for Wearable/Flexible Energy Storage', Angewandte Chemie - International Edition, 50, 1683–1687.

Bärtsch, M., Braun, A., Kötz, R. and Haas, O. (1998) 'High power electrochemical double-layer capacitor', Proceedings of the 38th power sources conference, Cherry Hill, NJ. , 17-21.

Becker, H.I., Gen Electric. (1957) 'Low voltage electrolytic capacitor', U.S. Patent 2,800,616.

Bellini, A., Shor, L. and Guceri, S.I. (2005) 'New developments in fused deposition modeling of ceramics', Rapid Prototyping Journal, 11(4), pp. 214-220.

Black Magic 3D, (2016). Conductive graphene PLA filament [online] Available at: http://www.blackmagic3d.com/aboutus.asp

Boos, D.L., Standard Oil Co. (1970) 'Electrolytic capacitor having carbon paste electrodes', U.S. Patent 3,536,963.

Cai, J., Lv, C. and Watanabe, A. (2017) ‘High-performance all-solid-state flexible carbon/TiO 2 micro-supercapacitors with photo-rechargeable capability’, RSC Adv. Royal Society of Chemistry, 7(1), pp. 415–422.

Cakici, M., Kakarla, R. R. and Alonso-Marroquin, F. (2017) ‘Advanced electrochemical energy storage supercapacitors based on the flexible carbon fiber fabric-coated with uniform coral-like MnO2 structured electrodes’, Chemical Engineering Journal, 309, pp. 151–158.

Cetiner, S. (2014) ‘Dielectric and morphological studies of nanostructured polypyrrole-coated cotton fabrics’, Textile Research Journal, 84(14), pp. 1463–1475.

Chang, C. (2004) ‘Direct slicing and G-code contour for rapid prototyping machine of UV resin spray using PowerSOLUTION macro commands’, The International Journal of Advanced Manufacturing Technology, 23(5-6), pp. 358-365.

Chen, P., Chen, H., Qiu, J. and Zhou, C. (2010) ‘Inkjet printing of single-walled carbon nanotube/RuO 2 nanowire supercapacitors on cloth fabrics and flexible substrates', Nano Research, 3(8), pp. 594-603.

Chen, T. and Dai, L. (2014) ‘Flexible supercapacitors based on carbon nanomaterials’, J. Mater. Chem. A, 2(28), pp. 10756–10775.

Chen, X., Lin, H., Deng, J., Zhang, Y., Sun, X., Chen, P., Fang, X., Zhang, Z., Guan, G. and Peng, H. (2014) ‘Electrochromic fiber-shaped supercapacitors’, Advanced Materials, 26(48), pp. 8126–8132.

Chen, Y., Xu, J., Yang, Y., Zhao, Y., Yang, W., He, X., Li, S. and Jia, C. (2016) ‘Enhanced electrochemical performance of laser scribed graphene films decorated with manganese dioxide nanoparticles', Journal of Materials Science: Materials in Electronics, 27(3), pp. 2564-2573.

Chen, Y., Zhang, X., Zhang, H., Sun, X., Zhang, D. and Ma, Y. (2012) ‘High-performance supercapacitors based on a graphene–activated carbon composite prepared by chemical activation’, RSC Advances, 2(20), p. 7747.

Cheng, T., Zhang, Y., Yi, J., Yang, L., Zhang, J., Lai, W. and Huang, W. (2016) 'Inkjet-printed flexible, transparent and aesthetic energy storage devices based on PEDOT: PSS/Ag grid electrodes', Journal of Materials Chemistry A, 4(36), pp. 13754-13763.

Choi, K., Yoo, J., Lee, C.K. and Lee, S. (2016) 'All-inkjet-printed, solid-state flexible supercapacitors on paper', Energy & Environmental Science, 9(9), pp. 2812-2821.

Chuizhou Meng (2013) 'A Review of Flexible and Weaveable Fiber-Like Supercapacitors', Journal of Postdoctoral Research, 1(12), pp. 16–30.

Corni, I., Ryan, M. P. and Boccaccini, A. R. (2008) 'Electrophoretic deposition: From traditional ceramics to nanotechnology', Journal of the European Ceramic Society, 28(7), pp. 1353–1367.

Dubal, D.P., Ayyad, O., Ruiz, V. and Gómez-Romero, P., (2015) 'Hybrid energy storage: the merging of battery and supercapacitor chemistries', Chem. Soc. Rev., 44(7), pp.1777–1790.

El-Kady, M. F. and Kaner, R. B. (2013) 'Scalable fabrication of high-power graphene micro-supercapacitors for flexible and on-chip energy storage.' Nature communications. Nature Publishing Group, 4, p. 1475.

Foster, C.W., Down, M.P., Zhang, Y., Ji, X., Rowley-Neale, S.J., Smith, G.C., Kelly, P.J. and Banks, C.E., (2017) '3D Printed Graphene Based Energy Storage Devices', Scientific Reports, 7(March), p.42233.

Fu, K., Yao, Y., Dai, J. and Hu, L. (2017) 'Progress in 3D Printing of Carbon Materials for Energy-Related Applications', Advanced Materials, 29(9), p. 1603486.

Functionalize, (2014). F-Electric filament. [online] Available at: http://functionalize.com/about/#HowitBegan

Gao, W., Zhang, Y., Ramanujan, D., Ramani, K., Chen, Y., Williams, C.B., Wang, C.C., Shin, Y.C., Zhang, S. and Zavattieri, P.D. (2015) 'The status, challenges, and future of additive manufacturing in engineering', Computer-Aided Design, 69, pp.65-89.

Gardner, J. M., Sauti, G., Kim, J. W., Cano, R. J., Wincheski, R. A., Stelter, C. J., Grimsley, B. W., Working, D. C. and Siochi, E. J. (2016) '3-D printing of multifunctional carbon nanotube yarn reinforced components', Additive Manufacturing, 12, pp. 38–44.

Gibson, I., Rosen, D. and Stucker, B. (2014) 'Additive manufacturing technologies: 3D printing, rapid prototyping, and direct digital manufacturing', Springer.

Gilshteyn, E. P., Kallio, T., Kanninen, P., Fedorovskaya, E. O., Anisimov, A. S. and Nasibulin, A. G. (2016) 'Stretchable and transparent supercapacitors based on aerosol synthesized single-walled carbon nanotube films', RSC Adv. Royal Society of Chemistry, 6(96), pp. 93915–93921.

Godino, N., Gorkin, R., Bourke, K. and Ducrée, J. (2012) 'Fabricating electrodes for amperometric detection in hybrid paper/polymer lab-on-a-chip devices', Lab on a Chip, 12(18), p. 3281.

Godoi, F.C., Prakash, S. and Bhandari, B.R., (2016) '3D printing technologies applied for food design: Status and prospects', Journal of Food Engineering, 179, pp.44-54.

González, A., Goikolea, E., Barrena, J. A. and Mysyk, R. (2016) 'Review on supercapacitors: Technologies and materials', Renewable and Sustainable Energy Reviews, 58, pp. 1189–1206.

Guan, L., Yu, L., & Chen, G. Z. (2016) 'Capacitive and non-capacitive faradaic charge storage', Electrochimica Acta, 206, 464-478.

Hao, L., Mellor, S., Seaman, O., Henderson, J., Sewell, N. and Sloan, M. (2010) 'Material characterisation and process development for chocolate additive layer manufacturing', Virtual and Physical Prototyping, 5(2), pp. 57–64.

He, S., Chen, L., Xie, C., Hu, H., Chen, S., Hanif, M. and Hou, H. (2013) 'Supercapacitors based on 3D network of activated carbon nanowhiskers wrapped-on graphitized electrospun nanofibers', Journal of Power Sources, 243, pp. 880–886.

Hsieh, B.R. (2017) 'Printed Planar Supercapacitors (SCs) Having High Energy Density', The Electrochemical Society, 7, pp. 623-623.

Huang, C. W., Wu, C. A., Hou, S. S., Kuo, P. L., Hsieh, C. Te and Teng, H. (2012) 'Gel electrolyte derived from poly(ethylene glycol) blending poly(acrylonitrile) applicable to roll-to-roll assembly of electric double layer capacitors', Advanced Functional Materials, 22(22), pp. 4677–4685.

Hwang, J.Y., Li, M., El-Kady, M.F. and Kaner, R.B. (2017) 'Next generation activated carbon supercapacitors: a simple step in electrode processing leads to remarkable gains in energy density', Advanced Functional Materials, 27(15).

Jang, Y., Jo, J., Choi, Y., Kim, I., Lee, S., Kim, D. and Yoon, S.M. (2013) 'Activated carbon nanocomposite electrodes for high performance supercapacitors', Electrochimica Acta, 102, pp. 240-245.

Jeong, H. T., Kim, B. C., Higgins, M. J. and Wallace, G. G. (2015) 'Highly stretchable reduced graphene oxide (rGO)/single-walled carbon nanotubes (SWNTs) electrodes for energy storage devices', Electrochimica Acta, 163, pp. 149–160.

Jost, K., Stenger, D., Perez, C. R., McDonough, J. K., Lian, K., Gogotsi, Y. and Dion, G. (2013) 'Knitted and screen printed carbon-fiber supercapacitors for applications in wearable electronics', Energy & Environmental Science, 6(9), pp. 2698–2705.

Ju, H., Song, W. and Fan, L. (2014) 'Rational design of graphene/porous carbon aerogels for high-performance flexible all-solid-state supercapacitors', Journal of Materials Chemistry A, 2(28), pp. 10895-10903.

Kadimisetty, K., Mosa, I.M., Malla, S., Satterwhite-Warden, J.E., Kuhns, T.M., Faria, R.C., Lee, N.H. and Rusling, J.F., (2016) '3D-printed supercapacitor-powered electrochemiluminescent protein immunoarray', Biosensors and Bioelectronics, 77, pp.188–193.

Kaempgen, M., Chan, C.K., Ma, J., Cui, Y. and Gruner, G. (2009) 'Printable thin film supercapacitors using single-walled carbon nanotubes', Nano letters, 9(5), pp. 1872-1876.

Kampouris, D.K., Ji, X., Randviir, E.P., Banks, C.E., (2015) 'A new approach for the improved interpretation of capacitance measurements for materials utilised in energy storage', RSC Adv. 5, 12782–12791.

Kurra, N., Hota, M.K. and Alshareef, H.N. (2015) 'Conducting polymer micro-supercapacitors for flexible energy storage and AC line-filtering', Nano Energy, 13, pp. 500-508.

Lammel, C., Schneider, M., Weiser, M. and Michaelis, A. (2013) 'Investigations of electrochemical double layer capacitor (EDLC) materials - A comparison of test methods', Materialwissenschaft und Werkstofftechnik, 44(7), pp. 641–649.

Leary, M., Babaee, M., Brandt, M. and Subic, a (2013) 'Feasible build orientations for self-supporting fused deposition manufacture: A novel approach to space-filling tesselated geometries', Advanced Materials Research, 633(July 2015), pp. 148–168.

Lee, K. H., Lee, Y.-W., Lee, S. W., Ha, J. S., Lee, S.-S. and Son, J. G. (2015) 'Ice-templated Self-assembly of VOPO4-Graphene Nanocomposites for Vertically Porous 3D Supercapacitor Electrodes', Scientific reports. Nature Publishing Group, 5(August), p. 13696.

Lee, W.Y., Le, L., Kong, D., Ervin, M.H., Zunino III, J.L. and Fuchs, B.E. (2015) 'Inkjet-printed flexible electronic components from graphene oxide', U.S. Patent No. 9,165,721. Washington, DC: U.S. Patent and Trademark Office.

Lei, C., Markoulidis, F., Ashitaka, Z., Lekakou, C., (2013) 'Reduction of porous carbon/Al contact resistance for an electric double-layer capacitor (EDLC)', Electrochim. Acta. 92, 183–187.

Leigh, S.J., Bradley, R.J., Purssell, C.P., Billson, D.R. and Hutchins, D.A. (2012) "A simple, low-cost conductive composite material for 3D printing of electronic sensors", PloS one, 7(11), pp. e49365.

Li, J., Lemme, M.C. and Östling, M. (2014) 'Inkjet printing of 2D layered materials', ChemPhysChem, 15(16), pp. 3427-3434.

Li, J., Mishukova, V. and Östling, M. (2016) 'All-solid-state micro-supercapacitors based on inkjet printed graphene electrodes', Applied Physics Letters, 109(12), pp. 123901.

Li, L., Sun, Q., Bellehumeur, C. and Gu, P. (2002) ‘Composite modeling and analysis for fabrication of FDM prototypes with locally controlled properties’, Journal of Manufacturing Processes, 4(2), pp. 129-141.

Li, R. R., Peng, K. Kihm, Bai S., Bridges, D. Tumuluri, Z U., Zhang, Wu, T., Compagnini, G., Feng, Z., Hu, A. (2016) ’High-rate in-plane micro-supercapacitors scribed onto photo paper using in situ femtolaser-reduced graphene oxide/Au nanoparticle microelectrodes’, Energy & Environmental Science, 9,pp. 1458-1467.

Liu, N., Ma, W., Tao, J., Zhang, X., Su, J., Li, L., Yang, C., Gao, Y., Golberg, D. and Bando, Y. (2013) ‘Cable-type supercapacitors of three-dimensional cotton thread based multi-grade nanostructures for wearable energy storage’, Advanced Materials, 25(35), pp. 4925–4931.

Liu, W., Yan, X., Lang, J., Peng, C. and Xue, Q. (2012) ‘Flexible and conductive nanocomposite electrode based on graphene sheets and cotton cloth for supercapacitor’, Journal of Materials Chemistry, 22(33), p. 17245.

Liu, Z., Wu, Z. S., Yang, S., Dong, R., Feng, X. and Müllen, K. (2016) ‘Ultraflexible In-Plane Micro-Supercapacitors by Direct Printing of Solution-Processable Electrochemically Exfoliated Graphene’, Advanced Materials, 28(11), pp. 2217–2222.

Macdonald, E., Salas, R., Espalin, D., Perez, M., Aguilera, E., Muse, D. and Wicker, R.B. (2014) ‘3D printing for the rapid prototyping of structural electronics’, IEEE Access, 2, pp. 234-242.

Malone, E. and Lipson, H. (2007) "Fab@ Home: the personal desktop fabricator kit", Rapid Prototyping Journal, 13(4), pp. 245-255.

Meissner, E. (1997) 'Phosphoric acid as an electrolyte additive for lead/acid batteries in electric-vehicle applications', Journal of Power Sources, 67(1-2), pp. 135-150.

Meng, C., Liu, C., Chen, L., Hu, C. and Fan, S. (2010) ‘Highly flexible and all-solid-state paperlike polymer supercapacitors’, Nano Letters, 10(10), pp. 4025–4031.

Nadiyapara, H. H. and Pande, S. (2017) ‘A Review of Variable Slicing in Fused Deposition Modeling’, Journal of The Institution of Engineers (India): Series C, 98(3), 387-393.

Nakamura, M., Nishiyama, Y. and Henmi, C. (2008) "3D Micro-fabrication by inkjet 3D biofabrication for 3D tissue engineering", Micro-NanoMechatronics and Human Science, 2008. MHS 2008. International Symposium on. IEEE, 451-456.

NinjaFlex, (2014) Flexible 3D Printing with Strong Flexible Filament | NinjaFlex. [Online]. 2014. Available from: http://www.ninjaflex3d.com/ [Accessed December 2015].

Niu, Z., Zhang, L., Liu, L., Zhu, B., Dong, H. and Chen, X. (2013) ‘All-solid-state flexible ultrathin micro-supercapacitors based on graphene’, Advanced Materials, 25(29), pp. 4035–4042.

Nyström, G., Marais, A., Karabulut, E., Wågberg, L., Cui, Y. and Hamedi, M. M. (2015) ‘Self-assembled three-dimensional and compressible interdigitated thin-film supercapacitors and batteries’, Nature communications, 6(May), p. 7259.

Oliver, M., Gies, P.J., Pendalwar, S.L., Coalson, C.E. and Eschbach, F.O. (1997) ‘Polymer gel electrolyte’, U.S. Patent No. 5,639,573. Washington, DC: U.S. Patent and Trademark Office.

Oropallo, W. and Piegl, L.A. (2016) ‘Ten challenges in 3D printing’, Engineering with Computers, 32(1), pp.135-148.

Pandey, P. M., Venkata Reddy, N. and Dhande, S. G. (2007) ‘Part deposition orientation studies in layered manufacturing’, Journal of Materials Processing Technology, 185(1–3), pp. 125–131.

Pandolfo, A. G. and Hollenkamp, A. F. (2006) ‘Carbon properties and their role in supercapacitors’, Journal of Power Sources, pp. 11–27.

Park, J.S. (2016) ‘Design of 3D-Printable Conductive Composites for 3D-Printed Battery’, Doctoral dissertation, Applied Sciences: School of Mechatronic Systems Engineering.

Pei, Z., Hu, H., Liang, G. and Ye, C. (2017) 'Carbon-Based Flexible and All-Solid-State Micro-supercapacitors Fabricated by Inkjet Printing with Enhanced Performance', Nano-Micro Letters, 9(2), pp. 19.

Peterson, G.I., Larsen, M.B., Ganter, M.A., Storti, D.W. and Boydston, A.J. (2014) "3D-Printed Mechanochromic Materials", ACS applied materials & interfaces, 7(1), pp. 577-583.

Poggenpohl, S. and Sato, K. (2003) 'Models of dissertation research in design', 3rd Doctoral Education in Design Conference, Tsukuba, Japan.

Qiu, F., Harrison, D., Fyson, J. and Southee, D. (2014) 'Fabrication and Characterisation of Flexible Coaxial Thin Thread Supercapacitors', Smart Science, 2(3), pp. 107–115.

Ramachandran, R., Saranya, M., Santhosh, C., Velmurugan, V., Raghupathy, B.P.C., Jeong, S.K., Grace, A.N.C., (2014) 'Co9S8 nanoflakes on graphene (Co9S 8/G) nanocomposites for high performance supercapacitors', RSC Adv. 4, 21151–21162.

Randviir, E.P. & Banks, C.E., (2013) 'Electrochemical impedance spectroscopy: an overview of bioanalytical applications', Analytical Methods, 5(5), pp. 1098-1115.

Reprap, (2015) RepRap G-code- RepRap Wiki. [Online]. 2015. Available from: http://reprap.org/wiki/G-code [Accessed May 2015].

Sa'adu, L.; Hashim, M.; Baharuddin, M.B. (2014) 'A noble conductivity studies and characterizations of PVA-Orthophosphoric-filter paper electrolytes', Journal of Materials Science Research, 3 (4), 1.

Saeidi, N. and Lotfollahi, M.N. (2016) 'Effects of Powder Activated Carbon Particle Size on Activated Carbon Monolith's Properties', Materials and Manufacturing Processes, 31(12), 1634-1638.

Saengchairat, N., Tran, T. and Chua, C. (2017) 'A review: additive manufacturing for active electronic components', Virtual and Physical Prototyping, 12(1), pp. 31-46.

Sagu, J.S., Wijayantha, U., Gamage, K., Bohm, M., Bohm, S. and Rout, T.K. (2016) 'Aerosol-Assisted Chemical Vapor Deposition of Multi-Walled Carbon Nanotubes on

Steel Substrates for Application in Supercapacitors', Advanced Engineering Materials, 18(6), 1059-1065.

Schunemann, E. (2015) 'Paste deposition modelling, deconstructing the additive manufacturing process: Development of novel multi-material tools and techniques for craft practitioners', Doctoral dissertation, Brunel University London.

Screwfix, (2015). Dow corning 781 Acetoxy silicone sealant clear 310ml. [online] Available at: http://www.screwfix.com/p/dow-corning-781-acetoxy-silicone-sealant-clear-310ml/32576?_requestid=184669.

Sheha, E. and El-Mansy, M. (2008) 'A high voltage magnesium battery based on H 2 SO 4-doped (PVA) 0.7 (NaBr) 0.3 solid polymer electrolyte', Journal of Power Sources, 185(2), pp. 1509-1513.

Shen, J. (2015) 'Material system for use in three dimensional printing', United States: U.S. Patent and Trademark Office DaimlerChyrsler, AG. 7,049,363, 2006.

Sheng, K., Sun, Y., Li, C., Yuan, W. and Shi, G. (2012) 'Ultrahigh-rate supercapacitors based on electrochemically reduced graphene oxide for ac line-filtering', Scientific reports, 2, p. 247.

Singh, S., Ramakrishna, S. and Singh, R. (2017) 'Material issues in additive manufacturing: A review', Journal of Manufacturing Processes, 25, pp.185-200.

Strano, G., Hao, L., Everson, R. M. and Evans, K. E. (2013) 'A new approach to the design and optimisation of support structures in additive manufacturing', International Journal of Advanced Manufacturing Technology, 66(9–12), pp. 1247–1254.

Structur3D., (2014). Discov3rysystem. [online] Available at: http://www.structur3d.io/#discov3ry [Accessed January 2016].

Sudhakar, Y. N., Selvakumar, M., Bhat, D. K. and Senthil Kumar, S. (2014) 'Reduced graphene oxide derived from used cell graphite and its green fabrication as an eco-friendly supercapacitor', RSC Advances. Royal Society of Chemistry, 4(104), pp. 60039–60051.

Sun, G., An, J., Chua, C. K., Pang, H., Zhang, J. and Chen, P. (2015) 'Layer-by-layer printing of laminated graphene-based interdigitated microelectrodes for flexible planar micro-supercapacitors', Electrochemistry Communications, 51, pp. 33–36.

Sun, H., Fu, X., Xie, S., Jiang, Y., Guan, G., Wang, B., Li, H. and Peng, H. (2016) 'A Novel Slicing Method for Thin Supercapacitors', Advanced Materials, pp. 6429–6435.

Sun, H., Xie, S., Li, Y., Jiang, Y., Sun, X., Wang, B. and Peng, H. (2016) 'Large-Area Supercapacitor Textiles with Novel Hierarchical Conducting Structures', Advanced Materials, pp. 8431–8438.

Sun, W. and Chen, X. (2009) 'Fabrication and tests of a novel three dimensional micro supercapacitor', Microelectronic Engineering, 86(4–6), pp. 1307–1310.

Tyagi, A., Tripathi, K.M. and Gupta, R.K., (2015) 'Recent progress in micro-scale energy storage devices and future aspects', J. Mater. Chem. A, 3(45), pp. 22507–22541.

Tyler, D. J. (2005) 'Textile Digital Printing Technologies', Textile Progress, 37(4), pp. 1–64.

Ujjain, S. K., Ahuja, P., Bhatia, R. and Attri, P. (2016) 'Printable multi-walled carbon nanotubes thin film for high performance all solid state flexible supercapacitors', Materials Research Bulletin, 83, pp. 167–171.

Ultimaker.com, (n.d.). Ultimaker 2. [online] Available at: https://www.ultimaker.com/pages/our-printers/ultimaker-2 [Accessed December 2015]

Valentine, A.D., Busbee, T.A., Boley, J.W., Raney, J.R., Chortos, A., Kotikian, A., Berrigan, J.D., Durstock, M.F. and Lewis, J.A. (2017) 'Hybrid 3D Printing of Soft Electronics', Advanced Materials, 29(40).

Voxel8, (2014). Voxel8 materials. [online] Available at: http://www.voxel8.co/materials/ [Accessed 9 Oct. 2013].

Wang, Q., Yan, J. and Fan, Z. (2016) 'Carbon materials for high volumetric performance supercapacitors: design, progress, challenges and opportunities', Energy & Environmental Science, 9(3), pp. 729-762.

Wang, S., Yu, Y., Li, R., Feng, G., Wu, Z., Compagnini, G., Gulino, A., Feng, Z. and Hu, A. (2017) ‘High-performance stacked in-plane supercapacitors and supercapacitor array fabricated by femtosecond laser 3D direct writing on polyimide sheets’, Electrochimica Acta, 241, pp.153–161.

Wang, X., Lu, X., Liu, B., Chen, D., Tong, Y. and Shen, G., (2014) ‘Flexible energy storage devices: design consideration and recent progress’, Advanced Materials, 26(28), pp.4763-4782.

Wang, Y., Chen, J., Cao, J., Liu, Y., Zhou, Y., Ouyang, J. and Jia, D. (2014) 'Graphene/carbon black hybrid film for flexible and high rate performance supercapacitor', Journal of Power Sources, 271, pp. 269-277.

Wardyn, J. D., Sanderson, C., Swan, L. E. and Stagi, M. (2015) ‘Low cost production of 3D-printed devices and electrostimulation chambers for the culture of primary neurons’, Journal of Neuroscience Methods, 251, pp. 17–23.

Wei, M., Zhang, F., Wang, W., Alexandridis, P., Zhou, C., & Wu, G., (2017) ‘3D direct writing fabrication of electrodes for electrochemical storage devices’, Journal of Power Sources, 354, 134-147.

Wei, X. R., Zhang, Y. H. and Geng, G. H. (2016) ‘No-infill 3D Printing’, 3D Research, 7(3), pp. 1–12.

Welham, N.; Berbenni, V.; Chapman, P. (2002) ‘Increased chemisorption onto activated carbon after ball-milling’, Carbon, 40 (13), 2307-2315.

Wen, F., Hao, C., Xiang, J., Wang, L., Hou, H., Su, Z., Hu, W. and Liu, Z. (2014) 'Enhanced laser scribed flexible graphene-based micro-supercapacitor performance with reduction of carbon nanotubes diameter', Carbon, 75, pp. 236-243.

Wijnen, B., Hunt, E. J., Anzalone, G. C. and Pearce, J. M. (2014) ‘Open-Source Syringe Pump Library’, PloS one, 9(9), e107216.

Winter, M. and Ralph, B. J. (2004) ‘What are batteries, fuel cells, and supercapacitors?’, Chemical Reviews, 104(10), pp. 4245–4269.

Xia, L., Yu, L., Hu, D. and Chen, G.Z. (2017) 'Electrolytes for electrochemical energy storage', Materials Chemistry Frontiers, 1(4), pp.584-618.

Xu, J., Wang, D., Yuan, Y., Wei, W., Duan, L., Wang, L., Bao, H. and Xu, W. (2015) 'Polypyrrole/reduced graphene oxide coated fabric electrodes for supercapacitor application', Organic Electronics: physics, materials, applications, 24, pp. 153–159.

Xu, J., Wang, D., Yuan, Y., Wei, W., Duan, L., Wang, L., Bao, H. and Xu, W. (2015) 'Polypyrrole/reduced graphene oxide coated fabric electrodes for supercapacitor application', Organic Electronics: physics, materials, applications, 24, pp. 153–159.

Xu, J., Wang, D., Yuan, Y., Wei, W., Gu, S., Liu, R., Wang, X., Liu, L. and Xu, W. (2015) 'Polypyrrole-coated cotton fabrics for flexible supercapacitor electrodes prepared using CuO nanoparticles as template', Cellulose, 22(2), pp. 1355–1363.

Xu, S., Wei, G., Li, J., Ji, Y., Klyui, N., Izotov, V. and Han, W. (2017) 'Binder-free Ti3C2Tx MXene electrode film for supercapacitor produced by electrophoretic deposition method', Chemical Engineering Journal, 317, pp. 1026–1036.

Xu, S., Zhang, Y., Cho, J., Lee, J., Huang, X., Jia, L., Fan, J. a, Su, Y., Su, J., Zhang, H., Cheng, H., Lu, B., Yu, C., Chuang, C., Kim, T.-I., Song, T., Shigeta, K., Kang, S., Dagdeviren, C., Petrov, I., Braun, P. V, Huang, Y., Paik, U. and Rogers, J. a (2013) 'Stretchable batteries with self-similar serpentine interconnects and integrated wireless recharging systems.', Nature communications. Nature Publishing Group, 4, p. 1543.

Yadav, A. A., Jadhav, S. N., Chougule, D. M., Patil, P. D., Chavan, U. J. and Kolekar, Y. D. (2016) 'Spray deposited Hausmannite Mn3O4 thin films using aqueous/organic solvent mixture for supercapacitor applications', Electrochimica Acta, 206, pp. 134–142.

Yang, Y., Huang, Q., Niu, L., Wang, D., Yan, C., She, Y. and Zheng, Z. (2017) 'Waterproof, Ultrahigh Areal-Capacitance, Wearable Supercapacitor Fabrics', Advanced Materials, p. 1606679.

Yang, Z., Deng, J., Chen, X., Ren, J. and Peng, H. (2013) 'A highly stretchable, fiber-shaped supercapacitor', Angewandte Chemie - International Edition, 52(50), pp. 13453–13457.

Yeo, J., Kim, G., Hong, S., Kim, M. S., Kim, D., Lee, J., Lee, H. B., Kwon, J., Suh, Y. D., Kang, H. W., Sung, H. J., Choi, J. H., Hong, W. H., Ko, J. M., Lee, S. H., Choa, S. H. and Ko, S. H. (2014) 'Flexible supercapacitor fabrication by room temperature rapid laser processing of roll-to-roll printed metal nanoparticle ink for wearable electronics application', Journal of Power Sources, 246, pp. 562–568.

Yong, S., Owen, J. R., Tudor, M. J. and Beeby, S. P. (2015) 'Flexible solid-state fabric based supercapacitor', Journal of Physics: Conference Series, 660, 1, pp. 012074.

Yoon, S.M., Go, J.S., Yu, J., Kim, D.W., Jang, Y., Lee, S., Jo, J., (2013) 'Fabrication and characterization of flexible thin film super-capacitor with silver nano paste current Collector', Journal of nanoscience and nanotechnology, (13, 12), 7844-7849.

Zang, J., Cao, C., Feng, Y., Liu, J. and Zhao, X. (2014) 'Stretchable and high-performance supercapacitors with crumpled graphene papers', Scientific reports, 4, p. 6492.

Zhang, J., Dong, L., Xu, C., Hao, J., Kang, F. and Li, J. (2017) 'Comprehensive approaches to three-dimensional flexible supercapacitor electrodes based on MnO2/carbon nanotube/activated carbon fiber felt', Journal of Materials Science. Springer US, 52(10), pp. 5788–5798.

Zhang, R. R., Xu, Y. M., Harrison, D., Fyson, J., Qiu, F. L. and Southee, D. (2015) 'Flexible strip supercapacitors for future energy storage', International Journal of Automation and Computing, 12(1), pp. 43–49.

Zhang, R., Xu, Y., Harrison, D. and Fyson, J. (2016) 'A study of the electrochemical performance of strip supercapacitors under bending conditions', Int. J. Electrochem. Sci., 11, 7922–7933.

Zhang, R., Xu, Y., Harrison, D. and Fyson, J. (2017) 'A study of the electrochemical performance of strip supercapacitors under static and dynamic mechanical tests', Int. J. Electrochem. Sci., 12, 1463 – 1473.

Zhang, R.; Xu, Y.; Harrison, D.; Fyson, J.; Southee, D. (2016) 'Experimental design to optimise electrical performance of strip supercapacitors'. Int.J.Electrochem.Sci, (11), 675-684.

Zhang, S., Li, Y. and Pan, N. (2012) 'Graphene based supercapacitor fabricated by vacuum filtration deposition', Journal of Power Sources, 206, pp. 476–482.

Zhang, S., Peng, C., Ng, K. C. and Chen, G. Z. (2010) 'Nanocomposites of manganese oxides and carbon nanotubes for aqueous supercapacitor stacks', Electrochimica Acta, 55(25), pp. 7447–7453.

Zhang, Y., Lin, B., Wang, J., Tian, J., Sun, Y. Zhang, X., Yang, H., (2016) 'All-solid-state asymmetric supercapacitors based on ZnO quantum dots/carbon/CNT and porous N-doped carbon/CNT electrodes derived from a single ZIF-8/CNT template', J. Mater. Chem. A. 4, 10282–10293.

Zhang, Y., Feng, H., Wu, X., Wang, L., Zhang, A., Xia, T., Dong, H., Li, X. and Zhang, L., (2009) 'Progress of electrochemical capacitor electrode materials: A review', International Journal of Hydrogen Energy, 34(11), pp.4889–4899.

Zhang, Z., Deng, J., Li, X., Yang, Z., He, S., Chen, X., Guan, G., Ren, J. and Peng, H. (2015) 'Superelastic supercapacitors with high performances during stretching', Advanced Materials, 27(2), pp. 356–362.

Zhao, C., Shu, K., Wang, C., Gambhir, S. and Wallace, G. G. (2015) 'Reduced graphene oxide and polypyrrole/reduced graphene oxide composite coated stretchable fabric electrodes for supercapacitor application', Electrochimica Acta, 172, pp. 12–19.

Zhao, C., Wang, C., Gorkin, R., Beirne, S., Shu, K. and Wallace, G. G. (2014) 'Three dimensional (3D) printed electrodes for interdigitated supercapacitors', Electrochemistry Communications, 41, pp. 20–23.

Zhao, W., Zhang, M., Pan, P., Song, D., Huang, S., Wei, J., Li, X., Qi, W., Zhang, K., Zhao, J. and Yang, Z. (2017) 'Design and fabrication of flexible supercapacitor devices by using mesoporous carbon/polyaniline ink', Surface and Coatings Technology, 320, 595-600.

Zhi, M., Xiang, C., Li, J., Li, M. and Wu, N. (2013) 'Nanostructured carbon-metal oxide composite electrodes for supercapacitors: a review', Nanoscale, 5(1), pp. 72–88.

Zhou, Q., Ye, X., Wan, Z. and Jia, C. (2015) 'A three-dimensional flexible supercapacitor with enhanced performance based on lightweight, conductive graphene-cotton fabric electrode', Journal of Power Sources, 296, pp. 186–196.

Zhu, C., Liu, T., Qian, F., Han, T. Y. J., Duoss, E. B., Kuntz, J. D., Spadaccini, C. M., Worsley, M. A. and Li, Y. (2016) 'Supercapacitors Based on Three-Dimensional Hierarchical Graphene Aerogels with Periodic Macropores', Nano Letters, 16(6), pp. 3448–3456.

Zuo, W., Li, R., Zhou, C., Li, Y., Xia, J. and Liu, J. (2017) 'Battery-Supercapacitor Hybrid Devices: Recent Progress and Future Prospects', Advanced Science, 4(7).

XI. Appendix

List of appendices

A Paste extruder

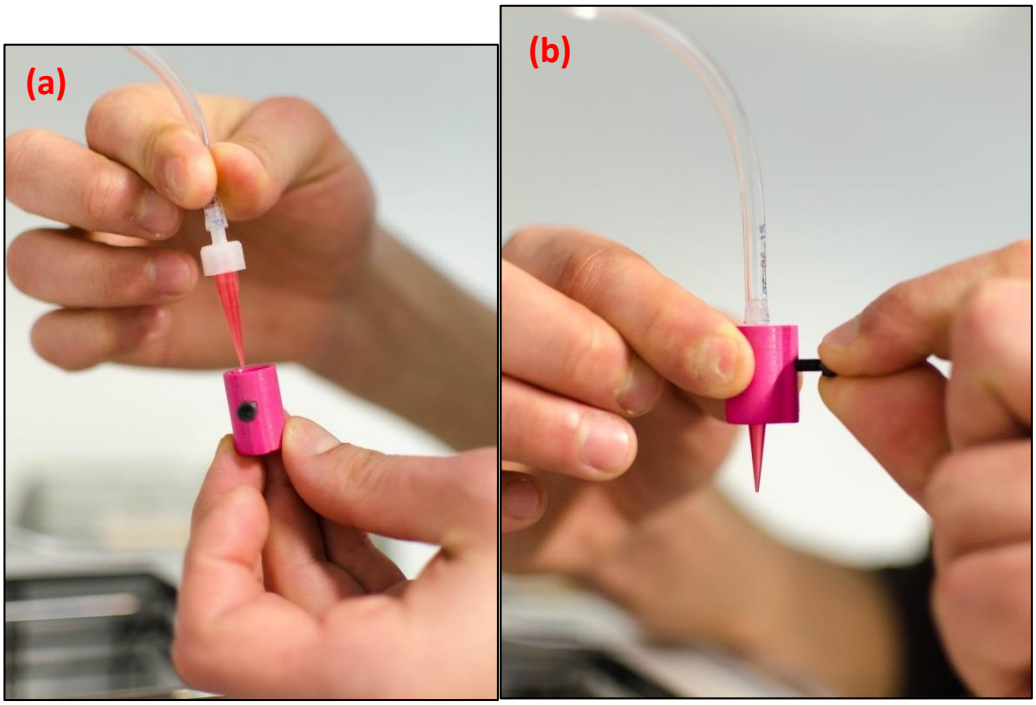

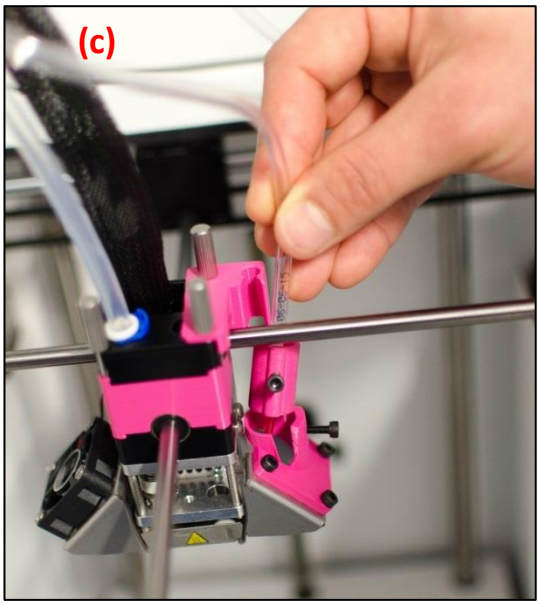
(c)

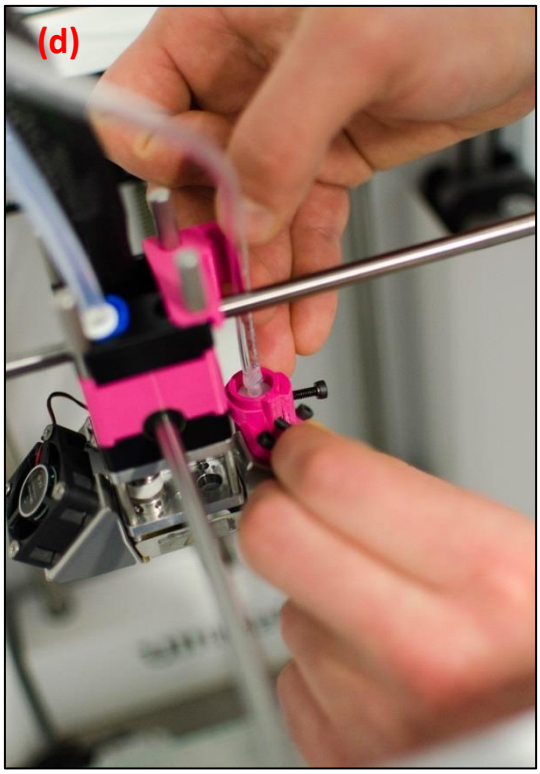
(d)

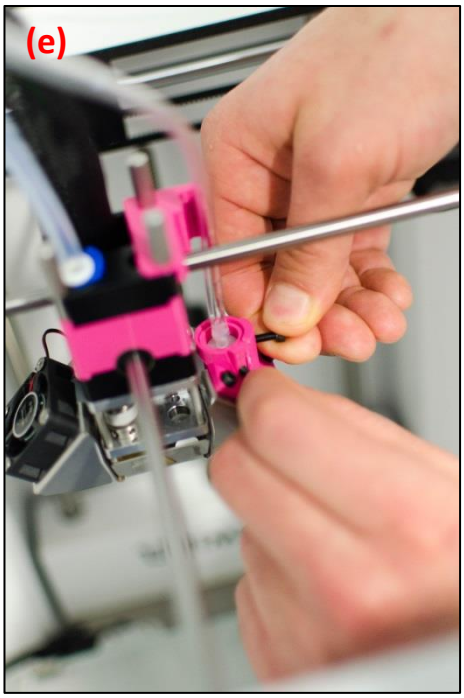
(e)

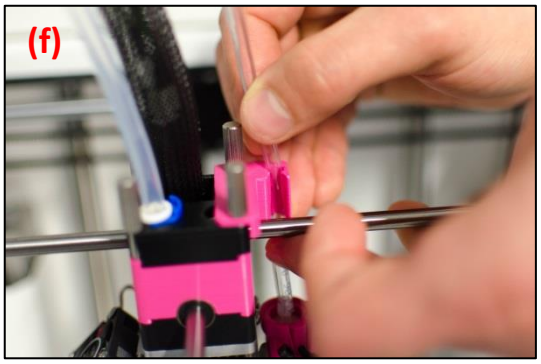
(f)

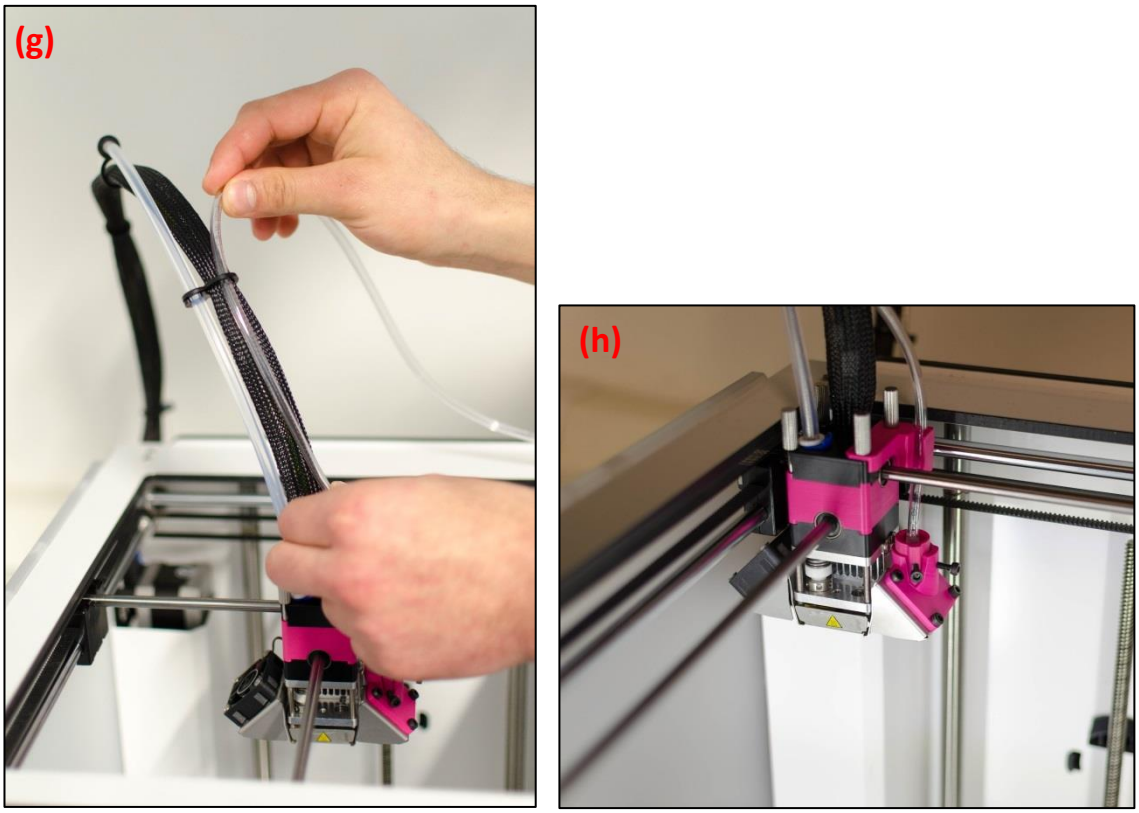

Figure 7.1*:* Images of 3D paste deposition head: a) barbed male luer w/locking nut and nozzle adaptor, (b) screw adapter, (c) nozzle hub, (d) extruder line fixture, (e) screw hub, (f) tube liner, (g) tube holder, and (h) final 3D dual head

B Barbed male luer w/locking nut

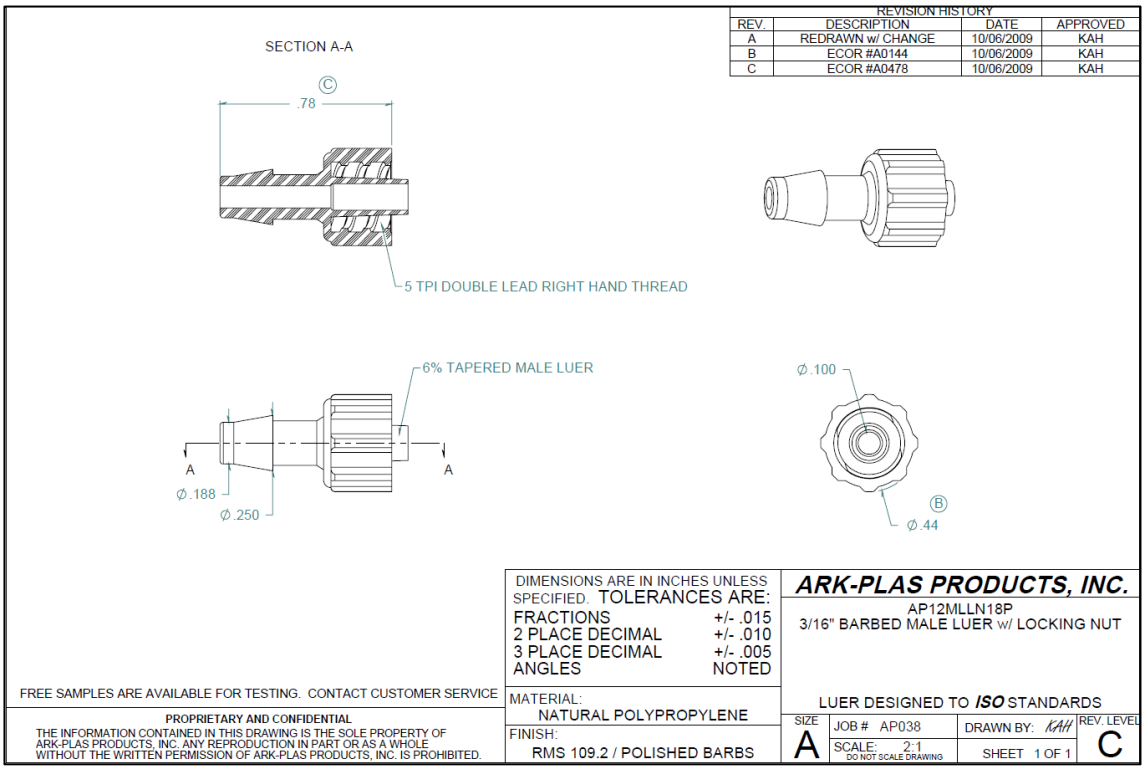

C Discov3ry gear box specifications

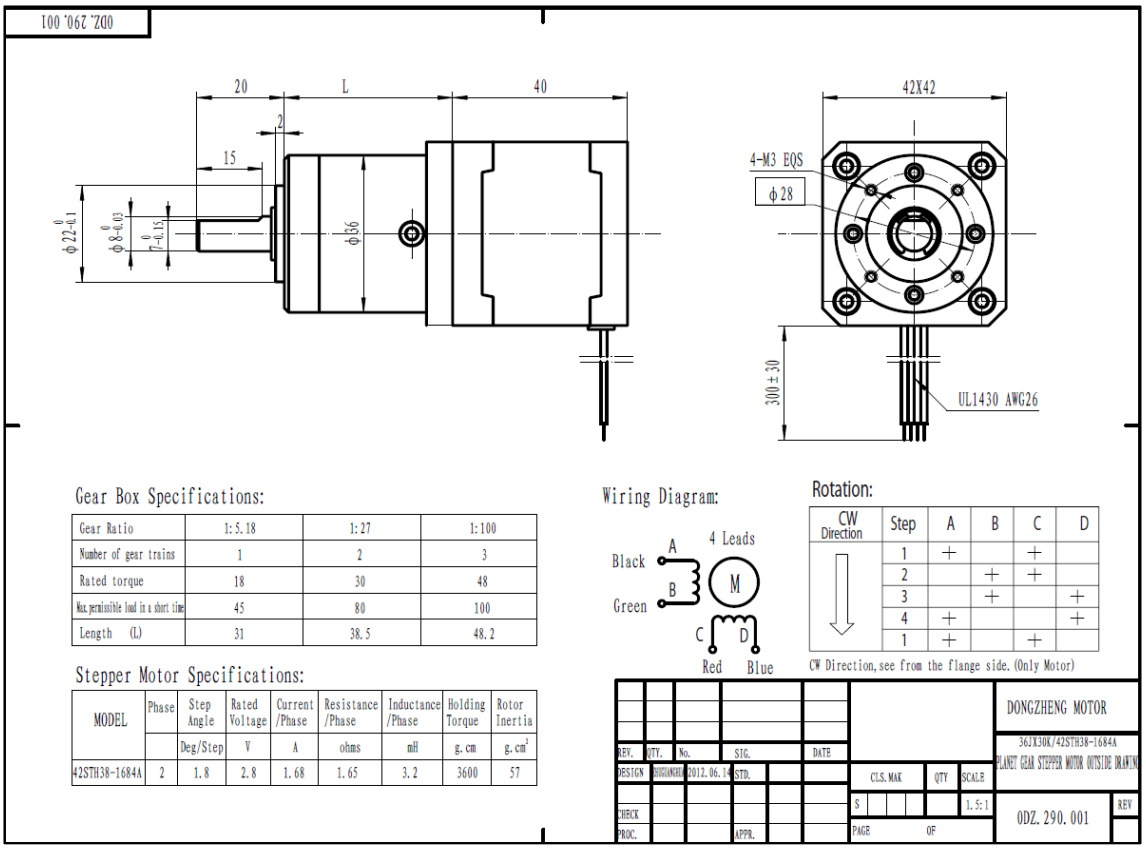

Gear Ratio	1:5.18	1:27	1:100
Number of gear trains	1	2	3
Rated torque	18	30	48
Max.permissible load in a short time	45	80	100
Length (L)	31	38.5	48.2

MODEL	Phase	Step Angle	Rated Voltage	Current /Phase	Resistance /Phase	Inductance /Phase	Holding Torque	Rotor Inertia
		Deg/Step	V	A	ohms	mH	g.cm	g.cm²
42STH38-1684A	2	1.8	2.8	1.68	1.65	3.2	3600	57

CW Direction	Step	A	B	C	D
	1	+		+	
	2		+	+	
	3		+		+
	4	+			+
	1	+		+	

D Dow corning(r) 781 acetoxy silicone

DOW CORNING

SAFETY DATA SHEET

According to article 31 and Annex II of the EU REACH Regulation

Version: 2.2
Revision Date: 07.10.2011
Superseded date: 30.05.2011

DOW CORNING(R) 781 ACETOXY SILICONE CLEAR

1. IDENTIFICATION OF THE SUBSTANCE/PREPARATION AND OF THE COMPANY

1.1 Product name : DOW CORNING(R) 781 ACETOXY SILICONE CLEAR

1.2 Identified uses : Adhesive, binding agents

Uses advised against : None known.

1.3 Company : Dow Corning Europe S.A.
rue Jules Bordet - Parc Industriel - Zone C
B-7180 Seneffe
Belgium

E-mail address (Safety Data Sheet) : sdseu@dowcorning.com

Customer Service :

English	Tel: +49 611237507
Deutsch	Tel: +49 611237500
Français	Tel: +32 64511149
Italiano	Tel: +32 64511170
Español	Tel: +32 64511163
	Fax: +32 64888683

1.4 Emergency Phone Number :

Dow Corning (Barry U.K. 24h)	Tel: +44 1446732350
Dow Corning (Wiesbaden 24h)	Tel: +49 61122158
Dow Corning (Seneffe 24h)	Tel: +32 64 888240

2. HAZARDS IDENTIFICATION

2.1 Classification of the substance or mixture

According to EU Directives 67/548/EEC or 1999/45/EC:

Not hazardous.

2.2 Label elements

Labelling according to EEC Directive

S-phrases : S24 Avoid contact with skin.
S51 Use only in well-ventilated areas.

DOW CORNING(R) 781 ACETOXY SILICONE CLEAR

Personal protection equipment

Respiratory protection	:	Suitable respiratory protection should be worn if the product is used in large quantities, confined spaces or in other circumstances where the OEL may be approached or exceeded. Depending on the working conditions, wear a respiratory mask with filter(s) E or use a self-contained respirator. The choice of a filter type depends on the amount and type of chemical being handled in the workplace. Regarding filter characteristics, contact your respiratory protection supplier.
Hand protection	:	Chemical protective gloves should be worn: Butyl rubber. Nitrile rubber. Neoprene rubber. Silver shield(TM). 4H(TM). Viton(TM). Regarding glove's breakthrough time,contact your chemical protective glove supplier.
Eye/face protection	:	Safety glasses should be worn.
Skin protection	:	Protective equipment is not normally necessary.
Hygiene measures	:	Exercise good industrial hygiene practice. Wash after handling, especially before eating, drinking or smoking.
Additional information	:	These precautions are for room temperature handling. Use at elevated temperature or aerosol/spray applications may require added precautions.
Environmental exposure controls	:	Refer to section 6 and 12.

9. PHYSICAL AND CHEMICAL PROPERTIES

Form	:	Paste
Colour	:	Colorless
Odour	:	Acetic acid
Flash point	:	> 100 °C (Closed Cup)
Explosive properties	:	No
Specific Gravity	:	1.02
Oxidizing properties	:	No

The above information is not intended for use in preparing product specifications. Contact Dow Corning before writing specifications.

10. STABILITY AND REACTIVITY

10.1 Reactivity	:	Cures in the presence of water or moisture, releasing a small amount of acetic acid.
10.2 Stability	:	Stable under normal usage conditions.

E Activated carbon

SIGMA-ALDRICH

sigma-aldrich.com

SAFETY DATA SHEET

according to Regulation (EC) No. 1907/2006
Version 5.0 Revision Date 08.05.2012
Print Date 09.02.2016

1. IDENTIFICATION OF THE SUBSTANCE/MIXTURE AND OF THE COMPANY/UNDERTAKING

1.1 Product identifiers

Product name : Activated charcoal

Product Number : 05105
Brand : Sigma-Aldrich
CAS-No. : 7440-44-0

1.2 Relevant identified uses of the substance or mixture and uses advised against

Identified uses : Laboratory chemicals, Manufacture of substances

1.3 Details of the supplier of the safety data sheet

Company : Sigma-Aldrich Company Ltd.
The Old Brickyard
NEW ROAD, GILLINGHAM
Dorset
SP8 4XT
UNITED KINGDOM

Telephone : +44 (0)1747 833000
Fax : +44 (0)1747 833313
E-mail address : eurtechserv@sial.com

1.4 Emergency telephone number

Emergency Phone # : +44 (0)1747 833100

2. HAZARDS IDENTIFICATION

2.1 Classification of the substance or mixture

Not a hazardous substance or mixture according to Regulation (EC) No. 1272/2008.
This substance is not classified as dangerous according to Directive 67/548/EEC.

2.2 Label elements

The product does not need to be labelled in accordance with EC directives or respective national laws.

2.3 Other hazards - none

3. COMPOSITION/INFORMATION ON INGREDIENTS

3.1 Substances

Synonyms : Charcoal activated

Formula : C
Molecular Weight : 12.01 g/mol

4. FIRST AID MEASURES

4.1 Description of first aid measures

If inhaled
If breathed in, move person into fresh air. If not breathing, give artificial respiration.

In case of skin contact
Wash off with soap and plenty of water.

9. PHYSICAL AND CHEMICAL PROPERTIES

9.1 Information on basic physical and chemical properties

a)	Appearance	Form: powder Colour: black
b)	Odour	odourless
c)	Odour Threshold	no data available
d)	pH	6.0 - 9 at 40 g/l at 25 °C
e)	Melting point/freezing point	Melting point/range: 3,550 °C
f)	Initial boiling point and boiling range	no data available
g)	Flash point	no data available
h)	Evaporation rate	no data available
i)	Flammability (solid, gas)	no data available
j)	Upper/lower flammability or explosive limits	no data available
k)	Vapour pressure	< 0.01 hPa at 20 °C
l)	Vapour density	no data available
m)	Relative density	0.250 - 0.600 g/cm3
n)	Water solubility	insoluble
o)	Partition coefficient: n-octanol/water	no data available
p)	Autoignition temperature	no data available
q)	Decomposition temperature	no data available
r)	Viscosity	no data available
s)	Explosive properties	no data available
t)	Oxidizing properties	no data available

9.2 Other safety information

Bulk density	250 - 550 kg/m3 at 20 °C

10. STABILITY AND REACTIVITY

10.1 Reactivity

no data available

10.2 Chemical stability

no data available

10.3 Possibility of hazardous reactions